# DYNAMICS AND SYNCHRONIZATION IN NEURONAL MODELS

**PhD Thesis**

**This thesis was supervised by Prof. Claudio Mirasso at the Institute for Cross-Disciplinary Physics and Complex Systems in Palma de Mallorca between 2004 and 2009.**

PhD Thesis

Dynamics and Synchronization in Neuronal Models

T. Pérez

**Toni Pérez**

**IFISC**

Instituto de Física Interdisciplinar y Sistemas Complejos

IFISC

Instituto de Física Interdisciplinar y Sistemas Complejos

## TESIS DOCTORAL

# Dynamics and Synchronization
# in Neuronal Models

*Tesis presentada por Toni Pérez, en el Departamento de Física de la Universitat de les Illes Balears, para optar al grado de Doctor en Física*

Toni Pérez

Palma de Mallorca, July 2009

**Dynamics and Synchronization
in Neuronal Models**

Toni Pérez
Instituto de Física Interdisciplinar y Sistemas Complejos
IFISC (UIB-CSIC)

PhD Thesis

Director: Prof. Claudio R. Mirasso Santos

This document was typeset with LaTeX $2_\varepsilon$

Claudio R. Mirasso Santos, Profesor Titular de Universidad

CERTIFICA

que esta tesis doctoral ha sido realizada por el Sr. *Toni Pérez* bajo su dirección en el Instituto de Física Interdisciplinar y Sistemas Complejos y, para que conste, firma la presente

Palma de Mallorca, 3 de Julio de 2009

Claudio R. Mirasso Santos

*A Sandra*
*por su incondicional apoyo.*

# Agradecimientos

Quiero expresar mi sincero agradecimiento a Claudio Mirasso, el cual confió en mí y me brindó la oportunidad de realizar esta tesis. Desde mis inicios en el estudio de la dinámica y sincronización de láseres de semiconductor y durante toda la realización de esta tesis ha fomentado un ambiente inmejorable de trabajo, estando siempre abierto a nuevas ideas y discusiones. Junto a él, no sólo me he formado como investigador, sino que además he encontrado a un amigo. No quisiera dejar pasar la oportunidad para agradecer también la maravillosa hospitalidad y amabilidad de Alejandra.

En el plano personal, Sandra ha tenido que convivir con lo bueno y lo malo de este proceso. Le estoy infinitamente agradecido por todo su cariño, comprensión y apoyo en el pasado, presente y futuro.

Junto a Raúl Vicente he vivido grandes momentos tanto científicos como personales. A pesar del natural distanciamiento actual, tengo que agradecerle los buenos ratos de trabajo juntos en nuestros inicios, toda su ayuda y apoyo durante todo este período y toda la diversión que hemos disfrutado tanto en nuestra querida isla como por media Europa. Como decía el estribillo de aquella canción que nos apropiamos aquel verano: *Nada de esto fue un error...*

He tenido el privilegio de poder realizar esta tesis en un entorno científico y humano excepcional. Quisiera expresar toda mi gratitud y afecto por todos los integrantes del IFISC, tanto presentes como pasados. Nombrarlos a todos llevaría muchas líneas, por lo que espero que cada cual sepa entender a su manera lo agradecido que le estoy. Especial mención se merecen Marta y Rosa, las cuales han sabido escuchar cuando lo necesitaba y Víctor por hacerme ver las cosas desde otra perspectiva.

Quisiera expresar mi gratitud a David por su amistad durante todos estos años y por ayudarme revisando la ortografía de la tesis, a Marina por compartir tantos momentos *inasc* conmigo y a Reyes por los buenos instantes pasados durante la experiencia ECTS, fira incluida, y por estar siempre dispuesta a compartir un momento conmigo.

A Elías Manjarrez y Lourdes Martínez les agradezco la oportunidad de poder colaborar con ellos en un área completamente diferente a la mía y el haber hecho mi estancia en Puebla muy agradable.

Thanks to Atsushi Uchida I had the opportunity to know and enjoy the Japanese customs. His hospitality together with his charming family made my stay in Saitama unforgettable. Dōmo arigatō gozaimashita.

Por último, pero no por ello menos importante, quisiera agradecer el cariño y apoyo de mi familia. Sin ellos esto no hubiese sido posible.

*Toni Pérez.*
*Palma, julio de 2009.*

# Contents

# Resumen

Desde hace muchos años los científicos han estado estudiado el sistema nervioso y sus constituyentes. Uno de los más notables avances en la descripción de la estructura y las unidades funcionales del sistema nervioso provino del fisiólogo español Santiago Ramón y Cajal a finales del siglo XIX con su doctrina neuronal. Ramón y Cajal rompió la creencia establecida de que el sistema nervioso estaba compuesto por un solo retículo o continuo. Usando una técnica de coloración histológica, Cajal pudo resolver en detalle la estructura y concluir que el sistema nervioso estaba compuesto de neuronas individuales en lugar de ser un continuo. Por este descubrimiento, Cajal recibió el premio Nobel de Medicina en 1906.

Actualmente, la neurociencia es un amplio campo donde muchas disciplinas convergen para tratar cuestiones como: de que manera se guardan los recuerdos? cual es el código neuronal? como puede ser el cerebro tan rápido?... desde diferentes puntos de vista y usando diferentes aproximaciones. Con la llegada de los ordenadores y posteriormente con el incremento de la potencia de cálculo, la neurociencia computacional surgió como un área fundamental en el análisis y estudio de los sistemas neuronales. Una gran variedad de modelos matemáticos aparecieron para describir la dinámica neuronal cubriendo diferentes niveles de complejidad. Mucho de ellos están basados en una descripción detallada de la anatomía, las reacciones químicas o los circuitos neuronales. Otra clase de modelos describen cualitativamente el comportamiento neuronal y los circuitos neuronales basándose en datos experimentales. Es difícil deter-

minar cual es el nivel de detalles apropiado que un modelo debe cubrir. Un buen modelo debería contener detalles suficientes que permitan describir los principales aspectos biofísicos, pero debe ser lo suficientemente simple para proveer una clara interpretación de los resultados.

Esta tesis está principalmente dedicada al modelado y simulación de sistemas neuronales con énfasis en diferentes aspectos. Empezamos con una introducción a los conceptos preliminares necesarios para un mejor entendimiento de los siguientes capítulos. Las bases fisiológicas de una neurona y sus principales mecanismos de operación se detallan en el capítulo 1. En este capítulo también se introduce los principales modelos neuronales que se usan durante la tesis.

En el capítulo 2 se investiga el papel del ruido cuando actua sobre neuronas. El fenómeno de resonancia estocástica es caracterizado en un conjunto de neuronas del sistema motor. Tras la introducción del modelo apropiado para describir la dinámica neuronal y los detalles del método de integración, la resonancia estocástica es cuantificada mediante la relación señal ruido. Finalmente, en colaboración con el laboratorio de Neurofisiología Integrativa de la Benemérita Autónoma Universidad de Puebla en México, se corroboró los resultados experimentales demostrando que el fenómeno de resonancia estocástica está presente en el sistema motor.

En el capítulo 3 se modela la propagación de señales a través de la médula espinal durante el desarrollo de una tarea motora. Basados en estudios previos, se propone un nuevo circuito neuronal capaz de reproducir los ritmos y la propagación de señales a lo largo de la médula observados durante una actividad motora como el rascado. También se reproducen los fallos espontáneos en la actividad observados experimentalmente durante el transcurso de esta tarea motora y se predice un nuevo tipo. Continuando la colaboración con el laboratorio de Neurofisiología Integrativa de la Benemérita Autonoma Universidad de Puebla en México, se ha podido corroborar los resultados numéricos mediante observaciones experimentales.

Posteriormente, se estudia el papel que juega la heterogeneidad en un conjunto de neuronas acopladas. En el capítulo 4 se demuestra que la presencia de diversidad en algunos parámetros de las neuronas puede

mejorar la respuesta del sistema a una modulación periódica externa. Primero se estudia un conjunto de neuronas descritas por el modelo de Fitzhugh-Nagumo cuando la interacción entre las neuronas está mediada por sinapsis químicas y eléctricas. También se ha estudiado una descripción neuronal que tiene en cuenta aspectos más biológicos como el modelo de Morris-Lecar. En la última parte del capítulo se desarrolla una aproximación teórica que cualitativamente reproduce los resultados numéricos.

La segunda parte de la tesis está centrada en el estudio del efecto de la topología y el retraso en las conexiones en una red neuronal. Se explora en el capítulo 5 como las propiedades topológicas y los retrasos en la conducción de diferentes clases de redes afectan la capacidad de las neuronas para establecer una relación temporal bien definida mediante sus potenciales de acción. En particular, el concepto de consistencia es introducido y estudiado en una red neuronal en el capítulo 6. El efecto de la inclusión de plasticidad sináptica en las conexiones entre las neuronas también se aborda en este capítulo.

Finalmente, en el último capítulo se resumen las principales conclusiones y resultados que se pueden extraer de la tesis. Esperamos que estos resultados puedan servir para estimular nuevas investigaciones y que puedan sacar provecho de ellos. También se describen la lineas abiertas y las posibles lineas futuras de trabajo.

# Preface

Since many years scientists have been studying the nervous system and its constituent elements. One of the most notable advances in the description of the structural and functional units of the nervous system came from the Spanish physician Santiago Ramón y Cajal in the late 19th century with his neuron doctrine. Ramon y Cajal broke down the widely believed concept that the nervous system was a reticulum or a continuum meshwork. Using a histological staining technique, Cajal could resolve in detail the structure and concluded that the nervous system was composed of individual neurons rather than a continuum. For this discovery, Cajal was awarded with the 1906 Nobel Price in Medicine.

Nowadays, neuroscience is a broad field where many disciplines converge to tackle questions like how are the memories stored? what is the neural code? how can the brain be so fast?... from different points of view and using different approaches. With the advent of computers and later on the increase of computational power, computational neuroscience emerged as a fundamental area in the analysis and study of neuronal systems. A variety of mathematical models appeared describing the dynamics of neurons covering different levels of complexity. Many of them are based on a detailed description of the anatomy, chemical reactions or circuitry of neuronal systems. Other kind of models qualitatively describe the behavior of neurons and neural circuits based on experimental data. It is difficult to determine which is the appropriate level of details covered

by a model. A good model should contain enough details in order to describe the principal biophysical aspects but must remain simple enough to provide a clear interpretation of the results.

This thesis is mainly devoted to the modeling and simulations on neuronal systems with emphasis in different aspects. We start with an introduction to the necessary preliminary concepts needed for a better understanding of the succeeding chapters. The physiological basis of a neuron and its principal mechanism of operation are provided in Chapter 1. In this chapter we also introduce the principal neuronal models used during the thesis.

Chapter 2 investigates the role of noise acting on neurons. The phenomenon of stochastic resonance is characterized on an ensemble of neurons of the motor system. After the introduction of the appropriate model describing the neuron dynamics and the numerical integration details, stochastic resonance is quantify by means of the signal-to-noise ratio. Finally, in collaboration with the Integrative Neurophysiology Laboratory of the Institute of Physiology of the Benemérita Universidad Autónoma de Puebla, Mexico, we experimentally corroborate the numerical results demonstrating that stochastic resonance phenomenon is also presented in the motor system.

In chapter 3 we model the propagation of signals through the spinal cord during a motor activity. Based on previous studies, we propose a new neuronal circuit capable of producing the rhythms and the propagation along the spinal cord of a specific motor activity such as the scratching. We also reproduce the experimentally observed spontaneous failures or absences of activity (deletions) during the scratching and predict a new kind of deletion. Continuing the collaboration with the Integrative Neurophysiology Laboratory of the Institute of Physiology of the Benemérita Universidad Autónoma de Puebla, Mexico, we support our numerical results with experimental observations.

Afterwards we study the role played by the diversity on an ensemble of interacting neurons. In chapter 4 we demonstrate that the presence of heterogeneity in some parameters of the neurons can enhance the response of the system to an external periodic modulation. First, we

study a set of neurons described by the Fitzhugh-Nagumo model when the interaction between the neurons is mediated by both chemical and electrical synapses. A neuronal model taking into account more biological details such as the Morris-Lecar is also considered. In the last part of the chapter we develop a mean-field theoretical framework that qualitatively reproduces the numerical results.

The second part of the thesis is centered in the study of the effect of the topology and delay in the connections in neuronal networks. We explore in chapter 5 how the topological properties and conductions delays of several classes of neural networks affect the capacity of neurons to establish well-defined temporal relations among the firing of their action potentials. In particular, the concept of consistency is introduced and studied in a neuronal network in chapter 6. The effect of the inclusion of synaptic plasticity in the connections between the neurons is also considered in this chapter.

Finally, the last chapter gives an overview and summarize the principal conclusions that can be extracted from the results of this thesis. We hope that these results will trigger new research that can take profit of them. We also describe the open prospectives and possible future research lines.

Chapter 1

# Introduction

In this chapter we introduce the most relevant concepts needed for a better understanding of succeeding chapters. We start the first part with a basic physiological description of the main subject of study of this thesis, the neuron. The principal properties of neurons and their principles of operation, i.e., the generation and transmission of electrical impulses are provided afterwards. Section 1.2 is devoted to introduce different mathematical models describing the dynamics of neurons with special attention to the Hodgkin-Huxley model. The concept of excitability and a brief overview of the principal bifurcations associated to neuronal dinamics are presented in section 1.3. Later, in section 1.4, the modeling of synaptic transmission and the plasticity mechanism are presented. The fundamental phenomenon of synchronization is introduced in section 1.5. Finally, in the last section of the Introduction we provide the basic concepts related to noise and how it affects the neuron behavior.

## 1.1

## Neurons

Neurons are the basic processing units of the nervous system. They are excitable cells specialized in the processing and transmission of information. Their size and shape can vary considerably but a typical neuron can be divided into three parts: the cell body or soma, the dendrites and the

axon.

The soma is the metabolic center of the neuron. It contains the nucleus of the cell where most protein synthesis occurs. The dendrites spread out from the cell body like the branches of a tree increasing the surface area available to receive contacts form other neurons. The dendrites size range from a few tens of $\mu m$ to several $mm$ in length. The main function of the dendrites is to collect incoming information from other neurons or sensory receptors. The dendrites receives these incoming impulses directly on their surface membrane or on tiny projections of membrane called dendritic spines. A schematic representation of a typical neuron can be seen in Figure 1.1.
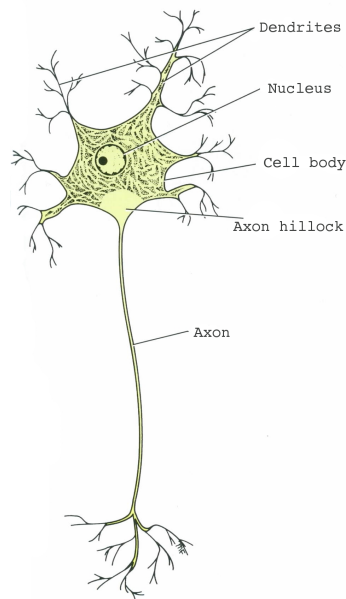


**Figure 1.1:** Scheme of a typical neuron.

Electrical impulses are conducted from the neuronal cell body to other neurons through the axon. The length of the axons covers a long range going from a few millimeters up to more than one meter. Most axons develop side branches along the route called axons collaterals in order to

bring information to several parts of the nervous system simultaneously. Large axons are surrounded by an insulating sheath called myelin, providing a fast and efficient conduction of action potentials. The myelin sheath is interrupted at very regular intervals called nodes of Ranvier. The function of these nodes is to optimize the conduction velocity. At the end of the axons lie an important specialized structures called synapses that are responsible of transmitting the nerve impulses form one neuron to another.

Neurons can be classified depending on their morphology or function. According to their structure, neurons can be unipolar, bipolar, multipolar (Figure 1.2). Unipolar neurons are those with a single axon. Many types of primary sensory neurons are unipolar. Typically these neurons have special structures for transducing some type of physical stimulus, such as light, sound, temperature, etc. into electrical activity. Bipolar neurons possess a single axon and a dendrite arising usually at opposite poles of the soma. They are part of the sensory pathways for smell, sight, taste, hearing and the vestibular system. Multipolar neurons represent the most common structure in the nervous system. They are characterized by one axon and two or more dendrites. Multipolar neurons have a diversity of shapes, some of them are so characteristic that are specially named. Examples of those neurons are: Purkinje cell, pyramidal cell, granule cell or motoneuron.

Neurons are functionally classified as sensory, motor, or interneuron. Sensory neurons conduct impulses from receptors to the brain and the spinal cord. Motorneurones conduct impulses from the brain and spinal cord to muscles and glands acting on the contraction of muscle fibers or the secretion of gland cells. Interneurones act as a link between sensory neurons and motor neurons. Interneurons are the responsible for the integration, facilitation, and inhibition.

### 1.1.1 Nernst Potential

Neurons, as many other cells are enclosed by a membrane which separates the interior of the cell from the extracellular medium. A cubic micron of cytoplasm might contain a huge number of particles like molecules of
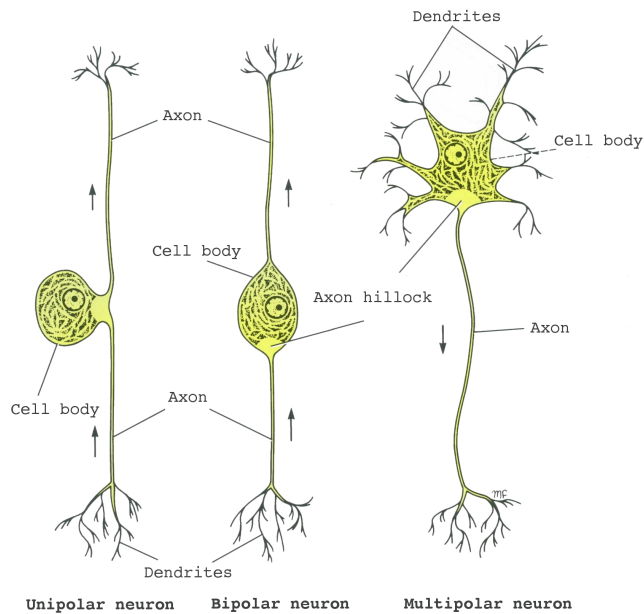
**Figure 1.2:** Morphological classification of neurons. Arrows indicate the direction of information propagation.

water, amino acids, nucleotides, ions and proteins, many of them carring electrical charges, either positive or negative. In a normal situation, there is an excess concentration of negative charge inside the neuron. This charge tends to distribute across the internal surface of the membrane. The membrane is able to maintain a separation between charges inside and outside the cell because acts as a partially permeable barrier to the diffusion of ions. Due to this insulating property, the membrane acts as a capacitor. The difference of concentration between intra and extracellular media generates an electrical potential usually called membrane potential.

From thermodynamics it is well known that the probability that a particle stays in a state with energy $E$ is proportional to the Boltzmann factor, $p(E) \propto e^{-E/kT}$, where $k$ is the Boltzmann constant and $T$ the temperature. The energy of a positive ion with charge $q$ at location $x$ is $E(x) = qu(x)$, where $u(x)$ is the potential at $x$. Therefore, the probability of finding an

ion in a region around $x$ is proportional to $e^{-qu(x)/kT}$. We can interpret this probability as an ion density due to the huge number of ions surrounding the membrane. Then, the relation between the density at $x_1$ and $x_2$ is

$$\frac{n(x_1)}{n(x_2)} = e^{-q\Delta u/kT} \tag{1.1}$$

where $\Delta u = u(x_1) - u(x_2)$ is the difference of electrical potential between $x_1$ and $x_2$ and $n(x_i)$ the ion density at $x_i$. Then, we can find an expression for the difference of electrical potential $\Delta u$ that is generated by a difference of ion density,

$$\Delta u = \frac{kT}{q} \ln\left(\frac{n_1}{n_2}\right). \tag{1.2}$$

Expression 1.2 is known as the Nernst potential.

### 1.1.2 Membrane Resting Potential

There are basically four relevant species of ions involved in the generation of the membrane potential of a neuron: $K^+$, $Na^+$, $Cl^-$ and organic anions ($A^-$). These ions are not equally distributed across the membrane, for example, $Na^+$ and $Cl^-$ are more concentrated outside the neuron, and $K^+$ and $A^-$ are more concentrated inside the neuron. The typical concentration of these ions is shown in Table 1.1. The membrane is partially permeable to many of these ions, $K^+$, $Na^+$ and $Cl^-$, and only large organic anions cannot cross the neuron membrane. Ions can diffuse across the membrane only at specialized intramembranous proteins pores called ionic channels. These channels are selective for the types of ions that they allow to pass. Of the three permeant ions, only $Cl^-$ is free to diffuse in or out of the neuron. Thus, the concentration ratio of $Cl^-$ reaches a value such its Nernst potential $E_{Cl}$ is equal to the membrane resting potential $V_R$.

Due to the different concentration of $K^+$ inside and outside the neuron, a chemical concentration gradient tends to push $K^+$ out of the neuron. The

**Table 1.1:** Typical concentrations of the principal ions in the intra-cellular and extracellular media at a temperature of $T = 25\,°C$.

| Ion | Cytoplasm (mM) | Extracellular media (mM) | Nernst Potential (mV) |
|---|---|---|---|
| $K^+$ | 400 | 20 | -77 |
| $Na^+$ | 50 | 440 | +56 |
| $Cl^-$ | 52 | 560 | -61 |
| $A^-$ | 385 | — | — |

electrical potential difference originated by the separation of the charges tends to push $K^+$ back into the neuron. As the diffusion of $K^+$ continues, the membrane potential continues increasing until it reaches a value in which $K^+$ is at equilibrium. If $K^+$ was the only permeable cation, the membrane resting potential $V_R$ would coincide with the $K^+$ Nernst potential $E_K = -77\,mV^*$. However, the membrane is also permeable to $Na^+$ and, because the concentration of $Na^+$ is higher outside than inside, tends to flow into the neuron. The Nernst potential for $Na^+$ is $E_{Na} = +56\,mV$. Then, at a resting membrane potential of $V_R = -77\,mV$, $Na^+$ is far away from its equilibrium, and a strong electrochemical force drives $Na^+$ through the membrane into the neuron. The influx of $Na^+$ depolarizes the membrane driving $V_m$ toward $E_{Na}$. However, since the membrane is only slightly permeable to $Na^+$, the membrane resting potential moves only slightly away from $E_K$. The reason for this is that when $V_m$ departs from $E_K$, an efflux of $K^+$ appears and tends to compensate the $Na^+$ influx. Finally, $V_m$ reaches a value at which the outward movement of $K^+$ balances the inward movement of $Na^+$.

Although these ion fluxes cancel each other, they cannot continue compensating to each other for a long time otherwise $[K^+]_i$ would be depleted, $[Na^+]_i$ would increase, and the ionic gradients would decrease gradually,

---

$^*$At $T = 25\,°C$, $kT = 25.8\,mV$. Then, $E_k = 25.8\ln\left(\frac{20}{400}\right) \approx -77\,mV$.

reducing the resting membrane potential. In order to prevent this re-
duction of the membrane potential, the membrane has another kind of
component: an enzyme called *Na-K adenosine triphosphatase*, which acts
as a pump, moving $Na^+$ out of the cell and $K^+$ in. This pump requires
energy, and this enzyme use the energy produced in the hydrolysis of
the adenosine triphosphate (ATP) to exchange ions across the membrane.
Figure 1.3 shows a schematic representation of the sodium, potassium
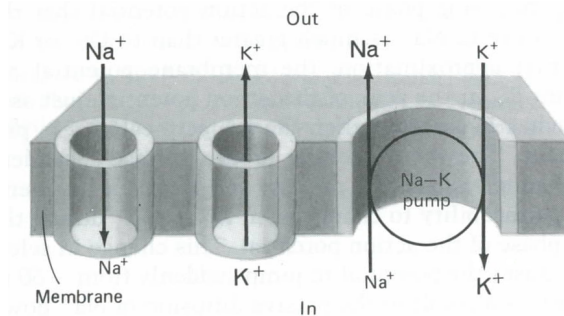and active-pump channels in the membrane.



**Figure 1.3:** Schematic representation of the different membrane
ionic channels.

When the neuron is at rest, the active fluxes driven by the pump and the
passive fluxes due to diffusion are balanced. The neuron is not in equi-
librium, but rather in a steady state where a certain quantity of energy is
consumed to maintain the ionic gradients across the membrane.

When the membrane potential is determined by two or more ions, each
ion has an influence on $V_m$ that is determined by its concentration ratio
and by the permeability of the membrane to that ion. In this case, the
membrane potential is given by the Goldman-Hodgkin-Katz equation:

$$V_m = \frac{RT}{F} \ln \left( \frac{P_K[K^+]_o + P_{Na}[Na^+]_o + P_{Cl}[Cl^-]_i}{P_K[K^+]_i + P_{Na}[Na^+]_i + P_{Cl}[Cl^-]_o} \right) \tag{1.3}$$

where $R$ and $F$ are the gas and the Faraday constants respectively and

$P_{Na}$, $P_K$ and $P_{Cl}$ the permeabilities of sodium, potassium and chlorine respectively.

### 1.1.3 **Action Potential**

At a resting state, the passive $Na^+$ and $K^+$ fluxes are balanced by the active fluxes driven by the Na-K pumps that keep constant the membrane potential. This steady-state balance changes however when the cell is depolarized. In addition to the passive ionic channels, the membrane also contains some channels that are voltage-sensitive and are opened when the membrane is depolarized. When a transient depolarization occurs, such an excitatory synaptic potential, some voltage-gated $Na^+$ channels are opened allowing an influx of $Na^+$. Then, a net influx of positives charges flows through the membrane generating an accumulation of positives charges inside the neuron causing a further depolarization. The increase in depolarization opens more voltage-gated $Na^+$ channels with the associated increase of the influx of positive charges, which accelerates the depolarization still further. This feedback cycle develops explosively, allowing $Na^+$ channels dominate over $K^+$ channels and driving the membrane potential closed to the $Na^+$ equilibrium potential $E_{Na}$ at the peak of the action potential ($V_m \approx +50\ mV$). At this voltage values, the voltage-dependent $K^+$ channels open causing an efflux of $K^+$. After the opening of the voltage-gated $K^+$ channels there is an inactivation of the $Na^+$ channels. The increase in $K^+$ efflux together with the decrease in $Na^+$ influx result in a net efflux of positive charges from inside the neuron, which continues until the cell reaches its membrane resting potential $V_R$. This process is illustrated in Figure 1.4.

### 1.1.4 **Nerve Impulse Propagation**

An action potential can propagate along the axonal membrane. In unmyelinated axons, the mechanism of propagation is based on the depolarization of the adjacent membrane area close to the generated action
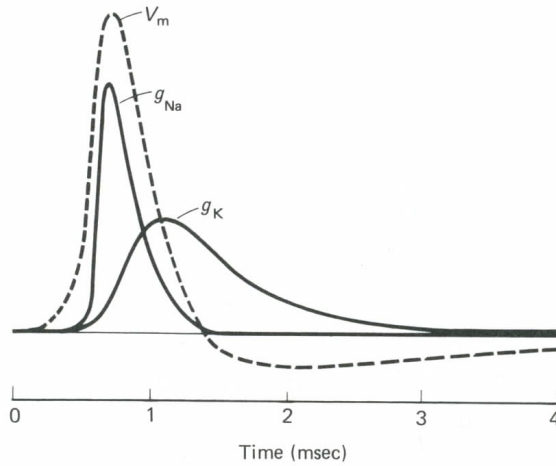
**Figure 1.4:** Voltage membrane during an action potential and evolution of $g_{Na}$ and $g_K$.

potential. During the generation of an action potential, positive charges flow into the axon and a positive charge spreads inside the axon neutralizing the negative charges on the adjacent membrane area. This neutralization of charges leads to a depolarization of the surrounding area, and the depolarization to the generation of an action potential in this adjacent area. This new generated action potential depolarizes the next adjacent area of the axonal membrane leading to the generation of another action potential in the next adjacent area. Figure 1.5 schematizes the impulse propagation across the axonal membrane.
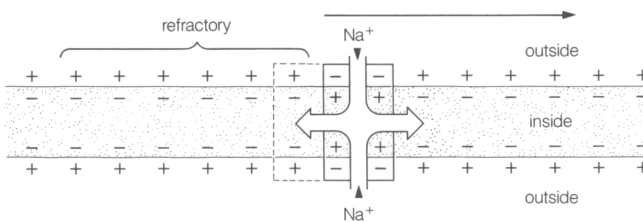


**Figure 1.5:** Propagation of the action potential.

**CHAPTER 1. INTRODUCTION**

Theoretically, actions potentials can propagate across both directions of axons (as observed in *in vitro* experiments), but there are two main reasons why only one propagation direction is preferential. Normally the action potential travels from the neuron body to the synapse across the axon. One of the main cause for that is the fact that the propagation of the action potential is generated at the beginning of the axons in a place called axon hillock. Another reason that prevents the propagation in both directions is the refractory time of the area preceding the action potential. The membrane usually needs ~ 1 *ms* to recovers from the previous depolarization, for this reason, new action potentials are generated in front of the previous ones.

In myelinated axons the propagation of action potentials is different. In this kind of axons, the action potentials are generated only in the nodes of Ranvier and the propagation is based on jumps from one node to the next. This propagation is known as a saltatory conduction. Between nodes, in the segment of the axon surrounded by myelin, the action potential propagates passively. This mechanism not only provides a faster conduction of the action potentials compared with unmyelinated axons, but also requires less metabolic demand on neurons. Saltarory conduction is sketched in Figure 1.6.
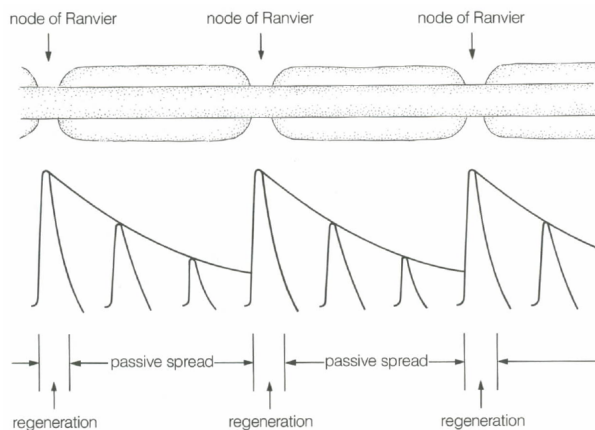


**Figure 1.6:** Schematic representation of saltatory conduction.

### 1.1.5 **Synapses**

The main role of neurons is to communicate with other neurons. This communication takes place at a site called synaptic junction or synapse. There are two different types of transmition, chemical and electrical, defining two different types of synapses. Chemical synapses are the most abundant in the nervous system and the information flows unidirectionally from the pre- to the postsynaptic neuron. This type of synapses does not involve a physical contact between the cells and the stimulus must cross a narrow gap called the synaptic cleft which separates pre- and postsynaptic neurons. When a presynaptic electrical potential arrives to the synapse, a chemical carrier, called neurotransmitter, is released from the presynaptic terminals. The neurotransmitters diffuse across the synaptic cleft and interact with the receptor molecules of the postsynaptic membrane opening some ionic channels. This allows a flux of ions through the postsynaptic membrane changing the electrochemical state of the membrane. The resulting change in voltage is called postsynaptic potential. The electrical excitability of the membrane can be increased or decreased depending on the nature of the neurotransmitter and the postsynaptic receptor, and then, the synapse can be excitatory or inhibitory. Figure 1.7 (a) sketches the typical structure of a chemical synapse.

Another type of synaptic junction is the electrical synapse. In this synapse, the membrane of pre- and postsynaptic neurons are contiguous, and therefore, the stimulus is able to pass directly from one neuron to the other without chemical mediation. This synapse provides bidirectional communication between neurons and is much faster than the chemical junctions. Figure 1.7 (b) shematizes the typical structure of an electrical synapse.

### 1.1.6 **Neurotransmiters**

There is a large variety of different molecules used in a chemical synaptic transmission. However, most chemical transmission is conducted by two amino acids: glutamate for excitation and GABA for inhibition. Their
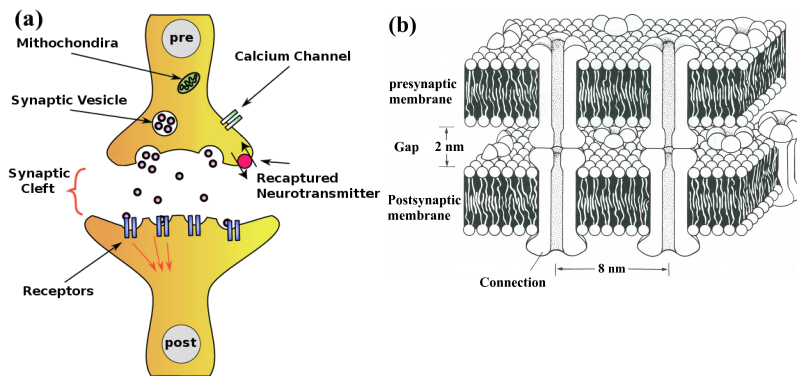
**Figure 1.7:** Schematic representation of the different types of synapses. (a) Sketch of a chemical synapse. (b) Illustration of an electrical synapse.

effects are local, fast (in a fraction of second) and they act directly on the receptors to open ionic channels. These two neurotransmiters are known as a classical or fast transmitters.

Other sort of neurochemicals like dopamine, serotonin, noradrenalin, neuropeptides or nitric oxide do not act directly on the receptors, having modulatory effects instead. These are called neuromodulators and their effects persist for a long time, from minutes to hours or even days. The neuromodulators influence the strength and the duration of the synaptic transmission mediated by classical neurotransmitters.

Fast and slow synaptic transmission are obtained from different mechanisms. Fast synaptic transmission involves receptors that are directly located on the ionic channel, so that the classical transmitters directly open the ionic channel. Slow transmission involves metabotropic receptors and second messengers that freely diffuse to reach the ionic channel. This process is much slower and can last from many second to minutes producing slow long lasting synaptic responses.

1.2

# Neuron Models

This section is devoted to introduce different neuronal models that will be used during this thesis. A brief historical overview is provided first, followed by an introduction to different neuronal models presented in an order of decreasing complexity.

### 1.2.1 Historical overview

One of the first models of neuronal excitability was introduced by the French physiologist Louise Lapicque in 1907 when he was studying the nerve excitability by stimulating the sciatic nerve of the frog [1]. At that time it was already known that the membrane acts as a capacitor and, in order to study the nerve membrane excitation by electrical stimulation, Lapicque used the concept of equivalent circuit of the axon membrane. Figure 1.8 shows the original equivalent circuit used by Lapicque to compare what his physiological experiment revealed about the laws of electrical excitation.
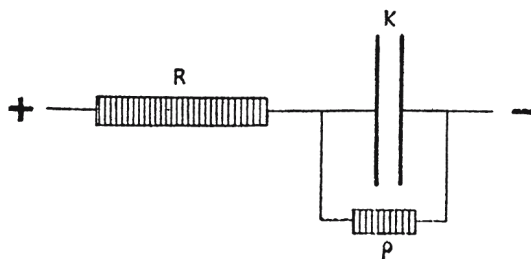


**Figure 1.8:** The equivalent circuit used by Louis Lapicque to study the nerve excitation. Extracted from [1].

The discovery of the squid giant axon by Young in 1936 [2] and the development of the voltage clamp technique by Kenneth Cole in the 1940s [3] were two important steps in the development of the electrophysiology.

But it was the work of Alan L. Hodgkin and Andrew Huxley in 1952 on the nerve conduction that the properties of ionic conductances underlying the nerve action potential were unveiled. Hodgking and Huxley proposed a mathematical model for the excitability and conduction in nerves [4]. Since then, several models have been developed. Among these models there are two of special relevance to this thesis: the one introduced in 1961 by Richard FitzHugh [5] and the one introduced by Cathy Morris and Harold Lecar in 1981 [6].

## 1.2.2 The Hodgkin-Huxley model

In a series of experiments done in 1952 [7–10], Hodgkin and Huxley determined that the current through the membrane of the squid giant axon has a component corresponding to the ions crossing the membrane and another contribution arising from the membrane capacitance. Thus, for a small patch of membrane the total current is

$$I = C_m \frac{dV}{dt} + I_{ion} \tag{1.4}$$

where $C_m$ is the membrane capacitance, $V$ is the membrane potential and $I_{ion}$ is the net ionic current flowing across the membrane. At that time it was already known that the ionic current for the squid giant axon has basically two mayor components corresponding to sodium $I_{Na}$ and potassium $I_K$ currents [11]. One of the major achievement of Hodgkin and Huxley was to measure the contribution of these two ionic currents. They also found a remaining small leakage current $I_L$ corresponding to chloride and other ions. In order to separate the ionic current into its components, Hodgkin and Huxley used a choline solution to reduce the sodium concentration $[Na^+]$ in the external fluid surrounding the axon. The inward current carried by $Na^+$ was cancelled leaving only the potassium ionic current component $I_K$. Subtracting the low-Na record from the ionic current measured in the usual concentration of ions, the contribution of the sodium ionic current was obtained (see Figure 1.9).
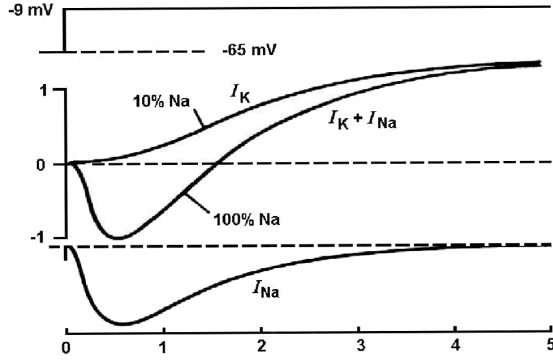
**Figure 1.9:** Quantitative measurements of ionic currents in the squid giant axon using voltage clamp technique. Extracted from [12].

The total ionic current was expressed thus as

$$I_{ion} = I_K + I_{Na} + I_L \tag{1.5}$$

where $I_K$ and $I_{Na}$ are the potassium and sodium currents and $I_L$ is the leakage current due to other ions. Having separated the current into components, the next step was to determine the relationship between the ionic current and the membrane potential. Hodgkin and Huxley measured what they called instantaneous current-voltage relation finding a linear current-voltage relation for the open channels, as in Ohm's law [9]. Thus, the ionic conductances were defined by

$$g_{Na} = \frac{I_{Na}}{V - V_{Na}} \tag{1.6}$$

$$g_K = \frac{I_K}{V - V_K} \tag{1.7}$$

$$g_L = \frac{I_L}{V - V_L} \tag{1.8}$$

Therefore, Eq. (1.4) becomes

$$C_m \frac{dV}{dt} = I - g_{Na}(V - V_{Na}) - g_K(V - V_K) - g_L(V - V_L) \tag{1.9}$$

15

They redefined the equivalent circuit representation of the axon membrane to include the three ionic currents they found in their experiments. Figure 1.10 shows the equivalent circuit of the axon membrane proposed by Hodgkin and Huxley. The capacitor represents the dielectric properties of the membrane. The three variable resistors represent the sodium, potassium and leakage conductances with their different electromotive forces.
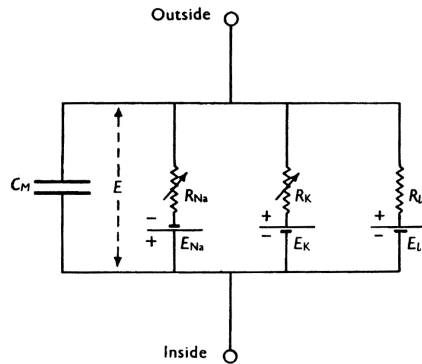


**Figure 1.10:** Equivalent circuit of axon membrane proposed by Hodgkin and Huxley. From [4].

The fact that Hodgkin and Huxley succeeded separating the components of the ionic current, allowed also to determine changes in the conductances $g_{Na}$ and $g_K$ by applying Eq. (1.6) and (1.7) to the separated currents. They found that, like the ionic currents, $g_{Na}$ and $g_K$ are voltage and time dependent. The sodium conductance of the axon membrane rises rapidly and then decays during a depolarization, or in other words, $g_{Na}$ activates and inactivates. Activation is the rapid process that opens sodium channels during a depolarization. On the contrary, inactivation is a slower process that closes sodium channels during a depolarization. The potassium conductance increases following a S-shape function during a depolarization event whereas during repolarization the decrease is exponential. Figure 1.11 illustrates the changes of $g_{Na}$ and $g_K$ in the squid axon during a depolarization (solid lines) and repolarization (dashed lines).
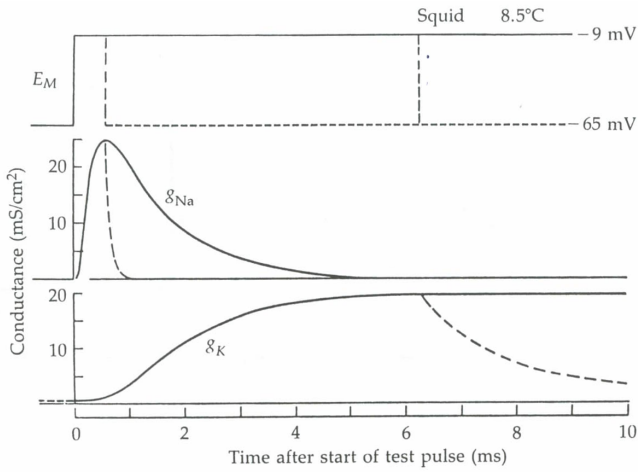
16

**Figure 1.11:** Ionic conductances changes during depolarization and repolarization.

Hodgkin and Huxley assumed that there were four independent identical particles, each with probability $n$ of being in the correct position to set up an open potassium channel. Thus, the probability that all four independent particles are correctly placed is $n^4$. Because the potassium channel is voltage-dependent, the hypothetical particles were assumed to be electrically charged. The voltage and time changes of $n$ follow a first-order kinetics reaction

$$1 - n \underset{\beta_n}{\overset{\alpha_n}{\rightleftharpoons}} n$$
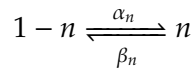
where $\alpha_n$ and $\beta_n$ are the voltage-dependent transition rates between permissive and nonpermissive positions. The rate at which the open probability for a subunit gate $n$ changes obeys the following equation

$$\frac{dn}{dt} = \alpha_n(V)(1 - n) - \beta_n(V)n \qquad (1.10)$$

17

Equation (1.10) can be rewritten by dividing by $\alpha_n (V) + \beta_n (V)$

$$\tau_n (V) \frac{dn}{dt} = n_\infty (V) - n \tag{1.11}$$

where $\tau_n (V)$ is the voltage-dependent time constant and $n_\infty (V)$ is the steady-state value defined by (see Figure 1.12)

$$\tau_n (V) \quad = \quad \frac{1}{\alpha_n + \beta_n} \tag{1.12}$$

$$n_\infty (V) \quad = \quad \frac{\alpha_n}{\alpha_n + \beta_n} \tag{1.13}$$

These quantities were experimentally fitted resulting in the following expressions:

$$\alpha_n (V) \quad = \quad \frac{0.01 (V + 55)}{1 - e^{-((V+55)/10)}} \tag{1.14}$$

$$\beta_n (V) \quad = \quad 0.125 e^{-((V+40)/80)} \tag{1.15}$$

Similarly, the sodium conductance can be described using the same formalism. However, because there are two opposite gating processes, activation and inactivation, there are two kind of gating particles. Three independent identical $m$ particles are involved in the activation and one $h$ particle is involved in the inactivation. Therefore, the probability that all the particles are all in an open position is $m^3h$. As for the $n$ parameter of the potassium conductance, $m$ and $h$ are assumed to undergo first-order transitions between permissive and nonpermissive positions:

$$1 - m \underset{\beta_m}{\overset{\alpha_m}{\rightleftharpoons}} m$$

$$1 - h \underset{\beta_h}{\overset{\alpha_h}{\rightleftharpoons}} h$$
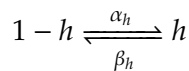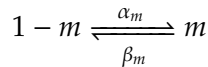
with rates satisfying the differential equations

$$\tau_m(V)\frac{dm}{dt} = m_\infty(V) - m \tag{1.16}$$

$$\tau_h(V)\frac{dh}{dt} = h_\infty(V) - h \tag{1.17}$$

where

$$\tau_m(V) = \frac{1}{\alpha_m + \beta_m} \tag{1.18}$$

$$\tau_h(V) = \frac{1}{\alpha_h + \beta_h} \tag{1.19}$$

$$m_\infty(V) = \frac{\alpha_m}{\alpha_m + \beta_m} \tag{1.20}$$

$$h_\infty(V) = \frac{\alpha_h}{\alpha_h + \beta_h} \tag{1.21}$$

and the experimentally fitted voltage-dependent transition rates

$$\alpha_m(V) = \frac{0.1(V+40)}{1 - e^{-((V+40)/10)}} \tag{1.22}$$

$$\alpha_h(V) = 0.07e^{-((V+65)/20)} \tag{1.23}$$

$$\beta_m(V) = 4e^{-((V+65)/18)} \tag{1.24}$$

$$\beta_h(V) = \frac{1}{1 + e^{-((V+35)/10)}} \tag{1.25}$$

To summarize, the Hodgkin and Huxley model for the squid giant axon describes the ionic current across the membrane in terms of three components

$$I_{ion} = \bar{g}_{Na}m^3h(V - V_{Na}) - \bar{g}_K n^4(V - V_K) - \bar{g}_L(V - V_L) \tag{1.26}$$

where $\bar{g}_{Na}$ and $\bar{g}_K$ are the maximal conductances for the sodium and

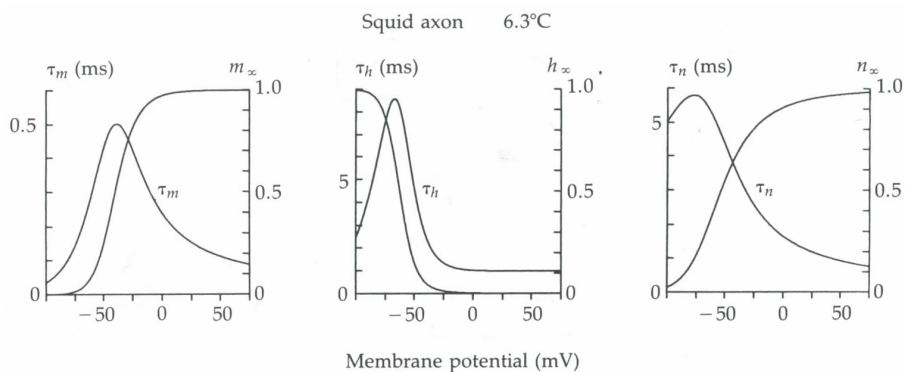**Figure 1.12:** Voltage-dependent time constants $\tau_m$, $\tau_h$ and $\tau_n$ and steady-state values $m_\infty$, $h_\infty$ and $n_\infty$.

potassium channels and $\overline{g}_L$ is a fixed background leakage conductance. The voltage-gated ion channels are described by the following set of differential equations

$$
\begin{aligned}
\dot{m} &= \alpha_m(v)(1-m) - \beta_m(v)m & (1.27) \\
\dot{h} &= \alpha_h(v)(1-h) - \beta_h(v)h & (1.28) \\
\dot{n} &= \alpha_n(v)(1-n) - \beta_n(v)h & (1.29)
\end{aligned}
$$

where the gating variables $m(t)$, $h(t)$, and $n(t)$ represent the activation and inactivation of the sodium channels and the activation of the potassium channels, respectively. The experimentally fitted voltage-dependent tran-

sition rates are

$$\alpha_m(V) = \frac{0.1(V + 40)}{1 - \exp\left(-(V + 40)/10\right)} \tag{1.30}$$

$$\beta_m(V) = 4\exp\left(-(V + 65)/18\right) \tag{1.31}$$

$$\alpha_h(V) = 0.07\exp\left(-(V + 65)/20\right) \tag{1.32}$$

$$\beta_h(V) = [1 + \exp\left(-(V + 35)/10\right)]^{-1} \tag{1.33}$$

$$\alpha_n(V) = \frac{(V + 55)/10}{1 - \exp\left(-0.1(V + 55)\right)} \tag{1.34}$$

$$\beta_n(V) = 0.125\exp\left(-(V + 65)/80\right) \tag{1.35}$$

### 1.2.3 Reduction of the Hodgkin-Huxley model

The Hodking-Huxley model involves four dynamical variables to describe the evolution of the membrane potential. The time scale associated with $m$ and $\tau_m$ is much smaller than those associated with $h$ and $n$. Thus, $m$ will reach its asymptotic value $\overline{m}(V)$ much faster than other changes in the model. If we are not interested in the response of the system at very short time scales we can assume $\dot{m} = 0$ and replace $m$ by its asymptotic value $\overline{m}(V)$.

On the contrary, it is not suitable to replace $h$ and $n$ by their asymptotic values with respect to $V$ because the model will lose the ability to generate actions potential. However, since $\tau_n$ and $\tau_h$ are approximately similar for any value of the membrane voltage and $n$ and $1 - h$ are rather similar, we can approximate the two variables $n$ and $1-h$ by a single effective variable $w$. Using the linear transformation $b - h \approx an$, with $a$ and $b$ constants, we can set $w = b-h = an$ or equivalently $h = b-w$ and $n = w/a$. Because $h$ and $n$ have longer time constant, these variables would reach their asymptotic values more slowly. Thus, we can approximate for the new variable $W$

$$n \approx \overline{n}(W) \tag{1.36}$$

$$h \approx \overline{h}(W) \tag{1.37}$$

The ionic current $I_{ion}$ can then be rewritten as

$$I_{ion}(V, m, n, h) \approx I_{ion}\left(V, \overline{m}(V), \overline{n}(W), \overline{h}(W)\right) \equiv f(V, W) \tag{1.38}$$

To find a equation for the new variable $W$, we can impose that the time dependence of $W$ in $f$ must be the same time-dependence induced into $I_{ion}(V, m, n, h)$ in the full model by the changing values of $n$ and $h$. Thus, the derivative of $I_{ion}$ and $f$ at a constant $V$ should be equal

$$\frac{\partial I_{ion}}{\partial n}\frac{dn(V)}{dt} + \frac{\partial I_{ion}}{\partial h}\frac{dh(V)}{dt} = \left(\frac{\partial f}{\partial \overline{n}}\frac{d\overline{n}(W)}{dW} + \frac{\partial f}{\partial \overline{h}}\frac{d\overline{h}(W)}{dW}\right)\frac{dW}{dt} \tag{1.39}$$

Using the original formulas for $dn/dt$ (Eq. 1.11) and $dh/dt$ (Eq. 1.17) together with the approximation $h \approx \overline{h}(W)$ and $n \approx \overline{n}(W)$ so that

$$\tau_n(V)\frac{dn}{dt} \approx \overline{n}(V) - \overline{n}(W) \tag{1.40}$$

$$\tau_h(V)\frac{dh}{dt} \approx \overline{h}(V) - \overline{h}(W) \tag{1.41}$$

Then, Eq. (1.39) becomes

$$\frac{dU}{dt} = g(V, W) \equiv \frac{A}{B} \tag{1.42}$$

with

$$A = \left(\frac{\partial I_{ion}}{\partial n}\right)\Bigg|_{n=\overline{n}(W)}\left(\frac{\overline{n}(V) - \overline{n}(W)}{\tau_n(V)}\right)$$

$$+ \left(\frac{\partial I_{ion}}{\partial h}\right)\Bigg|_{h=\overline{h}(W)}\left(\frac{\overline{h}(V) - \overline{h}(W)}{\tau_h(V)}\right) \tag{1.43}$$

$$B = \left(\frac{\partial f}{\partial \overline{n}}\frac{d\overline{n}(W)}{dW} + \frac{\partial f}{\partial \overline{h}}\frac{d\overline{h}(W)}{dW}\right) \tag{1.44}$$

After appling this reduction, the Hodgkin-Huxley model becomes

$$C_m \frac{dV}{dt} = f(V, W) + I,$$
(1.45)

$$\frac{dW}{dt} = g(V, W).$$
(1.46)

Different functions $f(V, W)$ and $g(V, W)$ yield to different reduced models. In the next section, a particular case of the family of models generated after this reduction is introduced.

### 1.2.4 **The FitzHugh-Nagumo model**

The idea of Richard FitzHugh was to use a modified version of the Van der Pol nonlinear relaxation oscillator to reproduce qualitatively the behavior of the Hodgkin-Huxley model [5]:

$$\ddot{x} + c(x^2 - 1)\dot{x} + x = 0.$$
(1.47)

Applying the Liénard transformation to the previous equation (for further details see [13])

$$y = \dot{x}/c + x^3/3 - x$$
(1.48)

the following pair of equations were obtained

$$\dot{x} = c(y + x - x^3/3)$$
(1.49)

$$\dot{y} = -xc$$
(1.50)

The FitzHug model is obtained by adding some terms to the equations (1.49-1.50)

$$\dot{x} = c(y + x - x^3/3 + z)$$
(1.51)

$$\dot{y} = -(x - a + by)/c$$
(1.52)

23

where $1 - 2b/3 < a < 1$, $0 < b < 1$ and $b < c^2$. $z$ is the stimulus intensity, corresponding to the membrane current in the Hodgkin-Huxley equations.

### 1.2.5 The Morris-Lecar model

The Morris-Lecar model was proposed after a study of the excitability of the giant muscle fiber of the barnacle [6]. According to voltage-clamp experiments they found two independent voltage-dependent conductances, $g_K$ and $g_{Ca}$, each one having a sigmoid voltage dependence. The equations describing the membrane potential and the slow recovery variable are

$$C_m \frac{dV}{dt} = I - g_{Ca} M_\infty (V - V_{Ca}) - g_K W (V - V_K) - g_L (V - V_L) \quad (1.53)$$

$$\frac{dW}{dt} = \phi \Lambda(V) [W_\infty - W] \quad (1.54)$$

where $C_m$ is the membrane capacitance. $V$ represents the membrane potential. $W$ represents the fractions of open channels. The quantities $M_\infty$, $W_\infty$ and $\Lambda(V)$ are given by

$$M_\infty(V) = \frac{1}{2}\left[1 + \tanh\left(\frac{V - V_1}{V_2}\right)\right] \quad (1.55)$$

$$W_\infty(V) = \frac{1}{2}\left[1 + \tanh\left(\frac{V - V_3}{V_4}\right)\right] \quad (1.56)$$

$$\Lambda(V) = \tanh\left(\frac{V - V_3}{2V_4}\right) \quad (1.57)$$

The Morris-Lecar model is a simplification of the Hodking-Huxley model reducing the number of dynamical variables. It displays an action potential when the value of the applied current $I$ leads a saddle-node bifurcation to a limit cycle. The inclusion of a slow calcium-dependent potassium channel allows the system to exhibit bursting behavior.

### 1.2.6 **The Integrate-and-Fire model**

It was Richard Stein who introduce in 1965 a leaky integrate-and-fire model [14]. This model describes the subthreshold membrane potential simplifying the biophysical properties of the membrane to an equivalent circuit consisting of a capacitor and a resistor in parallel (Figure 1.8). The membrane potential $v$ is determined by

$$\tau_m \frac{dv}{dt} = -(v - E_L) + R_m I(t) \qquad (1.58)$$

where $\tau_m = R_m C_m$ is the membrane time constant, $R_m$ the membrane resistance and $E_L$ the resting potential of the neuron. This model does not describe explicitly the form of an action potential. A spike is defined by a threshold criterion; when the membrane potential reaches a given value, it is reset to the value $V_{reset}$.

The main advantage of this model is that allows some theoretical analysis and is computationally much less demanding. For example, the firing rate in response to a constant current can be computed analytically. Equation (1.58) can be solved when $I$ is independent of time. The subthreshold membrane potential is given by

$$V(t) = E_L + R_m I + (V(0) - E_L - R_m I) e^{-t/\tau_m} \qquad (1.59)$$

where $V(0)$ is the value of $V$ at time $t = 0$. One can chose arbitrarily this value. For example, if we suppose that at $t = 0$ the neuron has just fired a spike, thus the membrane potential is at the reset potential, $V(0) = V_{reset}$. The next spike will occur when the membrane potential reaches the threshold at time $t = t_{isi}$

$$V(t_{isi}) = V_{th} = E_L + R_m I + (V_{reset} - E_L - R_m I) e^{-t_{isi}/\tau_m} \qquad (1.60)$$

Solving Eq. (1.60) for the time of the next spike $t_{isi}$, allows to determine the interspike-interval firing rate of the neuron,

$$\nu = \frac{1}{t_{isi}} = \left( \tau_m \ln \left( \frac{R_m I + E_L - V_{reset}}{R_m I + E_L - V_{th}} \right) \right)^{-1} \qquad (1.61)$$

## 1.3

# Excitability in Neurons

Excitability is a phenomenon observed in a large variety of natural systems among which are lasers, biological tissues, chemical reactions or neurons. An excitable system is characterized by three aspects: i) a resting state, ii) a threshold behavior and iii) a refractory time needed to recover from the excited state to the resting one. Figure 1.13 sketches the response of an excitable system to different inputs.

Neurons are excitable systems. They are usually at rest but can spike as a response to certain stimuli exhibiting excitable behavior.
The actual classification of neuronal excitability was proposed by Alan Hodgkin in 1948 [17]. He was studying the response of the isolated axon of the *Carcinus maenas* when applied repetitive discharges.  He found that when the applied current was weak the axon was quiet and when the discharge was strong enough the axon fired repeatedly.  Hodgkin classified the axons according to the frequency of emerging firing,

- Class I neural excitability. When the applied current is larger than a threshold value, the neuron fires at a frequency that increase with the applied current.

- Class II neural excitability. For an applied current above a threshold value, the neuron fires with a frequency that is relatively insensitive to changes in the strength of the applied current.

Another feature that distinguishes the two classes of neural excitability is the fact that in class I systems the action potential can be generated with arbitrarily low frequency whereas in class II the spikes start with nonzero frequency and this frequency is restricted to a certain frequency band (see Figure 1.14).
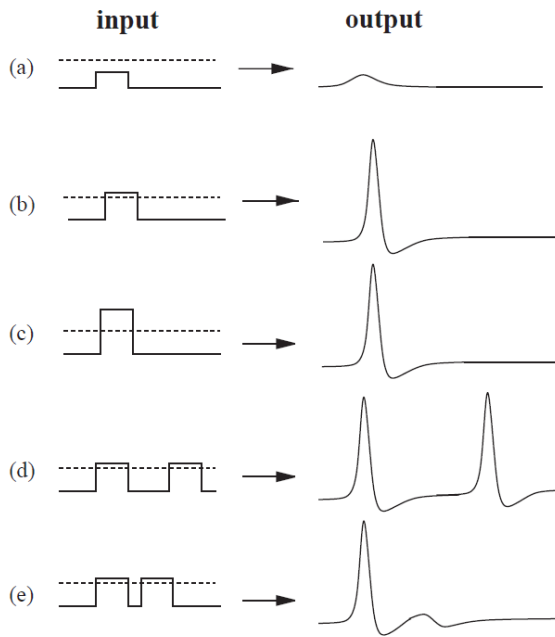
**Figure 1.13:** Response of an excitable system to different stimuli. a) A small subthreshold perturbation generates a small response. b) When the amplitude of the input exceeds the threshold it induces a large amplitude response. c) Larger input amplitudes do not change significantly the response amplitude. d) Two consecutive suprathreshold inputs generate excitations only if both are applied to the system in the resting state. e) When the separation between two consecutive inputs is smaller than the refractory time, the system does not respond to the second input. Adapted from [15].
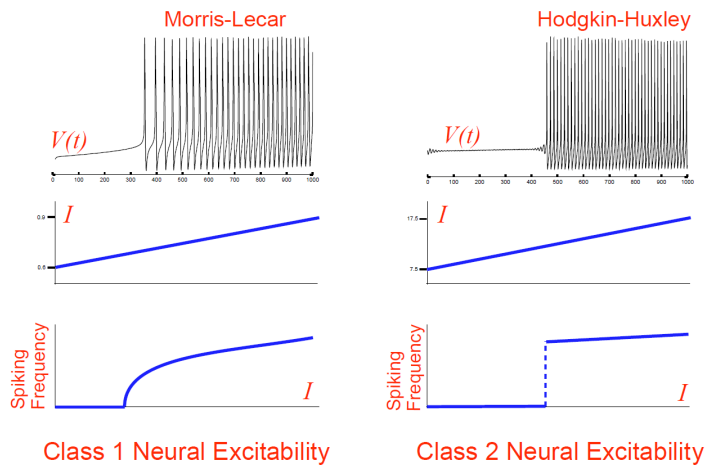
**Figure 1.14:** Neuronal excitability classification. Extracted from [16].

### 1.3.1 **Bifurcation analysis**

In general, neurons are excitable because they operate near a bifurcation from a resting to a firing state. Interestingly, the majority of neuron models undergo only four different types of bifurcations. In the following subsections these four types of bifurcation are described without any kind of mathematical rigor.

**Saddle-node bifurcation**

In this bifurcation, as the bifurcation parameter changes, a stable node and an unstable saddle collide and annihilate each other. Then, since the resting state given by the stable node no longer exists, the trajectory jumps to the coexisting limit cycle (see Fig. 1.15).
Within a more mathematical description, a k-dimensional dynamical system $\dot{x} = f(x, b)$, $x \in \mathbb{R}^k$ having an equilibrium point $f(x_0, b_0) = 0$ exhibits a saddle-node bifurcation if the equilibrium (fix point) is non-hyperbolic with a simple zero eigenvalue, the function $f$ is non-degenerate, and it is transversal with respect to $b$. The non-hyperbolicity implies that the Ja-
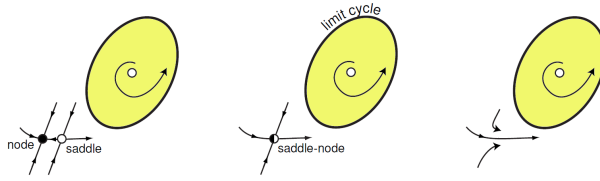
**Figure 1.15:** Phase portraits before (left), at (center) and after (right) saddle-node bifurcation. Adapted from [18].

cobian matrix has exactly one zero eigenvalue and the other eigenvalues have nonzero real parts. The remaining two conditions have complicated forms, however, for conductance-based model, assuming that the resting state is giving by $I(V, b)$, non-degeneracy implies that the second derivative of $I(V, b_0)$ with respect to $V$ is nonzero, $a = \frac{1}{2} \frac{\partial^2 I(V, b_0)}{\partial V^2} \neq 0$ at $V = V_0$. To satisfy transversality, $I(V, b)$ must be non-degenerated with respect to $b$, $c = \frac{\partial I(V_0, b)}{\partial b} \neq 0$ at $b = b_0$.

The dynamics of a multi-dimensional neuronal system near a saddle node bifurcation can be reduced to a topological normal form

$$\frac{dV}{dt} = c(b - b_0) + a(V - V_0)^2 \tag{1.62}$$

This equation, with a reset after a spike is also known as the quadratic integrate-and-fire neuron model.

## Saddle-node on invariant circle bifurcation

This bifurcation is similar to the saddle-node bifurcation described previously, but the collision occurs in an invariant circle that becomes a limit cycle after the saddle and the node annihilate each other.
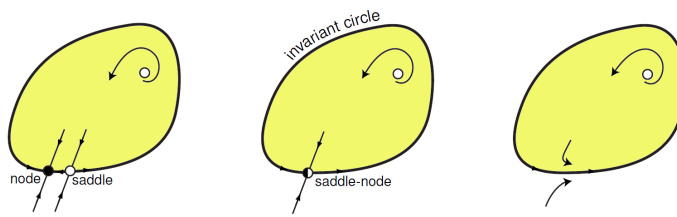
**Figure 1.16:** Phase portraits before (left), at (center) and after (right) saddle-node on invariant circle bifurcation. Adapted from [18].

## Subcritical Hopf bifurcation

This bifurcation occurs because a small unstable limit cycle shrinks to a stable fix point and when they touch, the unstable limit cycle disappears and the stable equilibrium loses its stability and become an unstable fix point. The trajectory diverges from the unstable fix point and approaches to a stable limit cycle.
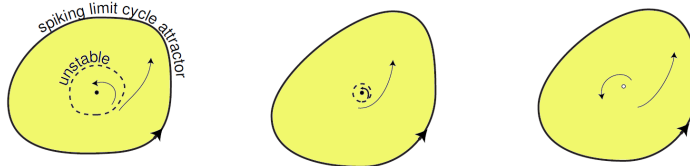


**Figure 1.17:** Phase portraits before (left), at (center) and after (right) subcritical Hopf bifurcation. Adapted from [18].

## Supercritical Hopf bifurcation

A stable fix point loses stability and gives rise to a small amplitude limit cycle. As the bifurcation parameter increases, the amplitude of the limit cycle increases as well.
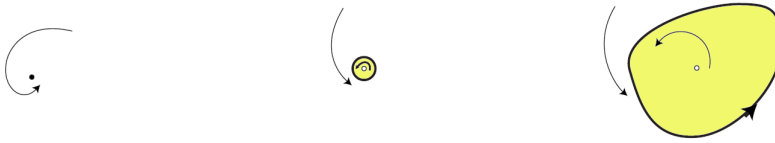
**Figure 1.18:** Phase portraits before (left), at (center) and after (right) supercritical Hopf bifurcation. Adapted from [18].

## 1.3.2  Bursting

A neuron has a bursting behavior when its activity changes periodically from rest state to repetitive firing. Bursting oscillations have been observe in many nerve and endocrine cells like thalamic neurons, hippocampal pyramidal neurons or pancreatic $\beta$-cells. The different kind of burting are classified in three different types according to the bifurcation mechanism that underlies the burting oscillation [19, 20].

### Square-Wave bursting

There is a coexistence of a rest state and spiking activity. The resting state disappears via a saddle-node bifurcation and the variable of the system is attracted to a stable limit cycle. This stable limit cycle disappears via a saddle separatrix loop bifurcation, and the variable of the system is attracted to the resting state again.
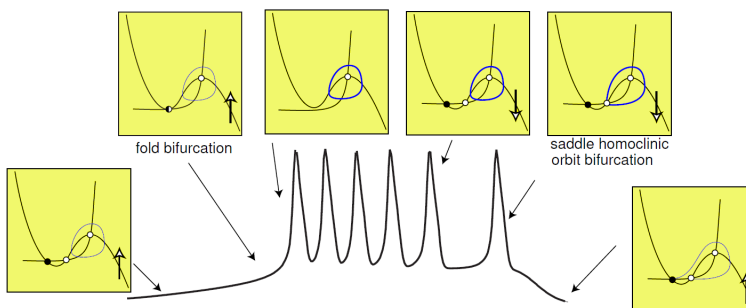


**Figure 1.19:** Square-wave burster. Adapted from [18].

## Parabolic bursting

This type of bursting is characterized by a resting state that disappears via a saddle-node on an invariant circle bifurcation, and the limit cycle corresponding to the firing state disappears via another saddle-node on an invariant circle bifurcation.
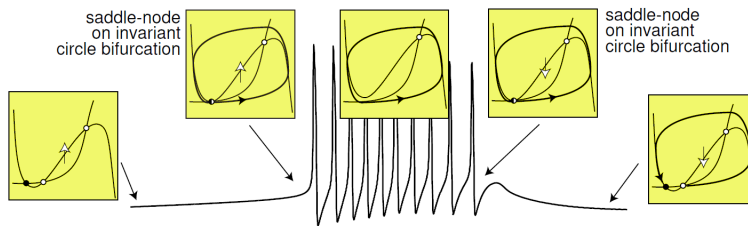


**Figure 1.20:** Parabolic burster. Adapted from [18].

## Elliptic bursting

An elliptic bursting is characterized by a situation in which the rest state disappears via a Hopf bifurcation and becomes oscillatory with a nonzero frequency and in some cases the amplitude of the spikes is small. The periodic orbit can disappear via another Hopf bifurcation carrying the system to the resting state.
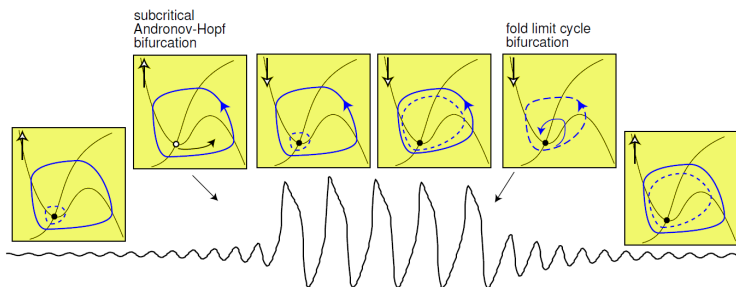


**Figure 1.21:** Elliptic burster. Adapted from [18].

An exhaustive analysis of other bursting mechanism can be found in [16].

1.4 ——————————————————————————————————————
## Coupling and Plasticity

### Alpha function

The main function of neurons is to transmit information from a neuron to another. The transmition of information between two neurons takes place through a synapse. In chemical synapses this process is governed by the release of neurotransmitters in the synaptic cleft. These neuro-transmitters diffuse across the synaptic gap and bind to the postsynaptic receptors. This process can be modeled following a first order kinetics for the neurotransmitter molecule $T$

$$R + T \underset{\beta}{\overset{\alpha}{\rightleftharpoons}} TR$$
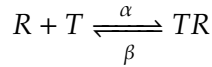
where the bound and unbound states of the postsynaptic receptor are represented by $R$ and $TR$ respectively. $\alpha$ and $\beta$ are the forward and backward rate constants for transmitter binding. The fraction of bound receptors $r$ can be described by the following rate equation

$$\frac{dr}{dt} = \alpha [T] (1 - r) - \beta r \tag{1.63}$$

where $[T]$ represent the concentration of neurotransmitters. This equation can be solved exactly assuming that the change in the concentration of neurotransmitters takes the form of a pulse. Thus,

1. During a pulse, $t_0 < t < t_1$, $[T] = T_{max}$ and the fraction of bound receptors $r$ is given by

$$r(t - t_0) = r_\infty + [r(t_0) - r_\infty] e^{-(t-t_0)/\tau_r} \tag{1.64}$$

were $r_\infty = \alpha T_{max} \tau_r$ and $\tau_r = (\alpha T_{max} + \beta)^{-1}$.

2. After a pulse, $t_1 < t$, the concentration of neurotransmitters tends to zero and the fraction of bound receptors is given by

$$r(t - t_1) = r(t_1) e^{-\beta(t-t_1)} \tag{1.65}$$

Usually the binding of neurotransmitter to a postsynaptic receptor is associated to the opening of ionic channels, thus, the total conductance is the result of multiplying the fraction of open channels by the maximal conductance of the synapse $\bar{g}_{max}$. Then, the synaptic current is defined as

$$I_{syn}(t) = \bar{g}_{syn}r(t)\left[V(t) - E_{syn}\right] \tag{1.66}$$

The binding process explained previously is based on the hypothesis of a constant and sufficient concentration of neurotransmitter molecules $T$. However, the neurotransmitters release probability $P_{rel}$ can depend on the previous activity of the synapse leading to the facilitation or depression of the synapse associated with plasticity phenomena. In the synaptic facilitation $P_{rel}$ increases with the activity of the synapse whereas during synaptic depression $P_{rel}$ decreases. The release probability between presynaptic spikes decays exponentially to $P_0$ following

$$\tau_p \frac{dP_{rel}}{dt} = P_0 - P_{rel} \tag{1.67}$$

where $\tau_p$ is the rate of decay. In the facilitation process, $P_{rel}$ changes by $P_{rel} \rightarrow P_{rel} + f_F(1 - P_{rel})$ where the factor $0 < f_F < 1$ controls the degree of facilitation. In the depresion, $P_{rel}$ is reduced by $P_{rel} \rightarrow f_D P_{rel}$, were $0 < f_D < 1$ controls the level of depresion. For a Poissonian spike train with firing rate $r$, it is easy to demonstrate that the average release probability $\langle P_{rel} \rangle$ in the case of facilitation is

$$\langle P_{rel} \rangle = \frac{P_0 + f_F r \tau_p}{1 + r f_F \tau_p} \tag{1.68}$$

and for depression is

$$\langle P_{rel} \rangle = \frac{P_0}{1 + (1 - f_D)r\tau_p} \tag{1.69}$$

The effects of synaptic facilitation and depression are illustrated in Figure 1.22.

### 1.4.1 Synaptic plasticity

Plasticity is a mechanism by which the synapses interaction strength is modulated according to the previous synaptic activity. One of the pioneers studying the plasticity effect was Donald Hebb that in 1949 conjectured that if an input from a neuron A often contributes to the firing of a neuron B, then the synapse from A to B should be strengthened [21]. Changes in the synapse are thought to be involved in learning, memory processes, pattern recognition, etc.
Different types of plasticity have been identified. In the following sections, a short overview of different types of plasticity is provided.

### Short-term plasticity

Short-term plasticity covers synaptic processes that affect the probability that a presynaptic impulse opens the channels of the postsynaptic neuron. The duration of the short-term plasticity lasts from milliseconds to tens of seconds. The modification of the synaptic transmition probability has basically two effects, depression and facilitation. Short-term depression is related to a decrease of the efficiency of the synapse inducing a decrease of the postsynaptic potential amplitude. Synaptic depression provides a mechanism to control the gain in the synapse. Short-term facilitation on the contrary, is associated with an increase of the efficacy of the synapse giving to an increase of the postsynaptic potential amplitude. Figure 1.22 illustrate these two processes.

### Long-term plasticity

Contrary to short-term plasticity, changes in the efficiency of the synapse during long-term plasticity can last from tens of minutes to days or even longer. As in short-term plasticity, two contrary effects have been also observed in long-term plasticity. Long-term potentiation is related with the enhancement of the synapse efficiency by high-frequency stimuli and it is considered to be related to one of the mechanisms that underlies learning and memory. Long-term depression is the weakening of the
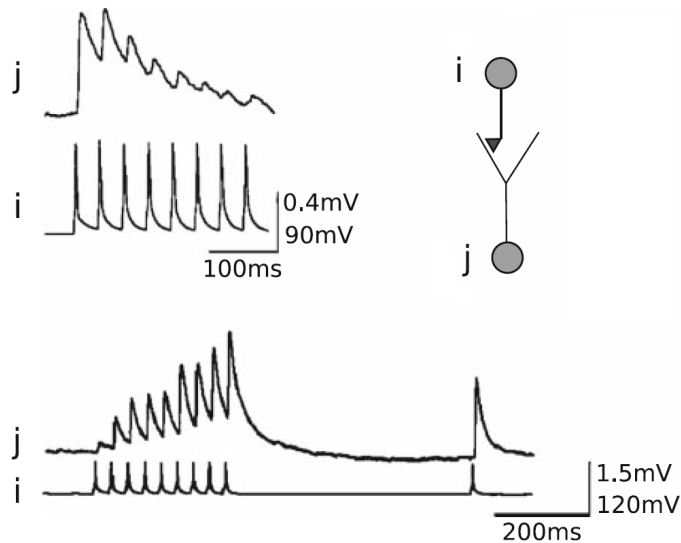
**Figure 1.22:** Illustration of the short-term plasticity, depression and facilitation effects. Adapted from [22].

synapse efficacy that can last form hours to days. It is believed that long-term depression is related with motor learning or erasing of old memory records.

**Spike timing dependent plasticity**

Spike Timing Dependent Plasticity (STDP) is a phenomenon related to the change in the synaptic weights $w$ between a pair of neurons associated with the spiking timing between both neurons. It was studied in 1997 by H. Markram [23] and one year later by L. Zhang and M. Poo who mapped the entire time course relating pre- and post-synaptic activity change [24]. For a single pair of presynaptic and postsynaptic action potentials with time difference $\Delta t = t_{post} - t_{pre}$ a change in the synaptic efficacy $\Delta w$ occurs.

This change is given by:

$$\Delta w = \begin{cases} -\lambda f_-(w) \times K(\Delta t) & if \ \Delta t \ \leq \ 0 \\ \lambda f_+(w) \times K(\Delta t) & if \ \Delta t \ > \ 0 \end{cases}$$

The temporal filter $K(\Delta t) = exp(- \mid \Delta t \mid /\tau)$ implements the spike-timing dependence of the learning. The time constant $\tau$ determines the temporal extent of the learning window. The learning rate $\lambda$ scales the magnitude of individuals weight changes. The temporal asymmetry of the learning is represented by the opposite signs of the weight changes for positive and negative time differences. The updating functions $f_+(w) = (1 - w)^\mu$ and $f_-(w) = \alpha w^\mu$, scale the synaptic changes and implement synaptic potentiation for $\Delta t > 0$, and depression otherwise.

A generalization of this rule takes into account the axonal delay. Then, to compute the temporal difference between pre- and postsynaptic events, one should also consider the time needed for the presynaptic impulse to arrive to the postsynaptic neuron.

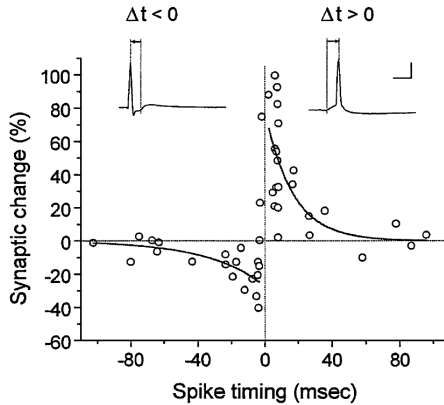$$t'_{pre} = t_{pre} + \tau \qquad (1.70)$$

where $\tau$ is the axonal delay.



**Figure 1.23:** Critical window for STDP. From [25].

## 1.5

# Synchronization

Synchronization is a fundamental phenomenon in nature [26]. It has been observed in many biological systems going from the flashes of a population of firefly to the spiking activity of pacemaker cells in the heart or the clapping of an audience. In neural systems, synchronization is believed to be involved in neural coding [27] and also in some pathological rhythmic brain activity related to epilepsy episodes or Parkinson's disease [28]. Synchronization appears as a multi-scale phenomenon in the brain [29] ranging from synchrony between pairs of single neurons [30, 31], different neuronal populations in the same area [32, 33] or distant areas which are far appart in the brain such as areas between occipital and frontal lobes or across hemispheres [34, 35].

### 1.5.1 Frequency and phase looking

In general, synchronization means an adjustment of frequencies of periodic self-sustained oscillators due to a weak interaction. There are many examples of this kind of oscillators in different fields: electronic circuits, lasers, chemical reactions like the Belousov-Zhabotinsky or biological pacemakers such as the sino-atrial node of the human heart. Common to all self-sustained oscillators there are some features: (i) the self-sustained oscillator is an active system capable of maintaining the same rhythm until a source of energy is available, (ii) the shape of the oscillations is determined by the internal parameters of the system and does not depend on the transient to the steady oscillation and (iii) the oscillation is robust against small perturbations.

One of the principal attribute of an oscillatory system is the characteristic time needed to repeat its intrinsic event. In a periodic oscillator, this time is determined by the period of the oscillation $T$. The inverse of the period defines the cyclic frequency $f = 1/T$ of the oscillator. The angular frequency is defined thus as $w = 2\pi f = 2\pi/T$. Another important quantity that characterize an oscillator is the phase. The signal $x(t)$ of an oscillator

can be written as

$$x(t) = A(t)e^{i(wt+\phi)} \tag{1.71}$$

being $A(t)$ the amplitude of the oscillations, $w$ the angular frequency and $\phi$ the phase of the oscillator. The phase of an oscillator plays an important role in the identification of synchronization.

When two or more oscillators with different intrinsic frequencies are weakly coupled they can adjust their rhythms and start to oscillate with a common period. This phenomenon is known as frequency locking. Figure 1.24 (a) illustrates a typical fingerprint of frequency locking. The graph of the detuning of effective frequencies $\Delta F = F_2 - F_1$ as a function of the natural frequencies mismatch $\Delta f = f_2 - f_1$ exhibits a plateau where $F_1 = F_2$ for a certain range of $\Delta f$. In this region the oscillators are synchronized with the same frequency. Higher orders of synchronization are also possible, usually at large detuning $\Delta f$, in which the ratio between the frequencies is a natural number $F_1/F_2 = n/m \in \mathbb{Q}$. The dependence of the width of this synchronization region with the coupling strength is characterized by the so call Arnold tongues. Figure 1.24 (b) represents the $n : m$ synchronization regions or Arnold tongues.

Associated to the frequency locking, the phase difference of the oscillators $\Phi = \phi_2 - \phi_1$ also remains bounded. A general condition of phase locking is $|n\phi_1 - m\phi_2| < constant$. The phase difference $\Phi$ of the oscillators determines different types of synchronization: in-phase synchrony corresponds to a situation in which $\Phi \approx 0$ denoting a state in which the oscillators have the same phase or very close; anti-phase synchronization appears between oscillators with a phase difference $\Phi \approx \pi$ corresponding to a situation in which the oscillators are at opposite position in the cycle (like two pendulums, one reaching the leftmost position while the other is in the rightmost position).

a)

$\Delta F$

$\Delta f$

synchronization
region

b)

$\varepsilon$

2 : 1     1 : 1     2 : 3     1 : 2                    1 : 3

$\omega_0/2$     $\omega_0$   $3\omega_0/2$   $2\omega_0$          $3\omega_0$
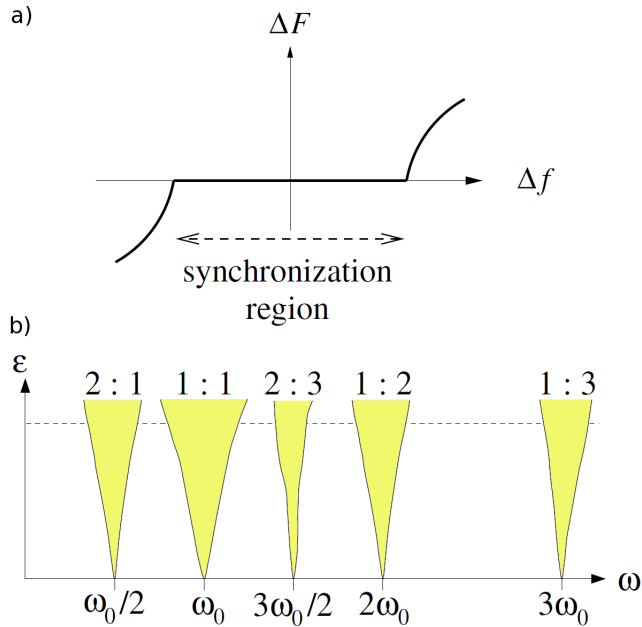
$\omega$

**Figure 1.24:** a) Frequency locking region. b) Arnold tongues.


## 1.5.2 Different types of synchronization

Different kinds of synchronization have been identified in dynamical
systems. In the following lines the principal types of synchronization
between two signal $x_1(t)$ and $x_2(t)$ of two interacting systems are described.

- Identical or complete synchronization: identical synchronization
  implies a perfect linking of the trajectories of the two systems $x_1(t) =$
  $x_2(t)$, so they remain close to each other in time [36]. Only identical
  systems can exhibit complete synchronization and any mismatch
  between them prevents this kind of solution.

- Lag synchronization: lag synchronization is related with the situ-
  ation in which the two systems are identically synchronized when
  they are compared at different times $x_1(t) = x_2(t - \tau)$ [37].

- Generalized synchronization: this kind synchronization implies a nontrivial, and some times complex, relationship between the variables of the two systems $x_2(t) = \mathcal{F}(x_1(t))$ [38]. It is usually easier to demonstrate the existence of this kind of synchronization than determine the relationship $\mathcal{F}$ between the systems. A simple method to check the existence of generalized synchronization was proposed in [39].

- Phase synchronization: this type of synchronization appears usually at weak coupling when the amplitudes of the systems are uncorrelated while the phase difference remains bounded [40].

An extensive review of synchronization in chaotic systems can be found in [41].

## 1.6

# Noise

Noise is present in nature and contrary to intuition noise can have a constructive role in many systems. This section is devoted to a basic introduction to some aspects of stochastic processes. First a brief historical overview is given, followed by the introduction to the white noise. Finally some aspects of the noise in neuronal systems are presented.

### 1.6.1 Historical overview

One of the first attempt to study a fluctuating behavior was done by the Scottish botanist Robert Brown in 1827 [42]. He observed that small pollen particles suspended in water presented an irregular motion. The first explanation of that erratic movement was related to a manifestation of live, but Brown realized soon that inorganic particles like minerals or glass also presented the same kind of movement. Figure 1.25 illustrate a computer generated version of the motion described by Brown.
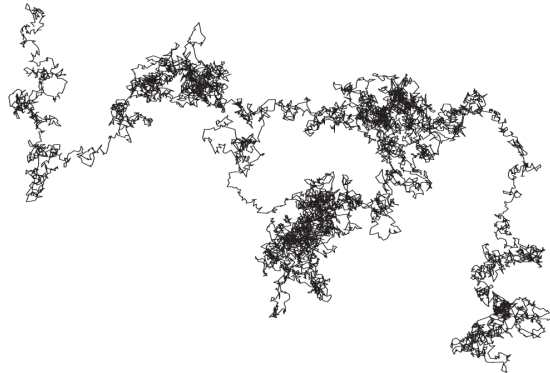


**Figure 1.25:** Representation of the Brownian motion.

A satisfactory explanation of the Brownian motion had to wait until Albert Einstein with one of his famous series of paper of 1905 [43] and independently by Marian Smoluchowskii one year later [44]. Einstein

argued that the motion was caused by the frequent impacts of the moving molecules of water on the pollen grains and that motion can only be described probabilistically in terms of statistically independent impacts. Assuming that the displacement of a particle is independent of all the other particles and the movements of a particle in different time intervals are independent, Einstein derived the diffusion equation

$$\frac{\partial \rho}{\partial t} = D \frac{\partial^2 \rho}{\partial x^2} \tag{1.72}$$

where $D$ is know as the diffusion coefficient and $\rho = \rho(x, t)$ is the probability density of finding a particle at $x$ at time $t$. The solution of the equation of diffusion when $\rho(x, 0) = \delta(x)$ is determined by

$$\rho(x, t) = \frac{1}{\sqrt{4\pi Dt}} e^{-x^2/(4Dt)} \tag{1.73}$$

and the average of the square of the displacement that a particle experiences is

$$\langle x^2 \rangle = 2Dt \tag{1.74}$$

Paul Langevin provided in 1908 a different approach to explain the Brownian motion [45]. Langevin supposed that there were two forces acting on a particle, one coming from the viscous drag due to the movement of the particle in the fluid and another fluctuating force coming from the impacts of the molecules of the liquid on the particle. Then, the equation of motion for the position of the brownian particle was

$$m \frac{d^2 x}{dt^2} = -6\pi \eta a \frac{dx}{dt} + \xi \tag{1.75}$$

where $\eta$ represent the viscosity and $a$ the radius of the assumed spherical particle. The fluctuating force was taken into account in the last term of Eq. 1.75 as $\xi$. Langevin estimated that the average of the square of the displacement was

$$\langle x^2 \rangle = \frac{kT}{3\pi \eta a} t \tag{1.76}$$

where $k$ is the Boltzmann's constant and $T$ is the temperature of the fluid. Then, the diffusion coefficient of Einstein was related to physical properties

$$D = \frac{kT}{6\pi\eta a} \tag{1.77}$$

Diffusion has an important role in biological systems for example in passive displacement of substances in the cells, the transport of neurotransmitters in the synaptic cleft, the transport of oxygen at alveolus, and others.

### 1.6.2  Random walk

In one dimension, the formulation of the random walk problem is equivalent to the situation in which a person moves along a line taking, at random, steps of equal length $\lambda$ to the left or to the right with the same probability. Figure 1.26 shows a schematic representation of this process. The probability of finding the person at a distace $x = r\lambda$ from the origin
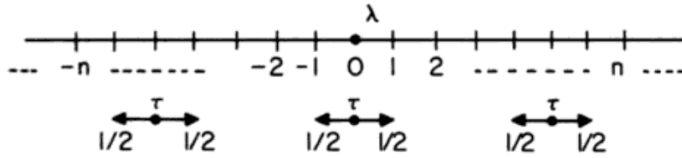


**Figure 1.26:** The random walk process in one dimension.

after a given time $t = n\tau$ follows the binomial distribution

$$P(x(n\tau) = r\lambda) = \binom{n}{\frac{n+r}{2}} 2^{-n} \tag{1.78}$$

The spectation value and the mean square deviation are $\langle x \rangle = 0$ and $\langle x^2 \rangle = n\lambda^2$ respectively. In the limit of large times, using the de Moivre-Laplace theorem, the binomial distribution can be approximated by a Gaussian one:

$$P(x(n\tau) \leqslant r\lambda) = \frac{1}{2} + \text{erf}\left(\frac{r}{\sqrt{n}}\right) \tag{1.79}$$

Figure 1.27 shows a caricature of the two dimensional version of the random walk, known as the drunkard's walk.
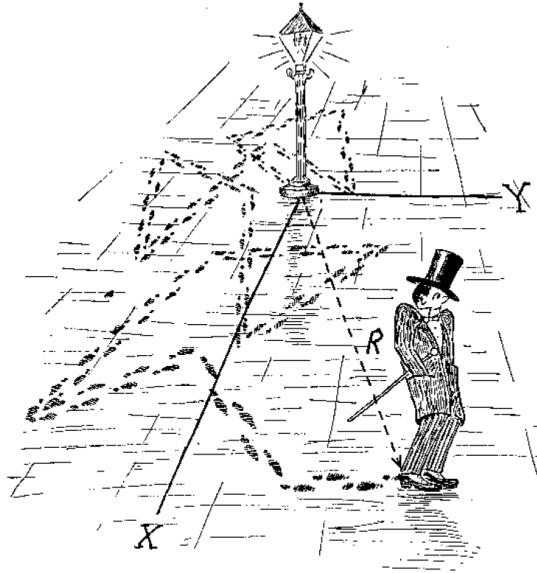


**Figure 1.27:** Illustration of the drunkard's walk.

### 1.6.3 **White noise**

Noise does not have a simple definition. Intuitively, noise represents fast and irregular fluctuations that deviates from the deterministic the behavior of a system. Historically the name was attributed to the irregular sound heard in electronic circuits and nowadays the term is widely used. In order to define the white noise we introduce first the so called Wiener process, $W(t)$, as a random walk process in the continuum limit $\tau \to 0$, $\lambda \to 0$ but $\lambda^2/\tau = 1$.

$$P(W(t) \leqslant x; t) = \frac{1}{\sqrt{2\pi t}} e^{-W^2/(2t)} \tag{1.80}$$

This process is continuous but not differentiable. $W(t)$ has a Gaussian distribution with zero mean and variance $t$. The associated probability

distribution function is

$$f(W; t) = \frac{1}{2} + \text{erf}\left(\frac{x}{\sqrt{t}}\right) \tag{1.81}$$

Since $W(t)$ is a Gaussian process, it is fully determined by its mean and correlation function

$$\langle W(t) \rangle = 0 \tag{1.82}$$
$$\langle W(t_1)W(t_2) \rangle = \min(t_1, t_2) \tag{1.83}$$

The withe noise random process is defined as the derivative of the Wiener process. But, since $W(t)$ has a Haussdorf dimension larger than the space in which the process is defined [46], the derivative of the Wiener process is defined in a special way, performing the derivative before taking the continuum limit previously described. We can define a Gaussian process $\xi_\epsilon(t)$ as a linear combination of a random walk process $x(t)$ in the following way

$$\xi_\epsilon(t) = \frac{x(t + \epsilon) - x(t)}{\epsilon} \tag{1.84}$$

that is completely defined by its mean and correlation functions

$$\langle \xi_\epsilon(t) \rangle = 0 \tag{1.85}$$
$$\langle \xi_\epsilon(t_1)\xi_\epsilon(t_2) \rangle = \begin{cases} 0 & if \quad |t_1 - t_2| \geq \epsilon \\ \lambda^2/(\tau\epsilon)(1 - |t_1 - t_2|/\epsilon) & if \quad |t_1 - t_2| < \epsilon \end{cases} \tag{1.86}$$

Then, the white noise is obtained in the limit $\xi(t) \equiv \lim_{\epsilon \to 0} \xi_\epsilon(t)$ which is characterized by the mean value and correlation

$$\langle \xi(t) \rangle = 0 \tag{1.87}$$
$$\langle \xi(t_1)\xi(t_2) \rangle = \delta(t_1 - t_2) \tag{1.88}$$

The white noise can be understood as an ideal physical stochastic process with delta correlation. In nature however, any physical process has a finite correlation time. To describe these situations, the Ornstein-Uhlenbeck

noise $\xi_{OU}$ is used. This noise is defined as a Gaussina Markov process characterized by

$$\langle \xi(t) \rangle \;\; = \;\; 0 \tag{1.89}$$

$$\langle \xi(t_1)\xi(t_2) \rangle \;\; = \;\; \frac{1}{2\tau}e^{-|t_1-t_2|/\tau} \tag{1.90}$$

The Ornstein-Uhlenbeck noise has a non zero correlation time, i.e. the value of the noise at different times are not independent variables. The white noise is recovered in the limit $\xi(t) = \lim_{\tau \to 0} \xi_{OU}$. The Ornstein-Uhlenbeck is usually know as colored noise.

### 1.6.4 **Langevin equation**

Langevin was a pioneer studying the effect of a stochastic term in a differential equation. When the stochastic process appears linearly, the stochastic differential equation is called Langevin equation. The general formulation of the Langevin equation reads

$$\frac{dx}{dt} = f(x,t) + g(x,t)\xi(t) \tag{1.91}$$

The situation in which the function $g(x,t)$ is constant is referred as additive noise case. On the contrary, when $g(x,t)$ is a non-constant function, the noise is called multiplicative. During this thesis both colored and white noises will be used in the additive form. Numerical integration of stochastic differential equation were done using the Heun method [47]. A review of the stochastic effects in physical systems can be found in [48].

### 1.6.5 **Noise in neurons**

Experimental recordings of neuronal activity present a high irregularity. Even in the situation in which it is assumed that neurons spike periodically, fluctuations of the firing period are observed. There are two kind of noise, an intrinsic noise coming from internal fluctuations at the level of the neuronal dynamics, and an extrinsic noise coming from the network

and connections with other neurons. At an intrinsic level, there exist basi-
cally two mechanisms that contribute as a sources of noise. One is thermal
noise, where the membrane potential fluctuates with temperature due to
the limited amount of electric carriers (Johnson noise). However, this con-
tribution is small compared with other noise sources in neurons. Another
intrinsic source of noise comes from the fluctuations in the conductance
due to the finite number of ionic channels present in the membrane. At
a constant membrane potential, the number of open channels fluctuates
around $nP(V)$ where $n$ is the total number of ion channels and $P(V)$ is the
fraction of open channels. These fluctuations can be critical for the gen-
eration of action potentials when the membrane potential is close to the
threshold. This type of noise is known as channel noise. At an extrinsic
level, a source of noise is the fluctuations in the arrival times of inputs
coming from thousands of other neurons. Another source of noise is the
synaptic transmission failures.

## Poisson process

In general, the probability that a neuron fires at a given time could depend
on the entire history of the preceding spikes. When the intervals between
successive spikes are independent and the firing probability extends only
to the preceding spike, the process that generates the sequence of spikes is
call renewal process. When the firing sequence of a neuron do not depend
on the preceding events, so that the spikes are statistically independent, a
good approximation to describe the firing sequence is given by the Poisson
process. When the firing rate is time independent $r(t) = r$, homogeneous
Poisson process, the probability $P[t_1, t_2, ..., t_n]$ that a sequence of $n$ spikes
occurs can be expressed as

$$P[t_1, t_2, ..., t_n] = n! P_T[n] \left( \frac{\Delta t}{T} \right)^n \qquad (1.92)$$

where it is assumed that the spike times are ordered $t_1 \leq t_2 \leq ... \leq$
$t_n \leq T$ and $P_T[n]$ is the probability that an arbitrary sequence of $n$ spikes
occurs within a time interval $T$. This probability is the product of three
factors: the probability of generating $n$ spikes in the interval $[0, t']$, the
probability of not generating spikes in the remaining interval $[t', T]$ and

the combinatorial factor equal to the number of ways of putting $n$ spikes into M bins ($M = T/\Delta t$).

$$P_T[n] = \lim_{\Delta t \to 0} \frac{M!}{(M-n)!n!}(r\Delta t)^n(1 - r\Delta t)^{M-n} \tag{1.93}$$

We can take this limit by considering that $M$ grows as $\Delta t$ tends to zero and thus, $M - n \approx M$. Defining $\epsilon = -r\Delta t$

$$\lim_{\Delta t \to 0}(1 - r\Delta t)^{M-n} = \lim_{\epsilon \to 0}\left((1 + \epsilon)^{\frac{1}{\epsilon}}\right)^{-rT} = e^{-rT} \tag{1.94}$$

For a large $M$, $M!/(M-n)! \approx M^n$, then,

$$P_T[n] = \frac{(rT)^n}{n!}e^{-rT} \tag{1.95}$$

This is called the Poisson distribution. The average number of spikes generated by a Poisson process is

$$\langle n \rangle = \sum_{n=0}^{\infty} nP_T[n] \tag{1.96}$$

and the variance

$$\sigma_n^2 = \sum_{n=0}^{\infty} n^2 P_T[n] - \langle n \rangle^2 \tag{1.97}$$

To compute these quantities we can use the moment-generating function and its *kth* derivative

$$g(\alpha) = \sum_{n=0}^{\infty} \frac{(rT)^n e^{\alpha n}}{n!}e^{-rT} \tag{1.98}$$

$$\frac{d^k g}{d\alpha^k} = \sum_{n=0}^{\infty} \frac{n^k (rT)^n e^{\alpha n}}{n!}e^{-rT} \tag{1.99}$$

We need the first and second derivatives evaluated at $\alpha = 0$ to obtain $\langle n \rangle$ and $\sigma^2$. Rewriting Eq. 1.98

$$g(\alpha) = e^{-rT}\sum_{n=0}^{\infty} \frac{(rTe^{\alpha})^n}{n!} = e^{-rT}e^{rTe^{\alpha}} \tag{1.100}$$

Then, the first and second derivatives are given by

$$\frac{dg}{d\alpha} = (rT)e^{\alpha}e^{-rT}e^{rTe^{\alpha}} \tag{1.101}$$

$$\frac{d^2g}{d\alpha^2} = ((rT)e^{\alpha})^2\, e^{-rT}e^{rTe^{\alpha}} + (rT)e^{\alpha}e^{-rT}e^{rTe^{\alpha}} \tag{1.102}$$

Evaluating these expressions at $\alpha = 0$ give $\langle n \rangle = rT$ and $\sigma^2 = rT$.

# Part I

# Noise, diversity and signal propagation

# Stochastic Resonance in neuronal systems

Noise, when acting on excitable systems, not always has a degrading effect. In fact, when it affects a system that is driven by a periodic force, it may occur that the noise enhances the responce of the system to the modulation. The effect of the noise is more evident when the amplitude of the modulation is small enough to not to induce a responce of the system in the absence of noise. This phenomenon is known as Stochastic Resonance. Stochastic resonance is commonly understood as the enhancement, by noise, of the response of a non-linear system to a weak input signal. Thus, the minimal ingredients required for the occurrence of stochastic resonance are: i) a source of noise, ii) a weak input signal and iii) a non-linear system. Stochastic resonance has been observed in many biological systems going from mechanoreceptor hair cells of the cryfish [49], the cercal system of the cricket [50] or sensory neurons [51], to cite some of them. Stochastic resonace has been shown in electrophysiological experiments of muscle spindles [52] demonstrating that the sensitivity of the muscle spindle receptors to a weak movement signal is enhanced by introducing a particular level of noise through the tendon of the parent muscle. However, it is not clear from these experiments whether the

---

This chapter is based on the paper: L. Martínez, T. Pérez, C.R. Mirasso, and E. Manjarrez, J. Neurophysiol. **97**, 4007 (2006)

electrical activity of the spinal motoneurones also exhibits the stochastic resonance behavior.

In this chapter we study the role of noise acting on neurons belonging to the motor system. The phenomenon of stochastic resonance is observed and characterized at the level of both the spinal cord and the gastronemial nerve. In the first part of the chapter we introduce and describe the model while in the second part the numerical results are presented and compared with the experimental observations.

## 2.1
# Stochastic resonance in motoneurons

In sensory systems, the presence of a particular nonzero level of noise may significantly enhance the ability of an individual to detect weak sensory stimuli through the phenomenon of stochastic resonance. However, in the motor system it is not clear whether the electrical activity of motoneurons exhibits the stochastic resonance effect. The aim of this study is to demonstrate that such phenomenon is also exhibited by motoneurons.

### 2.1.1  The system

With the aim of demonstrating that the Stochastic Resonance phenomenon is also present in the motor system, we study an ensemble of heterogeneous independent motoneurons. The dynamic of each motoneuron is described by the Morris-Lecar model [6]

$$C_m \frac{dV_i}{dt} = I^{app} + I_i^{ion} - I_i^{ext} + \sqrt{D}\xi_{OU} \tag{2.1}$$

$$\frac{dW_i}{dt} = \phi\Lambda(V_i)\left[W_\infty(V_i) - W_i\right]. \tag{2.2}$$

$C_m$ is the membrane capacitance. $V_i$ and $W_i$ represent the membrane potential and the fractions of open channels of neuron $i$, respectively. $I^{app}$ is the external applied bias current. $\phi$ is the decay rate of $W_i$. The ionic

current $I^{ion}$ is defined as follows

$$I_i^{ion} = -g_{Ca}M_\infty(V_i)\,(V_i - V_{Ca}) - g_K W_i\,(V_i - V_K) - g_L(V_i - V_L) \qquad (2.3)$$

where $g_a$ and $V_a$, being $a = \{Ca, K, L\}$, represent the conductance and the resting potential of the calcium, potassium and leakage channels respectively. The gatering functions are taken into account as the quantities $M_\infty(V)$, $W_\infty(V)$ and $\Lambda(V)$ defined by

$$M_\infty(V) \;=\; \frac{1}{2}\left[1 + \tanh\left(\frac{V - V_1}{V_2}\right)\right] \qquad (2.4)$$

$$W_\infty(V) \;=\; \frac{1}{2}\left[1 + \tanh\left(\frac{V - V_3}{V_4}\right)\right] \qquad (2.5)$$

$$\Lambda(V) \;=\; \tanh\left(\frac{V - V_3}{2V_4}\right) \qquad (2.6)$$

where $V_{M1}$, $V_{M2}$, $V_{W1}$ and $V_{W2}$ are constant values. The external applied current is defined as [53]

$$I_i^{ext} = g_i^{ext} r(t)\,(V_i - E_s) \qquad (2.7)$$

where $g_i^{ext}$ is the conductance of the synaptic channel and $r$ represent the fraction of bound receptors described as

$$r(t) \;=\; \left(1 - e^{-\alpha t}\right) \qquad\qquad for\ t \le t_{on} \qquad (2.8)$$

$$r(t) \;=\; \left(1 - e^{-\alpha t_{on}}\right)e^{-\beta t} \qquad for\ t > t_{on} \qquad (2.9)$$

where $\alpha$ and $\beta$ are rise and decay time constants, respectively. Here $t_{on}$ represents the time at which the synaptic connection is activated. $E_s$ is the the synaptic reversal potential and determines the character of the synapse. An excitatory synapse is defined by a value of $E_s$ larger than the membrane resting potential. On the contrary, a value of $E_s$ smaller than the membrane resting potential is attributed to an inhibitory synapse. In this work, we consider only excitatory synapses coming from the applied external signal.

In nature, heterogeneity is intrinsic to the majority of the systems. Recently, it has been shown that diversity might play an important role in

forced excitatory systems [54]. The response of an excitable system to
an external weak periodic signal can be optimized when an intermediate
level of diversity in the elements composing the system is considered. In
order to account for the natural heterogeneity existing in motoneurons,
we include diversity in our system. To take into account this diversity,
we allow the conductance channel parameter $g_a$ to fluctuates around a
mean value: $g_a = (\sigma \cdot w_a + 1)\bar{g}_a$ where $w_a$ is a Gaussian distributed random
number of zero mean and unit variance. $\sigma = 0.1$ is the percentage of
heterogeneity that we consider.

There is experimental evidence that the size of a pool of motoneurons re-
ceiving the same afferent input is of the order of 300 alpha-motoneurons
[55]. To take into account this experimental evidence we consider a pool of
$N = 300$ motoneurons. Furthermore, because the proportion of possible
direct excitatory connections between motoneurons is low [56], we limit
our study to the situation where the neurons are uncoupled. A periodic
weak modulation that corresponds to the electrical excitation of the gas-
tronecmious nerve (see below) is applied to the system. Each neuron in
the ensemble receives an external periodic synaptic input. The amplitude
of the signal is selected weak enough in order to not to evoke spikes in
the absence of noise. In our simulations, $I_i^{ext}$ is a periodic synaptic pulse
with a period $T_m = 400$ $ms$ (i.e., 2.5 $Hz$), $t_{on} = 3$ $ms$ and amplitude $g^{ext}$
acording to the experimental conditions. We also allow the amplitude of
the external signal to fluctuates around a mean value $g^{ext} = (\sigma \cdot w_e + 1)\bar{g}_{ext}$
being $w_e$ a Gaussian distributed random number of zero mean and unit
variance. The rest of parameters are shown in Table 2.1. Figure 2.1 shows
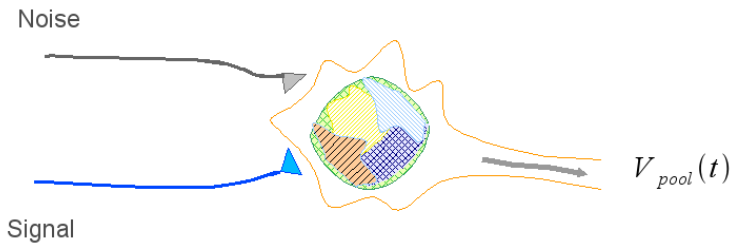a schematic representation of the system.



**Figure 2.1:** Schematic representation of the system under study.

**Table 2.1:** Parameters of the Morris-Lecar model.

| Parameter | Value | Units |
|---|---|---|
| $C_m$ | 5 | $\mu F/cm^2$ |
| $I^{app}$ | 65 | $\mu A/cm^2$ |
| $\bar{g}^K$ | 8 | $\mu S/cm^2$ |
| $\bar{g}^{Ca}$ | 4.4 | $\mu S/cm^2$ |
| $\bar{g}^L$ | 2 | $\mu S/cm^2$ |
| $V_K$ | $-80$ | $mV$ |
| $V_{Ca}$ | 120 | $mV$ |
| $V_L$ | $-60$ | $mV$ |
| $V_{M_1}$ | $-1.2$ | $mV$ |
| $V_{M_2}$ | 18 | $mV$ |
| $V_{W_1}$ | 2 | $mV$ |
| $V_{W_2}$ | 30 | $mV$ |
| $\phi$ | 0.04 | $ms^{-1}$ |
| $\alpha$ | 0.33 | $ms^{-1} \, mM^{-1}$ |
| $\beta$ | 0.2 | $ms^{-1}$ |
| $\bar{g}^{ext}$ | (specified in each case) | |
| $\tau_{syn}$ | 3 | $ms$ |
| $E_s$ | 0 | mV |

## 2.1.2 Synaptic noise

Recently it was shown that the total conductance resulting from a sum of thousands of synaptic inputs has a power spectrum that approximates a Lorentzian shape, i.e., which decays as $e^{-t/\tau}$. This was demonstrated in a detailed physiological model of cortical neurons subject to stochastic synaptic inputs [57]. The Gaussian nature of the Ornstein-Uhlenbeck process and its Lorentzian spectrum qualitatively matches the conductance underlying the synaptic noise, thus providing an effective stochastic representation that captures the amplitude of the conductances, their standard deviation and spectral structure. This motivates the use of the

Ornstein-Uhlenbeck process as a valid description of the synaptic noise.
The Ornstein-Uhlenbeck process can be obtained from the solution of the
following stochastic differential equation

$$\frac{d\xi_{OU}}{dt} = \frac{1}{\tau} (\xi_w - \xi_{OU}) \tag{2.10}$$

with the initial condition $\xi_{OU}(0)$ being a Gaussian random variable of
zero mean and variance $(2\tau)^{-1}$ and $\xi_w$ a white-noise process.

Following this idea, for the case of motoneurons, we assume that the ex-
ternal noise $\sqrt{D}\xi_{OU}$ that enters the pool of neurons through the synaptic
connections is modeled as an Ornstein-Uhlenbeck process, i.e. as a col-
ored noise source, with a correlation time of 0.5 $ms$. Integration of Eq.
(2.1)-(2.2) was done by using a stochastic Runge-Kutta method known as
the Heun method for colored noise following [48]. Figure 2.2 shows the
typical power spectra of the colored noise used in the numerical simula-
tions.
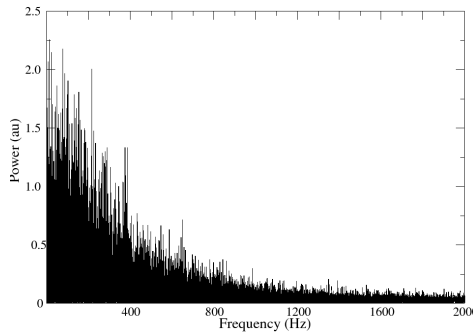


**Figure 2.2:** Power spectra of the colored noise used in the simula-
tions.

## 2.2
# Results

In this section we present the main results obtained from the numerical simulations of the system described in previous sections. To characterize the stochastic resonance we compute the signal to noise ratio (SNR) defined as

$$SNR = \frac{P(\omega)}{P_N(\omega)} \qquad (2.11)$$

where $P(\omega) = \frac{1}{2\pi T}|\int_0^T x(t)e^{-i\omega t}dt|^2$ is the power spectrum of the signal and $P_N(\omega)$ is the power spectrum of the background noise. We characterize the behavior of our system by the collective response $x(t) = N^{-1}\sum_{i=1}^{N} V_i(t)$.

First, we determine the response of the system as a function of the external modulation amplitude in the absence of noise. We normalize the amplitude of the external modulation $g^{ext}$ to the minimal amplitude necessary to obtain some response $T$ (threshold amplitude). Figure 2.3 shows the response amplitude $x(t)$ as a function of the modulation amplitude $g^{ext}$. The response amplitude of the system increases linearly for small amplitudes of the modulation. On the other hand, values of $g^{ext} \gtrsim 1.4T$ produce saturation of the response amplitude.

The next step is to consider a colored noise acting on the system and study the effect of increasing the noise amplitude. Figure 2.4 shows the signal-to-noise ratio for different amplitudes of the applied external signal as a function of the noise level. When the amplitude of the modulation is small enough (green filled squares), practically the system does not respond to the signal. For a value of the amplitude close to the threshold $T$ (blue filled circles), the response of the system is maximized at an intermediate value of the noise intensity. If the amplitude of the modulation is even larger (gray filled triangles), the system does not exhibit the resonant effect and its response degrades when increasing the noise intensity. Our results are consistent with the well established fingerprints of stochastic resonance: the effect of the noise is maximized when the
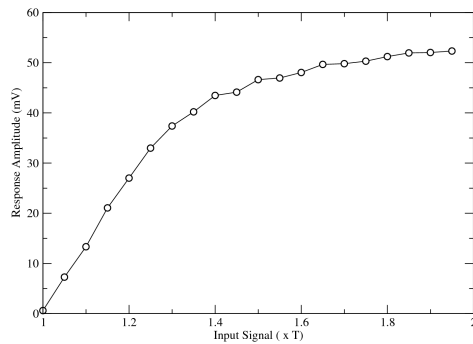
**Figure 2.3:** Amplitude of the respose of the system as a function of the external applied modulation amplitude $g^{ext}$.

system is close to its threshold; the resonant behavior appears only for subthreshold, or close to threshold, values of the modulation amplitude while suprathreshold amplitudes give a degradation of the response of the system. Figure 2.5 displays the time trace of one neuron for differents noise strength $D$. When the noise is small, the neurons slightly respond to the modulation. For an intermediate value of the noise strength, the system responds optimally to the modulation, while at higher values of the noise amplitude, the firing rate of the neurons increases deteriorating the capacity of the system to respond to the external modulation.
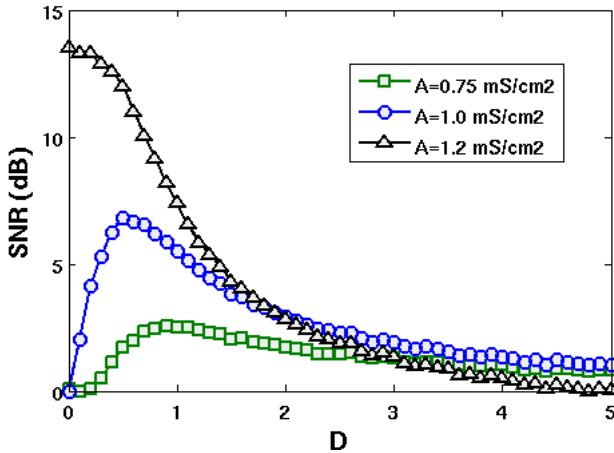
**Figure 2.4:** Signal-to-Noise ratio for different external modulation amplitude $\bar{g}^{ext} = A$ as a function of the noise strength $D$.

## 2.2.1 **Experimental Results**

In collaboration with the Integrative Neurophysiology Lab of the Institute of Physiology of the Benemérita Universidad Autónoma de Puebla, Mexico, we experimentally corroborated the numerical results. In the experiment, we studied the effects of continuous noisy stretches (input noise) to the lateral gastrocnemius-soleus (LGS) muscle on the amplitude of monosynaptic reflexes elicited by periodic electrical stimulation of the medial gastrocnemius (MG) nerve in the leg of the cat (further experimental details can be found in the publication associated to this chapter). Figure 2.6 A shows a schematic representation of the experimental setup. The amplitude of the monosynaptic reflex as a function of the external stimuli amplitude in the absence of noise is shown in Figure 2.6 B. The power spectra of the elicited response and the applied random stretches are displayed in Figure 2.6 C and D respectively.
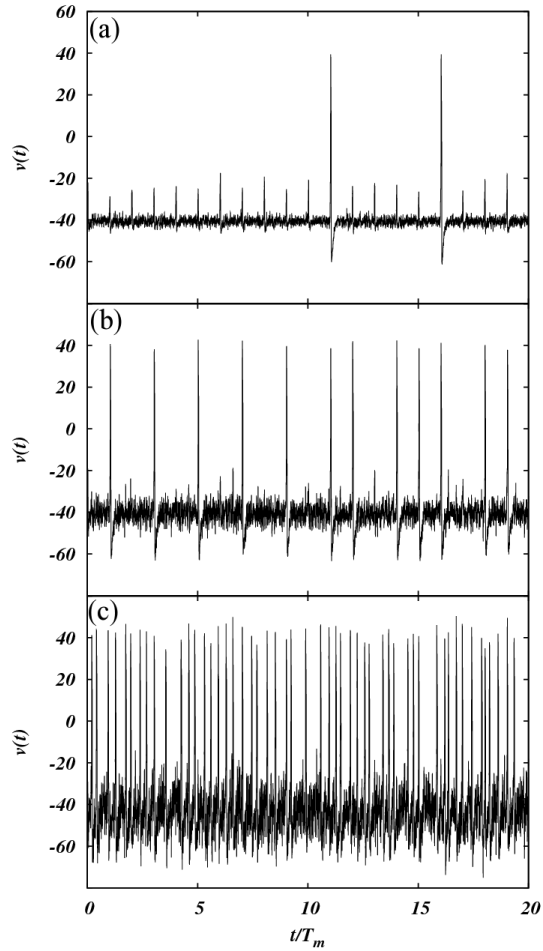
**Figure 2.5:** Temporal trace of one neuron as a function of the
noise strength $D$. The external modulation amplitude is set to
$A = 1.0 \ mS/cm^2$. (a) $D = 0.1$, (b) $D = 0.6$ and (b) $D = 3.0$.
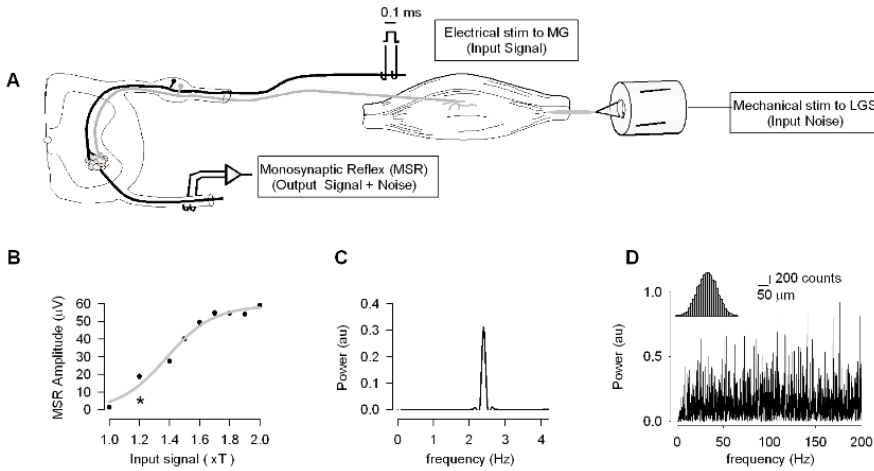
**Figure 2.6:** A: scheme of the experimental arrangement. B: amplitude of the monosynaptic reflexes versus the intensity of the electrical stimulation applied to the medial gastrocnemius nerve. C: power spectra of the elicited response. D: power spectra of the random stretches. Inset: amplitude distribution around 500 $\mu m$.

The main results of the experiment are synthetized in Figure 2.7. The response amplitude of successive monosynaptic reflexes for three levels of noise (low, intermediate, and high) is represented with open circles. The amplitude in control conditions is indicated with black filled circles. Note that the amplitude of the monosynaptic reflex significantly increases when an intermediate level of noise is applied to the LGS muscle. On the contrary, for a high level of noise, the amplitude significantly decreases.
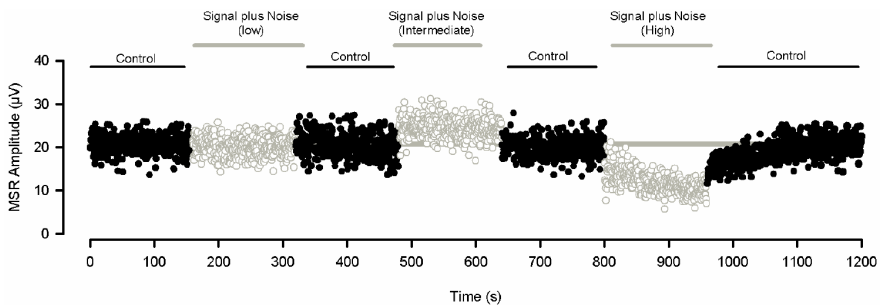
**Figure 2.7:** Amplitude of the successive monosynaptic reflexes for different noise strength.

In order to quantify this observation, we computed the signal to noise ratio (Eq. (2.11)) for different noise strengths, see Figure 2.8. The response of the system clearly exhibits a resonant behavior for intermediates values of the noise strength.
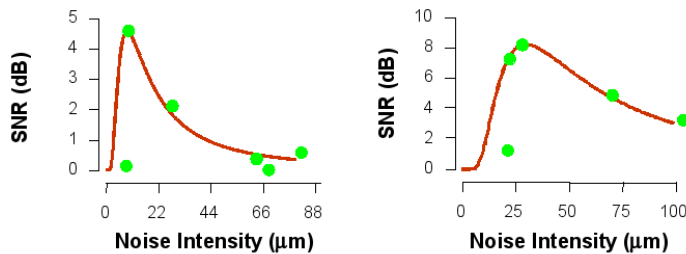


**Figure 2.8:** Computed signal to noise ratio from experimental data (green dots). Red line stands for the best fit $SNR \propto (a/D)^2 e^{-b/D}$ obtained. Both panels correspond to two different realizations of the experiment.

Despite the variability from experiment to experiment, we can conclude that the numerical results qualitatively match the experimental observations.

2.3

# Conclusions

In this chapter we have studied the effect of noise when it acts over a population of motoneurons.  In the first part of the chapter, we have simulated an ensemble of heterogeneous motoneurons described by the Morris-Lecar model. We have considered the situation in which the motoneurons receive convergent synaptic inputs from sources generating the noise and the periodic external signal. The stochastic resonance phenomena has been observed and quantified in our simulations.

In the second part of the chapter, we have presented the experimental study where we have found a qualitatively agreement with the numerical results providing a verification that stochastic resonance occurs also in the motor system at the level of the spinal cord.

In summary, we have demonstrated that noise can have a constructive role when acting over motoneurons located in the spinal cord.  In particular, the enhancement of the response of an ensemble of motoneurons to a weak modulation is obtained for an intermediated level of noise.

# Signal propagation during a motor activity

In this chapter we study the signal propagation during a motor activity. In particular, we center our study in the scratching activity. Scratching is a motor task in which one hind limb performs rhythmic movements to relieve irritating sensations from the skin on the neck, face and pinna. During scratching episodes the spinal cord exhibits sinusoidal-like cord dorsum potentials (CDPs), i.e., sinusoidal electrical waves [58]. Recently, it was demonstrated the rostrocaudal propagation of these waves along the spinal cord during fictive scratching in the cat [59]. It is well known that the neuronal circuitry controlling scratching in the cat is located in the hind limb enlargement of the spinal cord [60–62]. This circuitry, called central pattern generator (CPG), produces the flexor and extensor movements during scratching. However, the detail of the architecture conforming the CPG that allows for the persistence of such sinusoidal waves even in the presence of local failures or absences of activity is still unclear. Here we address this problem both theoretically and experimentally. The aim of this work is to propose a theoretical circuit that reproduces the sinusoidal electrical propagating activity of the CDPs.

---

The chapter is divided as follows: first, a briefly introduction to the different neuronal circuits related to the generation of the motor activity is provided. The proposed neural network involved in the generation of scratching activity and a detailed description of the neuron dynamics is presented in section 3.2. In the last part, we present the obtained numerical results and compared with the experimental observations. Finally, the conclusions are drawn.

## 3.1
# Central pattern generator

The basic rhythms of neural activity related to locomotor activity are generated by neurons of the spinal cord. These neurons are organized in circuits that produce the basic rhythmic movements. These circuits are known as central pattern generators (CPG). The first description of a CPG was provided by Graham Brown in 1911 [63] based on the concept of half-centre. According to this idea, the rhythm related to a locomotor activity is generated by the balance between mutual excitation and the reciprocal inhibition of two population of neurons. In this situation, a simple circuit as the one displayed in Figure 3.1 controls the rhythm and the generated pattern of neuron activity. One of the disadvantages of this kind of scheme is the fact that a failure in the balance of the connection between the population leads the system in one of the phases or states. Another limitation of the half-centre architecture is that it can settle only a unique pattern of neuronal activity.
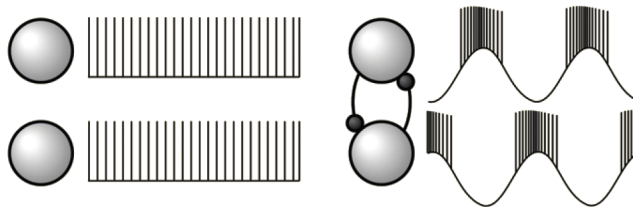


**Figure 3.1:** Basic representation of a CPG.

### 3.1.1 Two-level architecture

To overcome some of the limitations of the single half-centre network, different configurations have been suggested. An architecture based on multiple unit burst generators (UBG) [64] or others based on a bipartite half-centre organization [65], all of them organized in a single layer configuration were proposed. Eventhough these schemes afford to reproduce some complex pattern of locomotor activity, there are still some other aspects in which a single level architecture fails, for example, in the explanation of the deletions. A deletion is an absence of the expected activity of the neurons observed during fictive locomotion and scratching [66, 67]. When a non-resetting deletion occurs, the phase of the alternated activity, usually flexion-extension, is maintained after the deletion, suggesting that this kind of deletions are related with a change in the excitability of a part of the circuit involved in the generation of that locomotor activity. A single-level CPG cannot maintain the phase of the locomotor rhythm during the deletion because a single network is responsible of the generation of both the rhythm and the activity pattern of the neurons. Then, a perturbation in the network affects both the phase and the pattern of the locomotor activity. This is in contradiction with the observation that during a non-resetting deletion the phase of the activity is not altered.

Based on this experimental evidence, a two-level architecture has been recently proposed. It consists in a half-center generating the rhythm and a pattern formation network responsible of the activity pattern of the neurons [68]. The rhythm generator (RG) defines the rhythm and the duration of the different phases of the locomotor activity. The pattern formation network (PF) produces the specific synchronized activity of the neurons depending on the input received from the RG and the interaction between neurons within the same PF. This two-level based CPG has the advantage of a separated control of the locomotor rhythm at the RG layer and the pattern of activity at the PF level. Thus, a perturbation may affect the locomotor rhythm if it acts at the RG level or only the activity pattern if it acts at the PF level. A schematic representation of the two-level CPG is shown in Figure 3.2
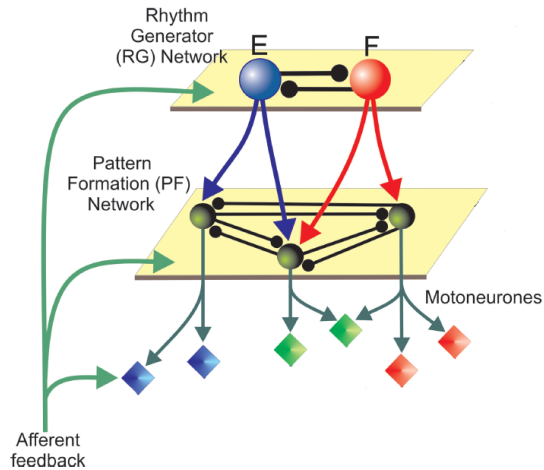
**Figure 3.2:** Two levels central pattern generator. Adapted from
[69].

### 3.1.2 **Spontaneous failures of activity: deletions**

As it was mentioned before, a deletion is a spontaneous lack of activity
during a locomotor activity. It has been observed in different motor tasks
and different animals [70, 71]. Deletions can be classified as resetting or
non-resetting, depending on whether the oscillation phase is altered or
not during the deletion [69]. A resetting deletion is characterized by a
phase shift of the post-deletion rhythm with respect to the pre-deletion
oscillations. In contrast, after a non-resetting deletion the phase of the
pre-deletion rhythm is not shifted after the deletion.

In this thesis we propose a theoretical neuronal circuit based on an ex-
tension of this two-level architecture with an asymmetrical connection
between the two layers. The description of this circuit and the detailed
neuronal dynamics is provided in the next section.

3.2

# Modeling a neuronal network involved in the fictive scratching

The fictive scratching is a motor task in which one limb performs rhythmic movements to mitigates an irritating sensation from the skin. During the fictive scratching, a rostrocaudal propagation of sinusoidal electrical waves have been observed [59]. Previous attempt to model the CPG involved in the fictive scratching were based on an single segment and did not consider the propagation [69]. We are interested in modeling the activity of the fictive scratching by considering also the rostrocaudal observed signal propagation.

We model the rhythm generation and the signal propagation along the spinal cord by means of a network composed of eight CPG units (or nodes [72]). These CPGs are connected via excitatory synapses with their nearest neighbors along the rostrocaudal-caudal direction. We consider the CPG network as consisting of a two-level architecture containing a half-center rhythm generator (RG) and a pattern formation (PF) network [69]. The RG, is formed of two populations of excitatory neurons that mutually project on each other via inhibitory interneuron populations and is the responsible for the duration of the flexor and extensor phases defining the scratching rhythm. It is also responsible for controlling the activity of the PF network by exciting the flexor and inhibiting the extensor half-center of the PF network. The flexor and extensor half-centers of the PF network consist of excitatory neuron populations that form reciprocal connections with one another through inhibitory interneuron populations. Based on the experimental evidence that rhythmic bursting activity in flexor motoneurons can continue in the absence of extensor burst [73] we connect the RG layer and the PF network through an asymmetric direct excitatory synapse on flexor PF neurons population and through an interposed inhibitory interneuron population on extensor PF neuron population [74]. Figure 3.3 shows a schematic representation of the proposed circuitry. To keep the model simple, but still realistic, we assume each population to be composed of twenty neurons described by a modified Morris-Lecar model [75]. We include heterogeneity within

each neuron populations by a random distribution of the leakage current
reversal potential $V_L$. Connections between populations are set such that
individual neurons of each population receive 15% of randomly chosen
connections from the other population.  Excitatory synaptic connections
from populations within the PF layer directly excite the motoneuron pop-
ulations (see for example connections from gray populations to extensor
and flexor motoneuron populations, respectively, in Figure 3.3 (a)).  In ad-
dition, reciprocal inhibitory synaptic connections via inhibitory interneu-
ron populations between the excitatory neuron populations, and flexor
and extensor motoneuron populations are also considered.  Excitatory
synaptic connections are assumed between adjacent rostrocaudal-caudal
elements along the propagation axis represented by light gray arrows in
Figure 3.3 (b).

(a)



(b)
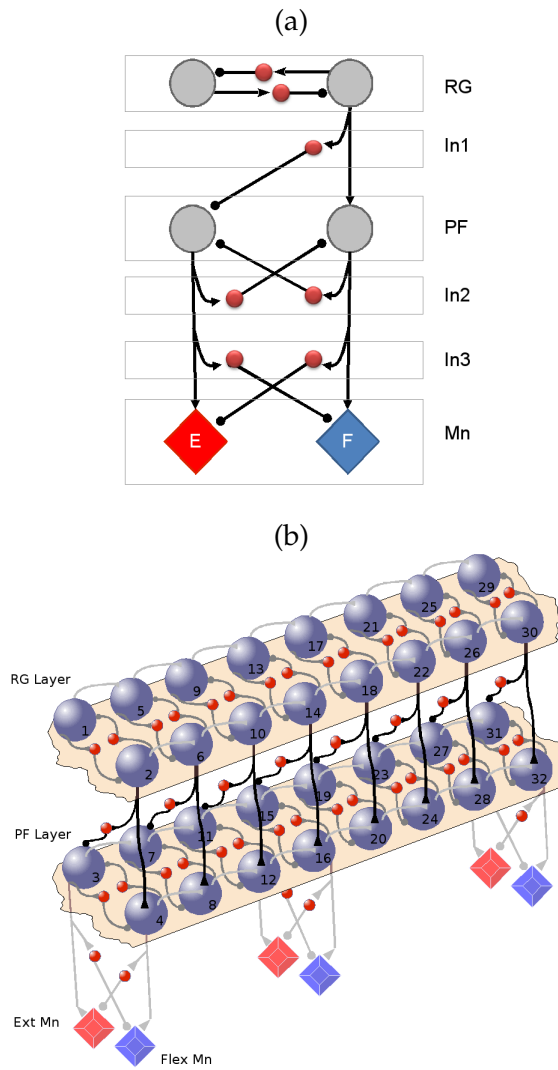


**Figure 3.3:** Representation of the neuronal circuit proposed. (a)
Single node detail. (b) Scheme of the global network.

### 3.2.1 **Neuron dynamic**

In this section we describe in more detail the model that we use to study the rhythm generation and signal propagation along the spinal cord. To model the neuronal activity within the CPG we use a square-bursting version of the Morris-Lecar model [75]. The equations read

$$
C_m\frac{dV_i}{dt} = I_i^{app} - g_{Ca}M_\infty(V_i)(V_i - V_{Ca}) - g_K W_i(V_i - V_K)
$$
$$
- g_L(V_i - V_L) - g_{KCa}z(y_i)(V_i - V_K) - I_i^{syn} \qquad (3.1)
$$
$$
\frac{dW_i}{dt} = \phi\Lambda(V_i)\left[W_\infty(V_i) - W_i\right] \qquad (3.2)
$$
$$
\frac{dy_i}{dt} = \epsilon\left(-\mu g_{Ca}M_\infty(V_i)(V_i - V_{Ca}) - y_i\right) \qquad (3.3)
$$

These equations describe the rate of change of the membrane potential $V(t)$, the slow recovering variable $W(t)$ and the calcium concentration $y(t)$. $C$ represents the membrane capacitance per unit of area. This conductance-based model describes the dynamical behavior of the membrane potential $V(t)$ taking into account four ionic currents for the calcium, potassium, leakage and calcium-dependent potassium channels with conductivities given by $g_{Ca}$, $g_K$, $g_L$ and $g_{KCa}$ respectively. The inclusion of the calcium-dependent potassium channel to the model allows to reproduce the bursting behavior observed experimentally in motoneurons. The dynamics of that channel is governed by the parameters $\mu$ and $\epsilon$. The parameter $\mu$ is determined by the ratio between the surface cell's area and the calcium volume. The parameter $\epsilon$ is the product of the calcium degradation rate and the ratio of free to total calcium. Since calcium is usually neutralized, $\epsilon$ is small and y has a slow dynamics. The nonlinear

functions governing the dynamics of the ionic currents are given by

$$M_\infty(V) = \frac{1}{2}\left[1 + \tanh\left(\frac{V + V_1}{V_2}\right)\right] \qquad (3.4)$$

$$W_\infty(V) = \frac{1}{2}\left[1 + \tanh\left(\frac{V - V_3}{V_4}\right)\right] \qquad (3.5)$$

$$\Lambda(V) = \tanh\left(\frac{V - V_3}{2V_4}\right) \qquad (3.6)$$

$$z(y) = \frac{y}{1 + y} \qquad (3.7)$$

where $V_{M1}$, $V_{M2}$, $V_{W1}$ and $V_{W2}$ are constant values. The value of the parameters used in the simulation can be found in Table 5.4 of Appendix A.

Numerical integration of the system of nonlinear differential equations (3.1-3.3) is done using a fourth order Runge-Kutta algorithm with a time step of $\Delta t = 0.001$ *ms*. An interval of time of $3$ $s$ is considered in order to allow the dynamic of the network to relax to a steady state before performing any measurement on the system.

### 3.2.2 Network Coupling

In the proposed network, we interconnect the neurons via chemical synapses. Then, the synaptic current of the neuron $i$ is defined as [53]

$$I_i^{syn} = g_{ij}^{syn} r_j (V_i - E_s) \qquad (3.8)$$

where $g_{ij}^{syn}$ is the maximum conductance of the synaptic channel between neuron $i$ and $j$. $E_s$ is the the synaptic reversal potential and determines the character of the synapse: when it is larger than the neuron's resting potential the synapse is excitatory, and when it is smaller, the synapse is inhibitory. $r_j$ represent the fraction of bound receptors described as

$$r_j = \left(1 - e^{-\alpha t}\right) \qquad for\ t \leq t_{on} \qquad (3.9)$$

$$r_j = \left(1 - e^{-\alpha t_{on}}\right)e^{-\beta t} \qquad for\ t > t_{on} \qquad (3.10)$$

where $\alpha$ and $\beta$ are rise and decay time constants, respectively. Here $t_{on}$ represents the time at which the synaptic connection is activated. The value of the connectivities used in the simulation can be found in Table 3.2 of Appendix A.

## 3.3

# Propagation of electrical waves

We start the activity of our network by increasing in $\Delta I = 0.5\ mA$ the applied current of the neuron populations belonging to the RG layer of all the CPGs, and also of neuron populations 3 and 4, belonging to the PF layer, in the first CPG. The remaining neurons are subject to a constant bias current of $I = 43.8\ mA$ which kept them just below the spiking threshold. In order to adjust the measured duration of the flexor and extensor phases, different burst durations are considered by varying the value of the parameter $\mu$ in the Equation (3.3). For example, neurons within populations 1, 3 and extensor motoneurons of the first CPG in Figure 3.3 (b), and the equivalent ones in the other CPG units, have a value of $\mu = 0.015$, which leads to an extensor phase of about 70 $ms$, while neurons within populations 2, 4 and flexor motoneurons, and the equivalent ones in the other CPG units, have a slightly larger value of $\mu = 0.017$ for which the flexor phase lasts about 140 ms. The proposed network generates an alternating rhythm that propagates in the rostrocaudal-caudal direction, illustrated in Figure 3.4.

**Figure 3.4:** Illustration of the activity propagation. Black traces correspond to the meanfield potentials recorded at the eight RG layers. Blue (red) line represent the activity of one flexor (extensor) motoneuron.

Figure 3.4 shows the mean field potential of the neurons belonging to the RG layer after a low-pass filter of cut-off frequency of 100 *Hz*. The temporal time traces of one of the flexor (blue) and extensor (red) motoneurons are also displayed. As it can be seen, the mean field potential propagates across the eight nodes. An alternating activity of the flexor-extensor phases is also obtained.

## 3.4
# Different kind of deletions

The observation of spontaneous failures in the activity of some groups of motoneurons during a motor task provides important clues concerning to the organization of the circuit involved in the generation of the rhythm and pattern of such activity.
With the aim of reproducing different kind of experimentally observed

deletions, we induce in our network a temporally change in the excitation
of part of the network.

### 3.4.1 Resetting deletion

In order to induce a resetting deletion, we apply a temporal reduction
of the current in the RG and PF populations of all the nodes. We bias
50% of the neurons of the RG and PF population at $I = 43.7 \; mA$ during
$\Delta t = 400 \; ms$ while the other 50% remain at $I = 44.3 \; mA$. After this
perturbation, the current of all the perturbed neurons is returned to its
original values of $I = 44.3 \; mA$. Figure 3.5 shows an example of resetting
deletion. A temporary lack of electrical activity of the eight CPGs (black
lines) and of the extensor motoneurons (red lines) can be clearly seen.
On the contrary, in flexor motoneurons (blue lines) the bursting period
increases due to the lack of inhibition induced by the extensor group of
the PF layer. Evenly spaced arrowheads indicate the averaged period of
the flexor-extensor cycle before the deletion. After the resetting deletion,
a clear phase shift of the post-deletion rhythm is induced, as it is shown
by the green arrowhead in Figure 3.5.

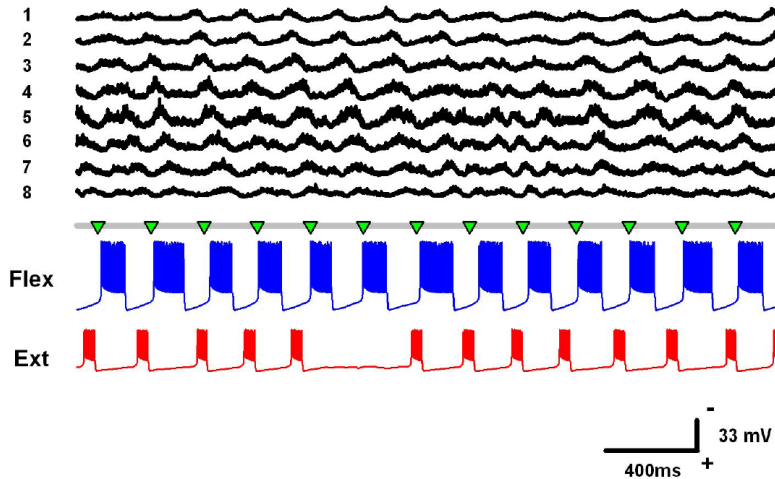**Figure 3.5:** Example of resetting deletion. Black traces correspond to the meanfield potentials recorded at the eight RG layers. A clear perturbation of the electrical activity of the eight CPGs is observed. Blue (red) line represents the activity of one flexor (extensor) motoneuron. Flexor motoneuron exhibit an increase of the bursting duration while extensor motoneuron shows a lack of burting activity during the deletion.

## 3.4.2 Non-resetting deletion

To induce a non-resetting deletion in our network we suddenly diminish the bias current of the neuron populations within the PF block of the CPGs. This sudden change is enough to generate a deletion that propagates along the segment. For example, when we diminish the applied current of 50% of the neurons of populations 3 and 4 to 43.7 mA during 100 ms (the other 50% remains unaltered at 44.3 mA), we observe that neurons belonging to population 3 are silent, while the neurons of population 4 continue their bursting activity, due to the asymmetric connection between RG and PF layers. This lack of activity also affects the extensor motoneuron pool of the same CPG, while the activity of the flexor motoneuron pool remains unaffected as it is shown in Figure 3.6. This evoked deletion propagates across the longitudinal CPG modules, under the same current reduction

of the subsequent PF nodes, as displayed in Figure 3.6. The two bottom
traces of this figure clearly show that the deletion affects the extensor
motoneuron of the last CPG.



**Figure 3.6:** Example of non-resetting deletion. Black traces corre-
spond to the meanfield potentials recorded at the eight RG layers.
The electrical activity of the eight CPGs remains unaltered during
the deletion. Blue (red) line represents the activity of one flexor (ex-
tensor) motoneuron. The flexor motoneuron bursting activity is not
affected by the deletion. On the contrary, the extensor motoneuron
activity presents a burting absence during the deletion.

Combining information provided by these two types of deletions, some
features of the CPG architecture involved in the generation of the fictive
scratching can be unveil. For example, the fact that after a non-resetting
deletion the phase of the activity is not altered, suggests that the CPG
has to have a rhythm generator that is not affected by the perturbations
originating the non-resetting deletions. And the fact that the mean field
potential is not affected during non-resetting deletions supports the hy-
pothesis of a CPG based in a two-level architecture.

### 3.4.3 **Recovering deletion**

The generality of our model allows us to observe, under certain conditions, new behaviors that, although we did not find experimentally yet, might be observed in other cases. For instance, if a local failure occurs in the RG layer, a resetting deletion that recovers during the propagation can occur. We numerically find that when reducing the applied current in only one CPG, a local deletion similar to those shown in Figure 3.5 is observed, although the wave recovers after traveling through few nodes. We illustrate this kind of delition in Figure 3.7.
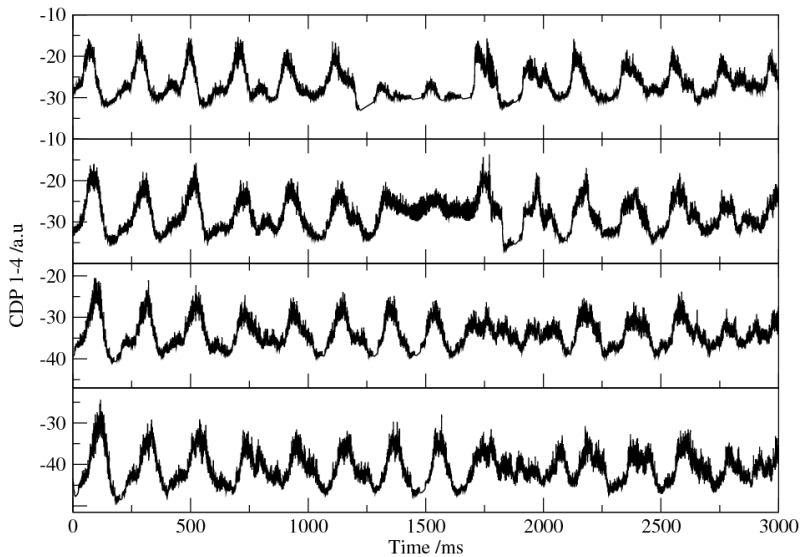


**Figure 3.7:** Example of a predicted recovering deletion. Black lines represent the meanfield potentials recorded at the first four RG layers. A failure of the activity that it recovers after the propagation throught a few nodes is observed.

3.5

# Experimental observations

As in the work presented in chapter 2, we carried out experimental stud-
ies in collaboration with the Integrative Neurophysiology Laboratory of
the Institute of Physiology of the Benemérita Universidad Autónoma de
Puebla, Mexico.

In a previous study performed in this Laboratory, the phenomenon of
propagation of electrical waves (sinusoidal CDPs) on the cat spinal cord
during scratching was analyzed in detail [59]. They observed, as our
model shows, a propagation of the electrical activity in a rostrocaudal
direction. Figure 3.8 illustrates this propagation and the alternating cycle
of flexor and extensor activity. This figure shows the recordings of the
cord dorsum potentials and electroneurograms of flexor tibialis anterior
(blue line) and extensor gastrocnemius (red line) nerves during a typical
fictive scratching episode. The magenta lines represent the phase gradient
associated with the travelling CDPs for each sctratching cycle. As it can
be seen, this propagation is reproduced numerically with our model, see
Figure 3.4. The duration of the exensor and flexor phases are also obtained
after a suitable internal parameter selection.

### 3.5.1 Deletions

Both types of deletions described in previous sections have also been
observed experimentally. Figure 3.9 shows an example of this two kind
of deletions. In the upper panel of Figure 3.9 the recordings of spinal
traveling waves and electroneurograms during scratching are shown.
The traces illustrate a resetting deletion of the extensor muscle motoneural
activity. The magenta lines indicate the rostrocaudal phase gradient of the
traveling waves. Flex and Ext indicate the recorded activity of the flexor
tibialis anterior and extensor gastrocnemius nerves respectively. During
this kind of deletion there is an absence of sinusoidal CDPs activity and a
change in the nerve activity phase after the deletion. In the bottom panel
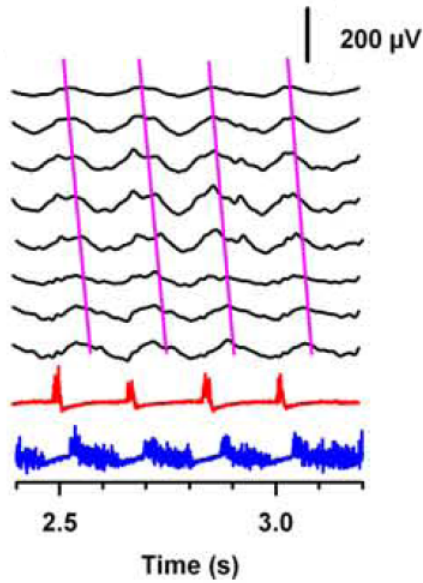an example of a non-resetting deletion is displayed. In contrast to the

**Figure 3.8:** Propagation of the experimentally recorded cord dorsum potentials (CDPs).

previous case, during a non-resetting deletion the traveling waves and the phase of the extensor muscle activity are unaltered.
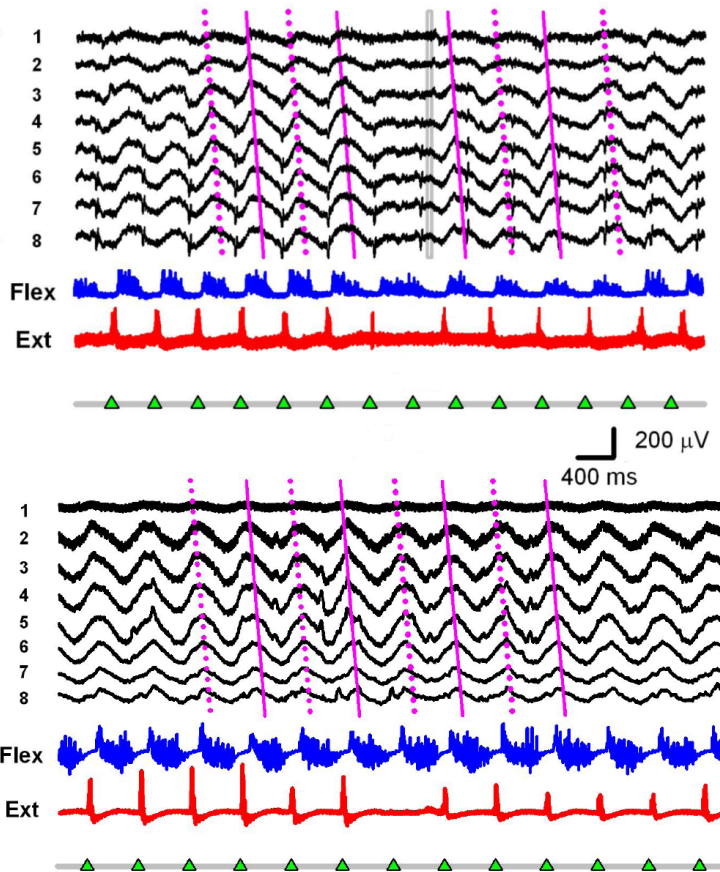
**Figure 3.9:** Illustration of the experimentally observed deltions.
Upper panel: a resetting deletion is clearly shown. Bottom panel:
Illustration of a non-resetting deletion.

## 3.6

# Conclusions

In this work we have demonstrated that the propagation of activity during the scratching motor task can be explained in terms of an asymmetric architecture formed by a Rythm Generator and a Pattern Formation layers. Populations of motoneurons described by a modified version of the Morris-Lecar model and specifically connected via interneurons account for the experimentally observed phenomena.

We have found that an alteration in the excitability of part of the network leads to the absence of activity during the scratching, i.e., the phenomenon of deletions was reproduced. Furthermore, both resetting and non-resetting deletions observed experimentally were obtained numerically. We have found that non-resetting deletions in extensor activity are not associated with disturbances of the traveling spinal wave. On the contrary, we found that resetting deletions are always associated with a failure in the traveling spinal wave.

A new kind of deletion, not observed experimentally yet, is predicted by our model. Further experimental corroboration of this predicted deletion is essential to elucidate the validity of the assumptions of our model.

Our results support the hypothesis that within the spinal cord there is a group of interneurons longitudinally organized similarly to the network proposed, that are capable of maintaining the CPG rhythm even during deletions in the extensor motoneuron activity. We suggest that the traveling electrical waves in the spinal cord during scratching are produced by the sequential activation of those circuits.

# Appendix A

**Table 3.1:** Parameters of the modified Morris-Lecar model.

| Parameter | Value | Units |
|---|---|---|
| $C_m$ | 5 | $\mu F/cm^2$ |
| $I^{app}$ | 43.8 | $\mu A/cm^2$ |
| $g_K$ | 8 | $\mu S/cm^2$ |
| $g_{Ca}$ | 4 | $\mu S/cm^2$ |
| $g_L$ | 2 | $\mu S/cm^2$ |
| $g_{KCa}$ | 0.25 | $\mu S/cm^2$ |
| $V_K$ | −84 | $mV$ |
| $V_{Ca}$ | 120 | $mV$ |
| $V_L$ | $-60 \pm 0.6$ | $mV$ |
| $V_{M_1}$ | 1.2 | $mV$ |
| $V_{M_2}$ | 18 | $mV$ |
| $V_{W_1}$ | 12 | $mV$ |
| $V_{W_2}$ | 1.4 | $mV$ |
| $\phi$ | 4.6 | $s^{-1}$ |
| $\epsilon$ | 0.0175 | $s^{-1}$ |
| $\mu$ | $0.015 - 0.017$ | $s^{-1}$ |
| $\alpha$ | 0.33 | $ms^{-1}\, mM^{-1}$ |
| $\beta$ | 0.2 | $ms^{-1}$ |
| $\tau_{syn}$ | 3 | $ms$ |
| $E_s$ | 0, −80 | mV |
| | (Ex,In) | |

**Table 3.2:** Synaptic connectivities.

| Connectivity | Value | Units |
|---|---|---|
| $g_{ex,int}$ | 0.3 | $nS$ |
| $g_{in,int}$ | $0.1 - 0.6$ | $nS$ |
| $g_{2,4}$ | 2.0 | $nS$ |
| $g_{4,flex}$ | 2.0 | $nS$ |
| $g_{3,ext}$ | 1.75 | $nS$ |
| $g_{int,flex}$ | 1.5 | $nS$ |
| $g_{int,ext}$ | 2.0 | $nS$ |
| $g_{exc,exc}$ | 0.1 | $nS$ |
| $g_{CPG,CPG}$ | 0.1 | $nS$ |

# Chapter 4

# Role of diversity in neurons

Synchronized behavior arising among the constituents of an ensemble is common in Nature. A few examples include the synchronized flashing of fireflies, cardiac cells of the sinoatrial node of the heart and the electrical pulses of neurons. This global behavior can originate from a common response to an external stimulus or might appear in autonomous, non-forced, systems. The theoretical basis for the understanding of synchronization in non-forced systems was put forward by Winfree [76] who showed that the interaction –i.e. coupling– between the constituents is an essential ingredient for the existence of a synchronized output. The seminal work on coupled oscillators by Kuramoto [77] offered a model case whose solution confirms the basic hypothesis of Winfree: while interaction helps towards the achievement of a common behavior, a perfect order can be achieved only in the absence of diversity –heterogeneity– among the components of an ensemble. In the Kuramoto model, diversity appears when the oscillators have different natural frequencies, those that they display when they are uncoupled from each other. While this result holds for systems that can be described by coupled oscillators, recent studies indicate that in other cases diversity among the constituents might actually have a positive role in setting a common behavior [54].

In this chapter we focus on the role of diversity in different neuron models. The dynamical features of many biological systems, such as neurons, can be described in terms of models of excitable systems. In the fist part of the chapter we consider the Fitzhugh-Nagumo (FHN) model [5] in-

troduced in the introductory chapter. The FHN model can be extended by coupling the individual elements and provides an interesting model of coupled neuron populations. In the initial studies of the dynamics of this and similar models, the individual units (e.g. neurons) were treated as identical. However, in reality individual units of such coupled systems are not identical; that is, there is a diversity in the population of these biological units. It is natural to ask what role diversity plays in the dynamical behavior of these systems. In general, it has been found that diversity can in fact be an important parameter in controlling the dynamics. In particular, it has been shown recently that a system has a better response to an external stimulus if there is some degree of diversity in the constituent units [54]. In the second part we deal with another model of an excitable system, the Morris-Lecar (ML) model [6]. This model can also be extended by coupling the individual elements and provides a second example in which one can explore the effects of diversity. Finally a theoretical approximation of the electrically coupled FHN system is presented.

## 4.1
# FitzHugh-Nagumo model

### 4.1.1 The system

We consider an ensemble of $N = 10^3$ excitable neurons, whose dynamical behavior is described by the FitzHugh-Nagumo model and is subject to an external sinusoidal forcing. The equations describing our system read:

$$\epsilon \dot{x}_i = x_i(1 - x_i)(x_i - b) - y_i + d - I_i^{syn} \tag{4.1}$$
$$\dot{y}_i = x_i - cy_i + a_i + A \sin(\Omega t) \tag{4.2}$$

where $x_i$ represents the membrane potential and $y_i$ the slow potassium gating variable of neuron $i$, respectively. The time scale of these variables are separated by $\epsilon = 0.01$. The rest of parameters are set to $b = 0.5$, $c = 4.6$, $d = 0.1$, $A = 0.05$ [78]. To take into account the natural diversity of the units, we allow the parameter $a_i$ to follow a Gaussian

distribution with mean $\langle a_i \rangle = a$ and correlations $\left\langle (a_i - a)(a_j - a) \right\rangle = \delta_{ij}\sigma^2$. We use $\sigma$ as a measure of the heterogeneity of the system and, in the following, we refer to $\sigma$ as the diversity.

The dynamics of a single neuron described by Eqs. (4.1)-(4.2) in the absence of the last right-hand side terms, the coupling and the modulation terms respectively, has a strong dependence on the diversity parameter $a_i$. Three different operating regimes are present: for $a_i \lesssim -0.09$ the system has a stable focus in the left branch of the cubic nullcline leading the system to an excitable regime, for $-0.09 \lesssim a_i \lesssim 0.01$ a limit cycle around an unstable focus appears (oscillatory regime) and for $0.01 \lesssim a_i$ a stable focus appears again, now at the right side of the cubic nullcline (excitable regime). Figure 4.1 (a) shows the nullclines $f(x)$ and $g(x, a_i)$ of the system in the three operating regimes described above, $a_i = -0.1, 0.0$ and $a_i = 0.06$. As shown in Figure 4.1 (b), in the oscillatory regime, the intrinsic firing frequency does not change drastically with respect to changes of $a_i$.
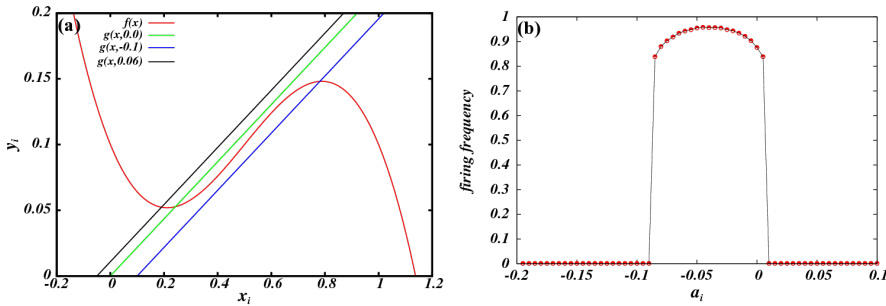


**Figure 4.1:** (a) Nullclines of the FHN system for different values of $a_i$. (b) Dependence of the firing frequency on $a_i$.

To illustrate the behavior of $x_i$ and $y_i$, we show in figure 6.3 the phase-portrait for different values of $a = -0.1, 0.0$ and $0.06$ corresponding to the three cases represented in figure 4.1 (a).

91
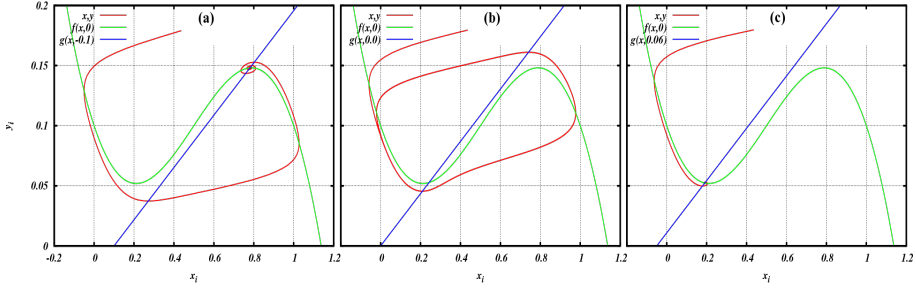
**Figure 4.2:** Phase-space portrait of the FHN system for different values of $a$. (a) $a = -0.1$, (b) $a = 0.0$ and (c) $a = 0.06$.

### 4.1.2 Coupling scenarios: electrical and chemical interactions

As it was mentioned in the Introduction, the most common way of communication between neurons is the chemical synapses were the transmission is carried out by an agent called neurotransmitter. In these synapses, neurons are separated by a synaptic cleft and the neurotransmitter has to diffuse to reach the postsynaptic receptors. There is another kind of synapse where the membrane of the neurons are in contact and thus, the transmission of the signal is achieved directly (electrical synapses). In this work we consider both electrical and chemical coupling between the neurons. In the electrical interactions, also known as diffusive coupling, the synaptic current is proportional to the membrane potential difference between a neuron and its neighbors:

$$I_i^{syn} = \frac{K}{N} \sum_{j=1}^{N} \left( x_i - x_j \right) \tag{4.3}$$

In the chemical coupling the synaptic current is described by:

$$I_i^{syn} = \frac{K}{N} \sum_{j=1}^{N} g_{ij} r_j(t) \left( x_i - E_s \right) \tag{4.4}$$

where $g_{ij}$ is the maximum conductance between neuron $i$ and $j$. We center our study in the homogeneous coupling configuration, where $g_{ij} = g$. The

character of the synapse is determined by the synaptic reversal potential $E_s$. An excitatory synapse is defined by a value of $E_s$ larger than the membrane resting potential. On the contrary, a value of $E_s$ smaller than the membrane resting potential is attributed to an inhibitory synapse. $r_j$ represents the fraction of bound receptors described as

$$r_j(t) \quad = \quad \left(1 - e^{-\alpha t}\right) \qquad\qquad\qquad for\ t \leq t_{on} \qquad (4.5)$$

$$r_j(t) \quad = \quad \left(1 - e^{-\alpha t_{on}}\right) e^{-\beta(t - t_{on})} \qquad\qquad for\ t > t_{on} \qquad (4.6)$$

where $\alpha$ = 2.5 $ms$ and $\beta$ = 3.5 $ms$ are the rise and decay time constans, respectively. Here $t_{on}$ represents the time at which the synaptic connection remains active.

### 4.1.3 Results

It is our aim to demonstrate that the diversity may play a constructive role in this kind of coupled excitable systems. To account for that, we center our study in the response of an ensemble of neurons subjected to an external weak periodic modulation. We expect that, similarly to the stochastic resonance phenomenon, there will be an optimal range of diversity in which the response of the system is maximized. In order to quantify the resonant effect with respect to the diversity, we compute the spectral amplification factor defined as

$$\eta \quad = \quad \frac{4}{A^2} \, | \, \langle e^{-i\Omega t} \bar{X}(t) \rangle \, |^2 \, . \qquad\qquad (4.7)$$

where $\bar{X}(t) = \sum_{i=1}^{N} x_i(t)$ and $\langle \cdot \rangle$ denotes a time average.

### Electrical coupling

In this section we concentrate in the situation in which the units are diffusively coupled. The mean value of the parameter distribution is fixed to $a$ = 0.06 and the coupling strength to $K$ = 0.6. Figure 4.3 shows the spectral amplification factor as a function of $\sigma$ for fixed values of the amplitude $A$ = 0.05 and two different values of the period $T$ of the external
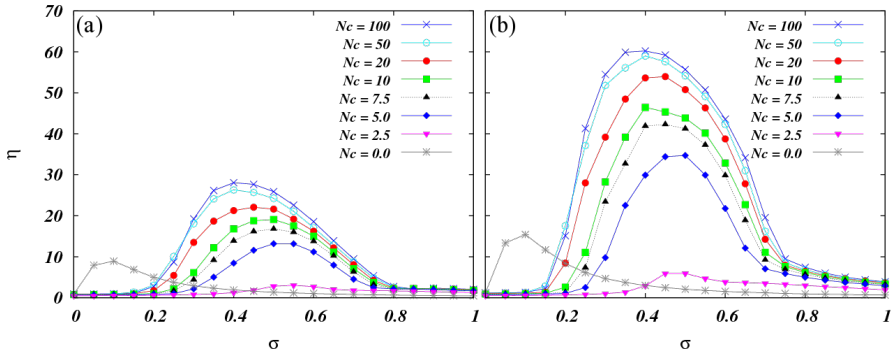
**Figure 4.3:** Spectral amplification factor $\eta$ as a function of $\sigma$ for an increasing percentage of connected neurons $Nc$. Parameters: $a = 0.06$, $K = 0.6$ and $A = 0.05$. (a) $T = 1.6$ and (b) $T = 1.11$.

modulation when the percentage of connected neurons $Nc$ increases. When the neurons are uncoupled, there is a moderate enhancement of the response of the system to the external modulation for low diversity values. On the other hand, when the neurons are coupled, the diversity induces a clear enhancement of the responce of the system to the weak external modulation for a certain range of diverity values present in the system. This enhancement is much larger than the one occurring when the neurons are uncoupled. Periods of modulation closer to the intrinsic firing period of the neurons yield an increasing value of $\eta$ (see Figure 4.1 (b)).

To illustrate the response of the system to the external sinusoidal modulation when the diversity is present, we show in Figure 4.4 the time traces of ten randomly chosen neurons and the rasterplots of the ensemble for different values of the diversity parameter. When the diversity is small, each neuron responds to the external modulation with subthreshold oscilations and the system remains under threshold. The right amount of diversity between the neurons leads to an improvement of their responses. In this situation, the neurons fire with the periodicity of the external modulation. Finally, for higher diversity values, the response of each neuron is completely different from each other and the firing frequency is much

higher than the period of the external modulation. Also the individual amplitudes are different to each other.
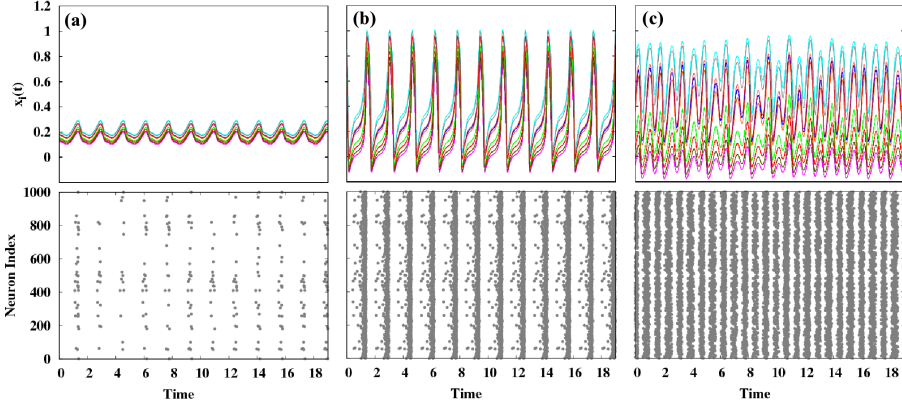


**Figure 4.4:** Time traces of ten randomly chosen neurons and raster-plot of the fully connected ensemble for three different values of the diversity: (a) $\sigma = 0.1$, (b) $\sigma = 0.4$ and (c) $\sigma = 0.9$. Other parameters: $a = 0.06$, $K = 0.6$, $A = 0.05$ and $T = 1.6$.

## Chemical coupling

We consider in this section the case in which the neurons are chemically coupled. In particular, for the FHN model we consider $E_s = 0.7$ for the excitatory synapses and $E_s = -2.0$ for the inhibitory ones. Figure 4.5 shows the spectral amplification factor as a function of the diversity $\sigma$ for a fixed value of the amplitude $A = 0.05$ and different periods $T$ of the external modulation when the percentage of connected $Nc$ neurons increases. The coupling strength is fixed to $K = 1.5$. In Figure 4.5 it can be seen that diversity also enhances the responce of the system when the neurons interact throught the chemical synapses. In this coupling configuration, increasing the percentage of connected neurons $Nc$ above the 2% does not have a significant effect in the response of the system to the external signal as in the electrical coupling case. Since the chemical synapses can be excitatory or inhibitory depending on the value of the parameter $E_s$, we
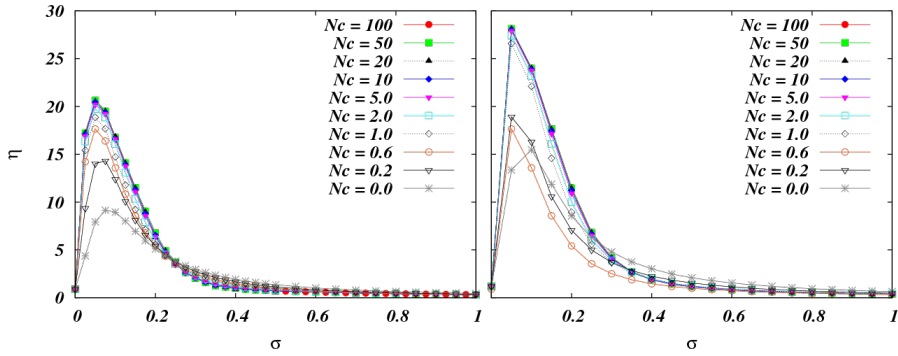
**Figure 4.5:** Spectral amplification factor $\eta$ as a function of $\sigma$ for an increasing $Nc$. The ratio of excitatory to inhibitory connections was fixed to 4. Other parameters: $a = 0.06$, $K = 1.5$ and $A = 0.05$. (a) $T = 1.6$ and (b) $T = 1.11$.

explore the effect of changing the ratio of excitatory/inhibitory synapses in our system. Figure 4.6 shows the spectral amplification factor when the fraction of excitatory neurons $Ne$ increases in the situation in which the neurons are globally coupled. In contrast with the previous situation, now the fraction of excitatory synapses presents in the system have a significant effect. When all the connections between neurons are excitatory, the response of the system is maximized. Then, when $Ne$ decreases, the maximum of the response also decreases. In the limit in which all the synapses are inhibitory, the diversity does not enhance the respose of the system to the external weak modulation.
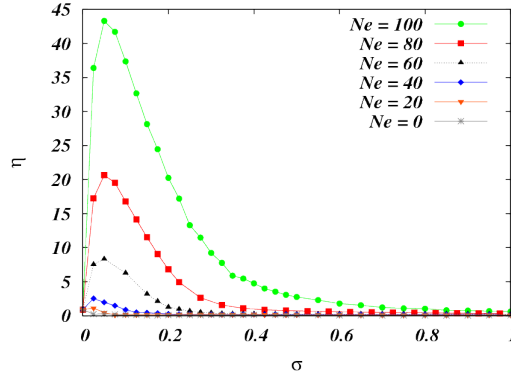
**Figure 4.6:** Spectral amplification factor $\eta$ as a function of $\sigma$ for an increasing number of excitatory synapses. The elements were gobally coupled. Other parameters as in Figure 4.5 (a).

## 4.2
# Morris-Lecar model

### 4.2.1 The system

As a second example of neuronal system we consider an ensemble of $N = 10^3$ neurons with a dynamics described by the Morris-Lecar model,

$$\frac{dV_i}{dt} = \frac{1}{C_m}\left(I^{app} - I_i^{ion} - I_i^{syn} - I^{ext}\right) \tag{4.8}$$

$$\frac{dW_i}{dt} = \phi\Lambda(V_i)\left[W_\infty(V_i) - W_i\right] \tag{4.9}$$

where $V_i$ and $W_i$ represent the membrane potential and the fraction of open potassium channels, respectively. $I^{app}$ is the external applied current, $I_i^{syn}$ is the synaptic current, and the ionic current is given by

$$I_i^{ion} = g^{Ca}M_\infty(V_i)\left(V_i - V_0^{Ca}\right) + g^K W_i\left(V_i - V_0^K\right) + g_i^L\left(V_i - V_0^L\right) \tag{4.10}$$

where $g^a$ and $V_0^a$ ($a = Ca, K, L$) are the conductance and the resting potentials of the calcium, potassium and leakage channels, respectively. We

define the following functions of the membrane potential:

$$M_\infty(V) = \frac{1}{2}\left[1 + tanh\left(\frac{V - V_{M_1}}{V_{M_2}}\right)\right] \tag{4.11}$$

$$W_\infty(V) = \frac{1}{2}\left[1 + tanh\left(\frac{V - V_{W_1}}{V_{W_2}}\right)\right] \tag{4.12}$$

$$\Lambda(V) = cosh\left(\frac{V - V_{W_1}}{2V_{W_2}}\right) \tag{4.13}$$

where $V_{M_1}$, $V_{M_2}$, $V_{W_1}$ and $V_{W_2}$ are constants. To take into account diversity in this model, the leakage conductance parameter is distributed around its mean value $g_0^L$ following a log-normal distribution in order to avoid negative values. We use the standard deviation of the distribution as a measure of the heterogeneity in the ensemble. A single neuron described by the ML model exhibits a bifurcation to a limit cycle when increasing the applied current $I^{app}$. This bifurcation can be saddle-node, involving type I excitability, or a subcritical Hopf bifurcation leading to excitability type II. We select the parameters to fulfill this last option. Table 5.4 summarizes the parameter values of the model that we use in our simulations.

Both chemical and electrical coupling schemes are also considered for this model. In the following sections we present the results concerning the chemical and electrical coupling configurations.

### 4.2.2 Results

#### Chemical coupling

In the chemical mediated interaction, when a neuron fires it sends a predefined pulse to all other neurons in the pool and the postsynaptic current has a predefined form as it was introduced in section 4.1.2. Interactions can be excitatory or inhibitory depending on the synaptic reversal potential. For the ML model we consider $E_s = 0.0 \ mV$ for the excitatory synapses and $E_s = -80.0 \ mV$ for the inhibitory ones. Figure 4.7 (a) shows

**Table 4.1:** Parameters of the Morris-Lecar model.

| Parameter | Value | Units |
|---|---|---|
| $C_m$ | 5 | $\mu F/cm^2$ |
| $I^{app}$ | 144 | $\mu A/cm^2$ |
| $g_0^K$ | 8 | $\mu S/cm^2$ |
| $g_0^{Ca}$ | 4.4 | $\mu S/cm^2$ |
| $g_0^L$ | 2 | $\mu S/cm^2$ |
| $V_K$ | $-80$ | $mV$ |
| $V_{Ca}$ | 120 | $mV$ |
| $V_L$ | $-60$ | $mV$ |
| $V_{M_1}$ | $-1.2$ | $mV$ |
| $V_{M_2}$ | 18 | $mV$ |
| $V_{W_1}$ | 2 | $mV$ |
| $V_{W_2}$ | 30 | $mV$ |
| $\phi$ | 0.04 | $ms^{-1}$ |
| $\alpha$ | 0.33 | $ms^{-1}\,mM^{-1}$ |
| $\beta$ | 0.2 | $ms^{-1}$ |
| $g_0^{syn}$ | 0.4 | $\mu S$ |
| $\tau_{syn}$ | 3 | $ms$ |
| $E_s$ | (specified in each case) | |

the spectral amplification factor as a function of the diversity for different fractions of coupled neurons $Nc$. There is an optimal range of values of the diversity of the neurons for which the system response is optimized. An interesting feature to analyze is the role played by the balance between excitatory and inhibitory synapses in the response of the system to the weak external signal. We show in Figure 4.7 (b) the spectral amplification factor as a function of the diversity when the percentage of excitatory connections $Ne$ in the network decreases. In this case, the response of the system is maximized when the ratio between excitatory and inhibitory connections is balanced.
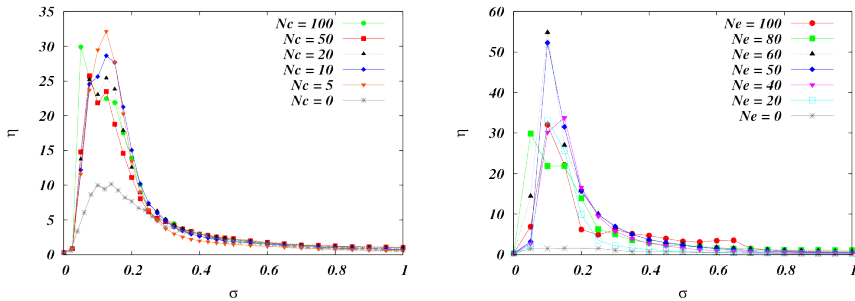
**Figure 4.7:** (a) Spectral amplification factor $\eta$ as a function of $\sigma$ when the fraction of connected neurons $Nc$ decrease.  (b) $\eta$ as a function of $\sigma$ for an decreasing number of excitatory synapses $Ne$.  Other parameters: $g_0^L = 2.0$, $A = 0.25$ and $T = 400$ $ms$.

## Electrical coupling

In this section we concentrate in the situation where the neurons are diffusively coupled. Figure 4.8 shows the spectral amplification factor as a function of the diversity for different fraction of connected neurons $Nc$. In this situation, when the neurons are diffusively coupled, the percentage of connected neurons $Nc$ has a significant effect. For $Nc \lesssim 10$, the response of the system improves with the number of coupled neurons. Beyond $Nc \approx 10$, increasing the number of connected neurons does not improve the response of the system. With the aim of illustrating the response of the system in this coupling configuration, Figure 4.9 shows time traces of ten randomly chosen neurons and the raster plots of the ensemble for different values of the diversity parameter. The phenomenon is clearly illustrated in this figure. When the neurons are almost identical, the system slightly reacts to the external signal. Only few neurons spike with the periodicity of the modulation being not enough to induce the rest of the neurons to fire. On the contrary, the right amount of diversity leads the fraction of neurons that follows the modulation to increase and, due to the coupling, pull the others entailing a collective response. If the neurons are too different to each other, there is a high resistance to be dragged and the system is not able to react to the signal because the neurons fire incoherently.
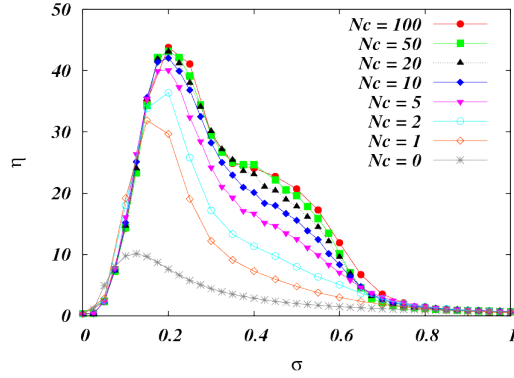
**Figure 4.8:** Spectral amplification factor $\eta$ as a function of the diversity $\sigma$ when the percentage of connected neighbors $Nc$ increases. Other parameters: $g_0^L = 2.0$, $A = 0.25$ and $T = 400\ ms$.
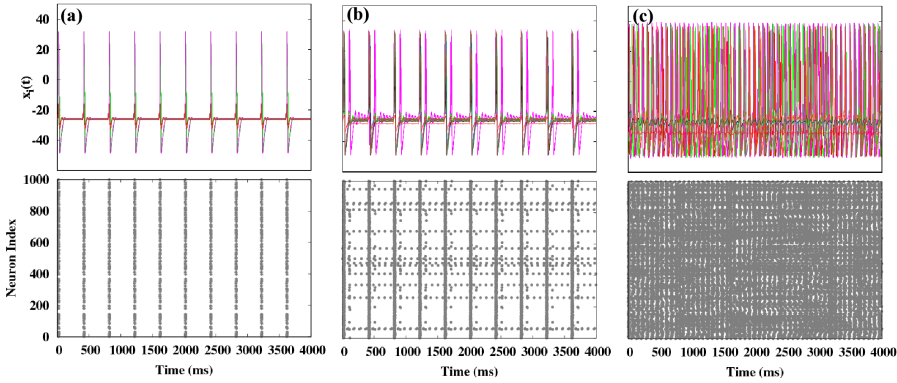


**Figure 4.9:** Time traces of ten randomly chosen neurons and rasterplot of the ensemble for three different values of the diversity: (a) $\sigma = 0.05$, (b) $\sigma = 0.2$ and (c) $\sigma = 0.8$. Other paremeters: $g_0^L = 2.0$, $A = 0.25$ and $T = 400\ ms$.

## 4.3

# Order Parameter Expansion

To gain insight into the obtained results we perform some theoretical analysis of the FHN model under the presence of diffusive coupling. To this end we follow the order parameter expansion developed in [79, 80]. This is simply an expansion of the dynamical variables around their mean-field values $x_j(t) = X(t) + \epsilon_j^x(t)$, $y_j(t) = Y(t) + \epsilon_j^y(t)$ and the diversity parameter around its mean value $a_j = a + \epsilon_j^a$. The validity of this expansion relies on the existence of a coherent behavior by which the individual units $x_j$ deviate in a small amount $\epsilon_j^x$ from the global behavior characterized by the mean-field variable $X(t)$. It also assumes that the deviations $\epsilon_j^a$ are small. For this particular model, there is no need to expand the equation for $\dot{y}_i$, since it is linear in all the variables, although we write the equation initially for a more general nonlinear dependence. We also expand the equation for $\dot{x}_i$ up to second order, with the resulting equations being

$$\epsilon \dot{x}_i = f(X,Y) + f_x(X,Y)\epsilon_i^x + f_y(X,Y)\epsilon_i^y + \frac{1}{2}f_{xx}(X,Y)\left(\epsilon_i^x\right)^2 \quad (4.14)$$

$$\dot{y}_i = g(X,Y,a) + g_x(X,Y,a)\epsilon_i^x + g_a(X,Y,a)\epsilon_i^a. \quad (4.15)$$

Here

$$f(x,y) = x(1-x)(x-b) - y + d - Kx \quad (4.16)$$

and

$$g(x,y,a) = x - cy + a. \quad (4.17)$$

If we average Eqs. (4.14)-(4.15) using $\langle \cdot \rangle = \frac{1}{N}\sum_i \cdot$ we obtain:

$$\epsilon \dot{X} = f(X,Y) + \frac{1}{2}f_{xx}(X,Y)\Omega^x \quad (4.18)$$

$$\dot{Y} = g(X,Y,a) \quad (4.19)$$

where we have used $\langle \epsilon_j^x \rangle = \langle \epsilon_j^y \rangle = \langle \epsilon_j^a \rangle = 0$ and defined the second moments $\Omega^x = \langle (\epsilon_j^x)^2 \rangle$, $\Omega^y = \langle (\epsilon_j^y)^2 \rangle$ and $\sigma^2 = \langle (\epsilon_j^a)^2 \rangle$; and the shape factors $\Sigma^{xy} = \langle \epsilon_j^x \epsilon_j^y \rangle$, $\Sigma^{xa} = \langle \epsilon_j^x \epsilon_j^a \rangle$ and $\Sigma^{ya} = \langle \epsilon_j^y \epsilon_j^a \rangle$. One can find the evolution

equations for the second moments, which follows simply from the first-order expansion $\dot{\epsilon}_j^x = \dot{x}_j - \dot{X}$, so that $\dot{\Omega}^x = 2\langle \epsilon_j^x \dot{\epsilon}_j^x \rangle$ and $\dot{\Sigma}^{xy} = \langle \dot{\epsilon}_j^x \epsilon_j^y + \epsilon_j^x \dot{\epsilon}_j^y \rangle$.

$$\epsilon \dot{\epsilon}_i^x = f_x \epsilon_i^x + f_y \epsilon_i^y + \frac{1}{2} f_{xx} \left[ \left( \epsilon_i^x \right)^2 - \Omega^x \right] \tag{4.20}$$

$$\dot{\epsilon}_i^y = g_x \epsilon_i^x + g_y \epsilon_i^y + g_a \epsilon_i^a \tag{4.21}$$

$$\dot{\Omega}^x = \frac{2}{\epsilon} \left[ f_x \Omega^x + f_y \Sigma^{xy} \right] \tag{4.22}$$

$$\dot{\Omega}^y = 2 \left[ g_x \Sigma^{xy} + g_y \Omega^y + g_a \Sigma^{ya} \right] \tag{4.23}$$

$$\dot{\Sigma}^{xy} = \frac{1}{\epsilon} \left[ f_x \Sigma^{xy} + f_y \Omega^y \right] + g_x \Omega^x + g_y \Sigma^{xy} + g_a \Sigma^{xa} \tag{4.24}$$

$$\dot{\Sigma}^{xa} = \frac{1}{\epsilon} \left[ f_x \Sigma^{xa} + f_y \Sigma^{ya} \right] \tag{4.25}$$

$$\dot{\Sigma}^{ya} = g_x \Sigma^{xa} + g_y \Sigma^{ya} + g_a \sigma^2 \tag{4.26}$$

The system of Eqs. (4.18)-(4.19) together with Eqs. (4.22)-(4.26) form a close set of differential equations for the mean-field variables $X(t)$ and $Y(t)$

$$\epsilon \dot{X} = -X^3 + (1+b)X^2 - (b + 3\Omega^x)X + (1+b)\Omega^x + d - Y \tag{4.27}$$

$$\dot{Y} = X - cY + a \tag{4.28}$$

$$\epsilon \dot{\Omega}^x = 2(-3X^2 + 2(1+b)X - b - K)\Omega^x - 2\Sigma^{xy} \tag{4.29}$$

$$\dot{\Omega}^y = 2 \left[ \Sigma^{xy} - c\Omega^y + \Sigma^{ya} \right] \tag{4.30}$$

$$\dot{\Sigma}^{xy} = \frac{1}{\epsilon} \left[ (-3X^2 + 2(1+b)X - b - K)\Sigma^{xy} - \Omega^y \right]$$
$$+ \Omega^x - c\Sigma^{xy} + \Sigma^{xa} \tag{4.31}$$

$$\epsilon \dot{\Sigma}^{xa} = (-3X^2 + 2(1+b)X - b - K)\Sigma^{xa} - \Sigma^{ya} \tag{4.32}$$

$$\dot{\Sigma}^{ya} = \Sigma^{xa} - c\Sigma^{ya} + \sigma^2 \tag{4.33}$$

Numerical integration of this system allows us to compute the spectral amplification factor (Eq. (4.7)) using the theoretical prediction of $X(t)$. Figure 4.10 shows this analytic result together with the numerical integration of the full system.

It can be seen that the order parameter expansion developed here fits
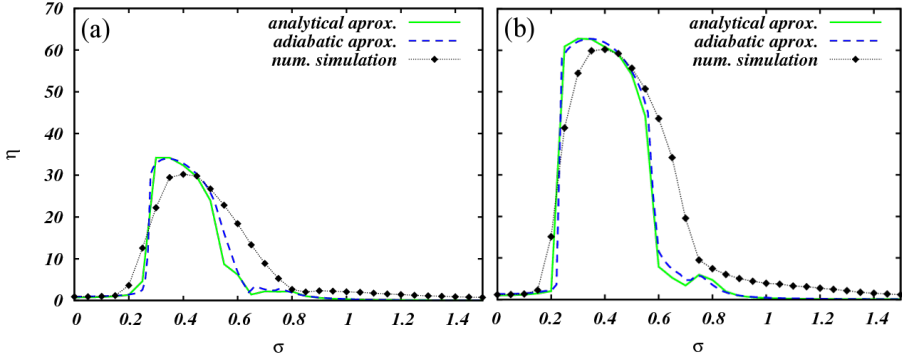
**Figure 4.10:** Order parameter expansion versus numerical integration of the fullsystem. An adiabatic approximation is also included (see text below). (a) $T = 1.6$ and (b) $T = 1.11$. Other parameter as in Figure 4.3.

quite well with the numerical integration of the full system.

We can also use (4.29)-(4.33) to obtain the value of $\Omega^x$. An adiabatic elimination of these variables, i.e., $\dot{\Omega}^x = \dot{\Omega}^y = \dot{\Sigma}^{xy} = \dot{\Sigma}^{xa} = \dot{\Sigma}^{ya} = 0$, yields:

$$\Sigma^{xa}_{ad} = \frac{\sigma^2}{cH(x) - 1} \tag{4.34}$$

$$\Sigma^{ya}_{ad} = \frac{H(x)\sigma^2}{cH(x) - 1} \tag{4.35}$$

$$\Sigma^{xy}_{ad} = \frac{H(x)\sigma^2}{(cH(x) - 1)^2} \tag{4.36}$$

$$\Omega^x_{ad} = \frac{\sigma^2}{(cH(x) - 1)^2} \tag{4.37}$$

$$\Omega^y_{ad} = \frac{H^2(x)\sigma^2}{(cH(x) - 1)^2} \tag{4.38}$$

with $H(x) = -3x^2 + 2(1 + b)x - b - K$. Substituting $\Omega^x_{ad}$ in (4.27)-(4.28), we can find a closed form for the equations describing the evolution of the

104

mean-field $X(t)$ and $Y(t)$:

$$\epsilon \dot{X} = -X^3 + (1+b)X^2 - \left[b + \frac{3\sigma^2}{(cH(X)-1)^2}\right]X$$

$$+ \frac{(1+b)\sigma^2}{(cH(X)-1)^2} + d - Y \tag{4.39}$$

$$\dot{Y} = X - cY + a \tag{4.40}$$

With the mean-field variable $X(t)$ obtained from the adiabatic elimination we can estimate the spectral amplification factor $\eta$. Figure 4.10 displays $\eta$ obtained from the adiabatic elimination together with the numerical simulation and the order parameter expansion. To illustrate the influence of the diversity, Figure 4.11 shows the nullclines $Y1(X, \sigma)$ and $Y2(X, a)$ of Eq. (4.39)-(4.40) for $a = 0.06$ and different values of the diversity $\sigma = 0.0$, 0.5, 0.8, 1.0, 1.2 and 1.4. The diversity changes the shape of the cubic nullcline $Y1$ leading to a lose of stability of the fix point of the system that, for a certain range of $\sigma$, become a limit cycle.
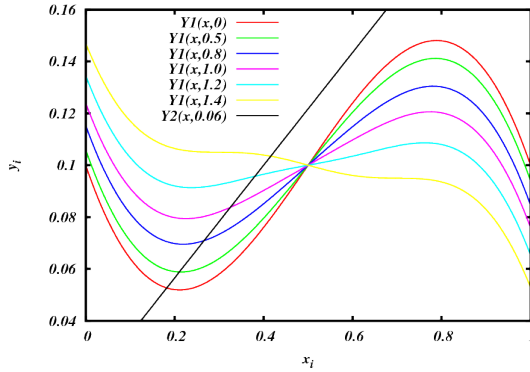


**Figure 4.11:** Nullclines of Eq. (4.39)-(4.40).

To schematize the behavior of the mean-field variables $X$ and $Y$ when the diversity changes, we show in Figure 4.12 the phase-portrait for different values of $\sigma = 0.0$, 0.5, 0.8, 1.0, 1.2 and 1.4 (corresponding to the values represented in Figure 4.11). It can be seen that there is a range of $\sigma$ for which the system exhibits a collective oscillatory behavior even in the

absence of the weak external modulation.
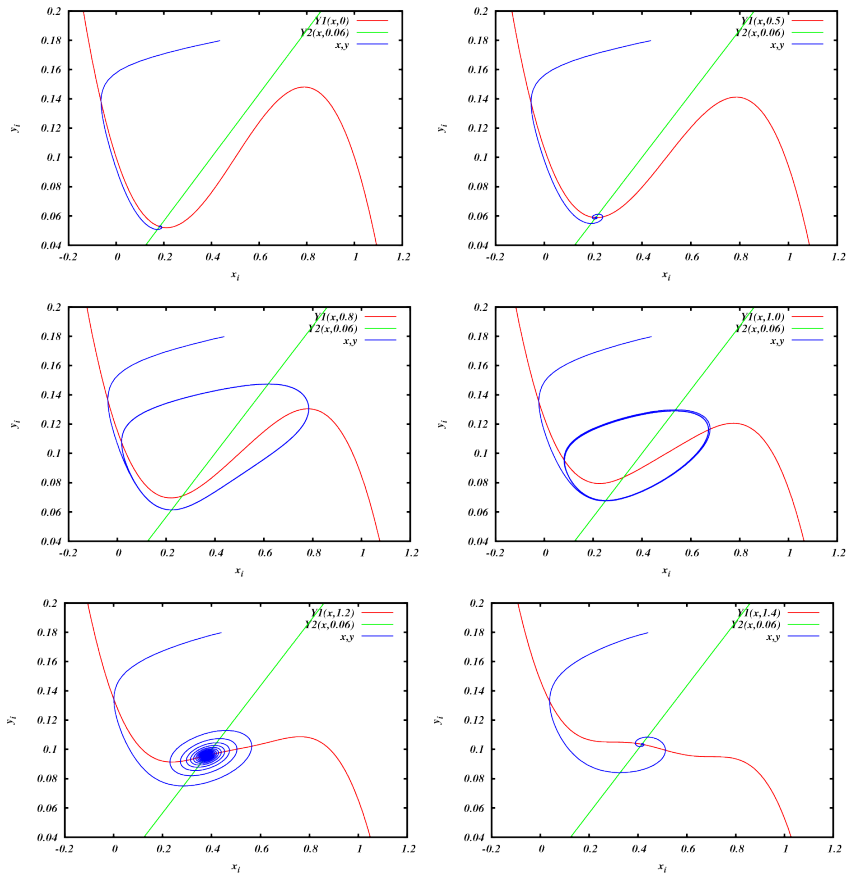


**Figure 4.12:** Phase-space portrait for different values of $\sigma = 0.0, 0.5, 0.8, 1.0, 1.2$ *and* $1.4$.

4.4

# Conclusions

In this chapter we have studied the effect of the diversity in an ensemble of neurons described by two different neuronal models. We have observed that under certain conditions diversity can enhance the response of the system to an external periodic modulation. We have also developed an order parameter expansion obtaining a good fit with the results obtained numerically for the diffusively coupled FHN system. The mechanism leading the system to a resonant behavior with the external signal is as follows: in the homogeneous situation, where all the units are identical, the weak external modulation cannot induce any spike in the system. When the diversity increases, a fraction of the neurons enters in the oscillatory regime and, due to the interactions, pull the other neurons leading the system to an oscillatory collective behavior following the external signal. For larger values of the diversity, the fraction of neurons inside the oscillatory regime decreases and the rest of neurons offer some resistance to be pulled by the oscillatory ones, thus, the system cannot respond to the external signal. We have also found that the number of coupled units become fundamental in the enhancement of the response of the system. These results suggest that the diversity present in biological systems may have an important role in order to enhance the response of the system to (or the detection of) weak signals.

**Part II**

# Topology, delay, and consistency

# Effect of the topology and delay in neuronal networks

As important as the intrinsic properties of an individual nervous cell stands the network of neurons in which it is embedded and by virtue of which it acquires much of its responsiveness and functionality. Synchronization on complex networks is an important topic under study in neuroscience [81, 82] due to its role in the processing and transmission of information across the nervous system [27, 83]. Also delays are intrinsic of neuronal systems due to the finite propagation speed in the transmission along the axons and due to the time lapses occurring in the synaptic processing [84]. These time delays can change the properties of the dynamics: delays can induce or destroy stable oscillations, enhance or suppress synchronization or generate complex spatiotemporal patterns [85, 86].

In this chapter we explore how the topological properties and conduction delays of several classes of neural networks affect the capacity of their constituent cells to establish well-defined temporal relations among the firing of their action potentials. This ability of a population of neurons to produce and maintain a millisecond-precise coordinated firing (either

---

evoked by external stimuli or internally generated) is central to neural
codes exploiting precise spike timing for the representation and commu-
nication of information.

The chapter is organized as follows: in the first part the description of
the system, the mathematical details of the neuronal model and the order
parameter used together with the description of the studied topologies are
provided. We consider two main situations: one in which all the axonal
delays take the same value (homogeneous delays) and the situation in
which the delays are different (heterogeneous delays). In section 5.2 we
present the result for the homogeneous delays and identical neurons.
Section 5.3 concerns to the situation in which the natural frequencies
of the neurons are different. An anatomical experimentally determined
network is considered in section 5.4. Afterwards, section 5.5 deals with
the situation in which the axonal delays are heterogeneous. Finally, in the
last section, the conclusions are presented.

## 5.1
# Description of the system

Our aim is to study the interplay between the conduction delays and the
topology of the network in an ensamble of delay interconnected neurons.
In order to understand the role played by the pathways in which the
neurons interact with each other, we consider different interconnection
topologies, ranging from a regular one-dimensional lattice to scale-free
networks. Figure 5.1 shows a schematic representation of the system.
We consider an ensemble of one thousand excitable neurons, whose dy-
namical behavior is described by the Hodgkin and Huxley model [4]

$$C_m \dot{v}_i = I_i - g_{Na} m^3 h(v_i - V_{Na}) - g_K n^4(v_i - V_K) - g_L(v_i - V_L) - I_i^{syn} \quad (5.1)$$

where $v_i$ represents the membrane potential of neuron $i$; $C_m = 1 \ \mu F/cm^2$ is
the membrane capacitance per unit area; $I_i$ is the external current; $I_i^{syn}$ is the
synaptic current; $g_{Na} = 120 \ mS/cm^2$, $g_K = 36 \ mS/cm^2$ and $g_L = 0.3 \ mS/cm^2$
are the maximum conductance of the sodium, potassium and leakage
channels and $V_{Na} = 50 \ mV$, $V_K = -77 \ mV$ and $V_L = -54.5 \ mV$ stand for
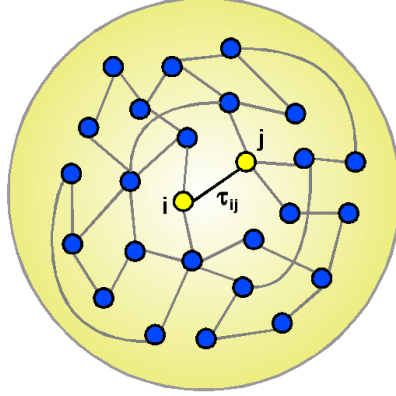
**Figure 5.1:** Schematic representation of the neuronal network considered.

the corresponding reversal potentials. The voltage dependent activating and inactivating variables are $h$, $m$ and $n$ respectively. According to Hodgkin and Huxley formulation these voltage-gated ion channels are described by the following set of differential equations

$$
\begin{aligned}
\dot{m} &= \alpha_m(v)(1-m) - \beta_m(v)m, & (5.2) \\
\dot{h} &= \alpha_h(v)(1-h) - \beta_h(v)h, & (5.3) \\
\dot{n} &= \alpha_n(v)(1-n) - \beta_n(v)h, & (5.4)
\end{aligned}
$$

where the gating variables $m$, $h$, and $n$ represent the activation and inactivation of the sodium channels and the activation of the potassium channels, respectively. The experimentally fitted voltage-dependent transition rates are

$$\alpha_m(V) = \frac{0.1(V + 40)}{1 - \exp\left(-(V + 40)/10\right)} , \tag{5.5}$$

$$\beta_m(V) = 4 \exp\left(-(V + 65)/18\right) , \tag{5.6}$$

$$\alpha_h(V) = 0.07 \exp\left(-(V + 65)/20\right) , \tag{5.7}$$

$$\beta_h(V) = [1 + \exp\left(-(V + 35)/10\right)]^{-1} , \tag{5.8}$$

$$\alpha_n(V) = \frac{0.01(V + 55)}{1 - \exp\left(-0.1(V + 55)\right)} , \tag{5.9}$$

$$\beta_n(V) = 0.125 \exp\left(-(V + 65)/80\right) . \tag{5.10}$$

The synaptic transmission between neurons is modeled, following [53], by a postsynaptic conductance change with the form of an alpha-function. The synaptic current is defined as

$$I_i^{syn} = \frac{g_{max}}{N} \sum_{spikes \in v(i)} \alpha\left(t - t_{spike} - \tau_{ij}\right)\left(V(t) - E_{syn}\right) , \tag{5.11}$$

where $g_{max}$ describes the maximum synaptic conductance and the sum is extended over the train of presynaptic spikes occurring at $t_{spike}$ produced by the neighbors connected to of the neuron $i$. For simplicity we assume only excitatory connections and take a value of $E_{syn} = 0$ mV for all the neurons. The alpha-function is defined as

$$\alpha(t) = \frac{1}{\tau_d - \tau_r} \left(\exp\left(-t/\tau_d\right) - \exp\left(-t/\tau_r\right)\right) , \tag{5.12}$$

where the parameters $\tau_d$ and $\tau_r$ stand for the decay and rise times and determine the duration of the response. Synaptic rise and decay times are set to $\tau_r = 0.1$ *ms* and $\tau_d = 3$ ms, respectively. The delay arising from the finite conduction velocity of axons is taken into account through the latency time $\tau_{ij}$. The first order differential equation describing the dynamic of the membrane potential of the neurons (Eq. (6.1)) are solved using a fourth order Runge-Kutta algorithm with time step $\Delta t = 0.02$ *ms*.

In order to avoid trivial spiking solutions, the initial conditions are chosen as follows: the membrane potential of each neurons are uniformly distributed in the range $[-65, 25]$ $mV$. During the first 250 $ms$ of simulation we randomly switch on the applied current of each neuron. Then, we leave the system to evolve over 250 $ms$. After this, we interconnect the neurons and leave the system to evolve for 1 $s$ before collecting any data.

### 5.1.1 Interconnection topologies

The synchronization of neurons may depend on the network in which they are embedded. To study the role played by the different synaptic pathways in the synchronization of our ensemble of neurons, we consider five different topologies: regular, small-world, random, scale-free and globally coupled networks.

In the regular lattice, neurons are connected with the four nearest-neighbors using periodic boundary conditions. To construct a small-world network we use the algorithm proposed by Watts and Strogatz [87]. The basic idea behind this algorithm is to start with a regular lattice, and with a certain probability $p$ that each link is rewired to another node randomly chosen from all possible nodes that avoid self-loops and link duplications. In the limit in which the rewaring probability is one, the random network is obtained.

The scale-free network was introduced by Barabási and Albert [88] and is based on a preferential attachment mechanism. The main feature of this network is that it does not have a characteristic defined scale. Most of the nodes are connected with few elements and only a few nodes are connected with many elements.

We also consider the situation where each neuron is connected with all others neurons conforming the network, we refer to this case as the all-to-all or mean-field configuration.

### 5.1.2 **Data analysis**

To characterize the synchronization in our network of neurons, we define
the phase of neuron $i$ as [89]:

$$\phi_i(t) \quad = \quad 2\pi \frac{t - \tau_k}{\tau_{k+1} - \tau_k}, \tag{5.13}$$

where $\tau_k$ is the time of the $k$th firing of the neuron $i$. The idea behind this
phase definition is that the phase of a neuron experiments a change of $2\pi$
between spikes. To measure the phase synchronization of neuron $i$ with
its neighbors, we define the quantity:

$$s_i(t) \quad = \quad \frac{1}{n_i} \sum_{j \in v(i)} \sin^2 \left( \frac{\phi_i(t) - \phi_j(t)}{2} \right), \tag{5.14}$$

with $n_i$ being the degree of neuron $i$, i.e., the number of connected neigh-
bors of the neuron $i$. Averaging over elements and integrating in time,
we obtain

$$S^{loc} \quad = \quad \lim_{T \to \infty} \frac{1}{T} \int_0^T \left( \frac{1}{N} \sum_{i=1}^{N} s_i \right) dt, \tag{5.15}$$

that gives a measure of the average of the local phase synchronization
in the coupled system. To measure the global synchronization over the
network we extend the sum over neighbors in Eq. (6.7) to all the neurons.
Then, the global phase synchronization of neuron $i$ is obtained

$$s_i'(t) \quad = \quad \frac{1}{N} \sum_{j=1}^{N} \sin^2 \left( \frac{\phi_i(t) - \phi_j(t)}{2} \right), \tag{5.16}$$

Following the previous definition of the local synchronization index, we
average over elements and time to obtain a global order parameter,

$$S^{glob} \quad = \quad \lim_{T \to \infty} \frac{1}{T} \int_0^T \left( \frac{1}{N} \sum_{i=1}^{N} s_i' \right) dt, \tag{5.17}$$

This order parameter is zero if the phases of all the neurons are equal and
one if they differ by $\pi$. When the phases of the neurons are randomly
distributed, the order parameter takes the value one-half.

5.2

# Homogeneous ensemble

First we analyze the ideal case of identical neurons and all the $\tau_{ij}$ equal to each other. We quantify the local and global synchronization by means of the indices defined in section 5.1.2. We investigate the effect of the randomness of the interconnections as well as the effect that the number of connected neighbors has in the synchronization of the system. The final firing frequency distribution of our ensemble in different situations is also presented. Then, we consider the situation in which the natural frequencies of the neurons are distributed around a mean value according to a Gaussian distribution. Finally, we particularize our study to an anatomical network determined experimentally from the macaque cortico-cortical network [90].

### 5.2.1 Axonal delays defines local and global synchronization properties

As we said before, we start our study by considering the situation in which the delays in the connection between neurons are all identical. Figure 5.2 shows the contour plot of the local and global synchronization indices, $S^{loc}$ and $S^{glob}$ respectively, when the coupling strength between the neurons and the delay along the connections are varied.
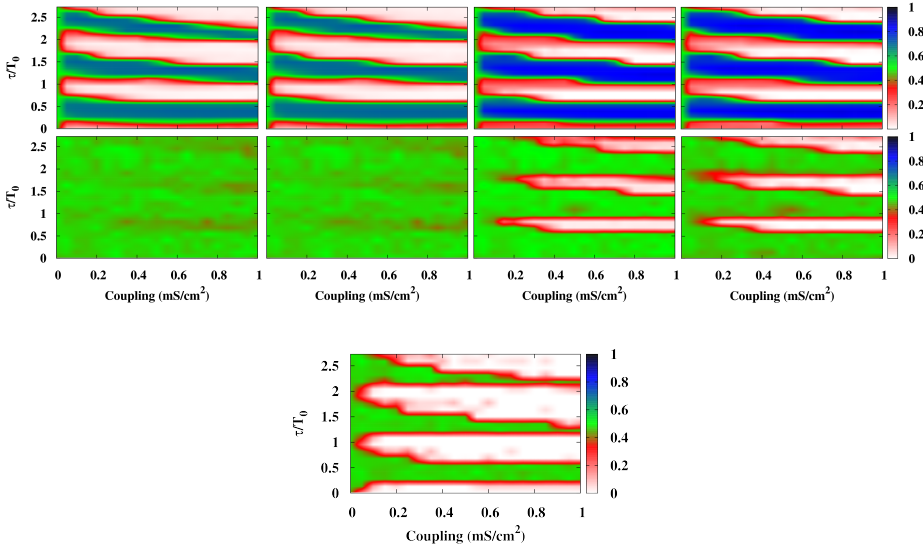
**Figure 5.2:** Upper panel: Contour plots of $S^{loc}$ (top row) and $S^{glob}$ (bottom row) in the coupling-delay phase space. Columns, from left to right, correspond to simulations with different topologies: regular, small-world, random and scale-free. Bottom panel: Contour plot of $S^{glob}$ for the globally coupled network.

The variation of the delay reveals a resonant-like effect in the synchronization even in the mean-field topology. Synchronization (white regions in Figure 5.2) appears for a delay close to (or multiple of) the natural period of the isolated neurons, which corresponds to $T_0 = 14.65$ ms for an injected current of $I = 10$ mA. While synchronized firing activity between one neuron and its neighbors (local synchronization) is achieved in all the networks that we have considered, a high randomness in the connections is required for a global synchronized activity to occur.

In order to illustrate the activity of the network, we show in Figure 5.3 raster plots for a fixed coupling strength and three delay values, for different topologies. It can be seen that for $\tau = 0.82\ T_0$ the neurons spike synchronously. In this situation, the neurons are locally and globally syn-

chronized except for the regular lattice. At a delay close to the natural period $\tau = 0.96 \, T_0$, a variety of behaviors appears. In the regular lattice for example, the neurons are spiking consecutively and the activity sequentially propagates forming a v-shape pattern. Other topologies like the random or the scale-free networks show an out of phase firing state. Interestingly, for $\tau = 1.1 \, T_0$ some of the topologies exhibit an anti-phase state. An example of this state is shown by the random network where neurons fire with a phase difference closed to $\pi$. This is corroborated by a value of $S^{loc}$, represented as a green square in the right y-axis (blue square stands for $S^{glob}$), closed to one.
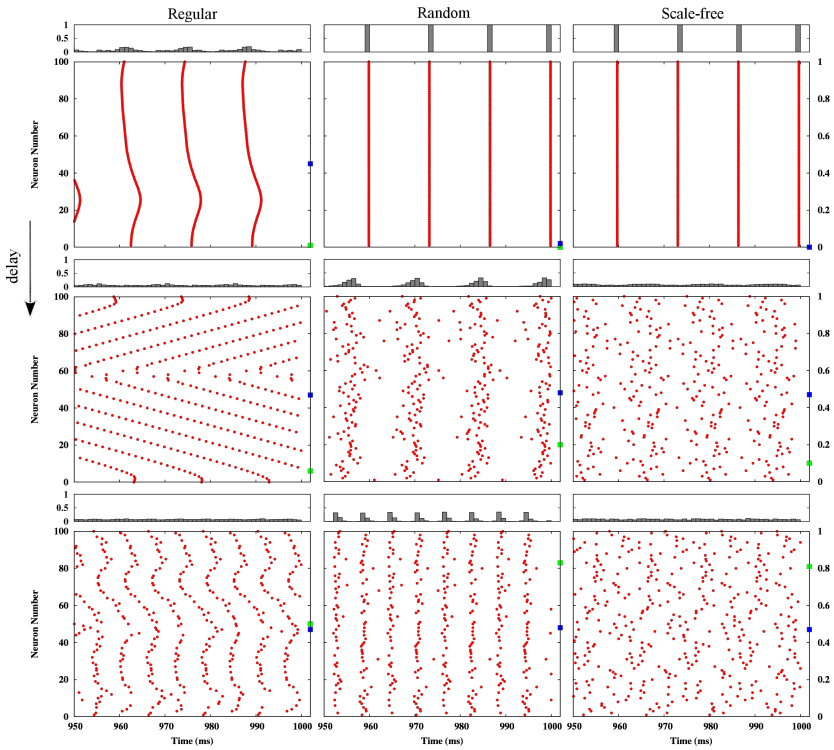
**Figure 5.3:** Raster plots for different values of the delay: $\tau/T_0 = 0.82$ (upper row), $\tau/T_0 = 0.96$ (middle row) and $\tau/T_0 = 1.1$ (bottom row). The coupling strength is fixed to $g_{max} = 0.8\,\mathrm{mS\,cm^{-2}}$ Columns, from left to right, correspond to simulations with different topologies: regular, random and scale-free. Green and blue squares plotted at the right y-axis represent the values of $S^{loc}$ and $S^{glob}$ respectively. Only the fist one hundred neurons are shown. Panels on top of each figure refer to firing histogram of the whole network in the corresponding situation.

To illustrate better this scenario, Figure 5.4 shows the membrane voltage time trace of one randomly chosen neuron and its neighbors in the random network. Three different states clearly emerge. Neurons spike in-phase when the network is locally and globally synchronized ($\tau = 0.82\ T_0$). Then, an increase of the delay in the connections ($\tau = 0.96\ T_0$) leads to a

degradation of the synchronization due to an out-of-phase firing of the neurons. Further increasing the delay, for $\tau = 1.1 \, T_0$, makes the neurons start to fire in anti-phase. Two clusters formed by neurons spiking with the same phase but with a phase difference close to $\pi$ with respect to the other group are observed.
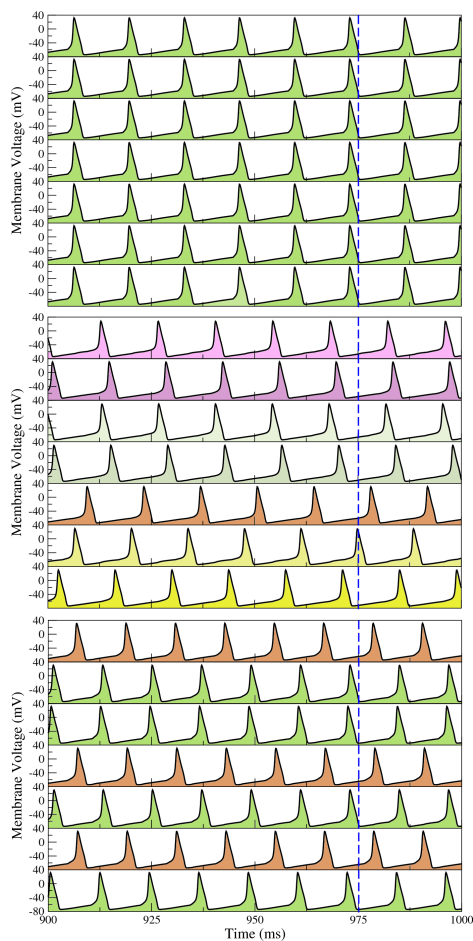


**Figure 5.4:** Time traces of the membrane potential of one neuron and its neighbors for different values of the delay in a random network. Upper row: $\tau/T_0 = 0.82$. Middle row: $\tau/T_0 = 0.96$. Bottom row: $\tau/T_0 = 1.1$. The coupling strength is fixed to $g_{max} = 0.8$ mS cm$^{-2}$.

## 5.2.2 **Role of the long-range connectivities and interaction strength in the synchronization**

In order to understand the role played by large-range interconnections, we randomize the regular one-dimensional lattice. Figure 5.5 shows the global and local order parameter as a function of the rewiring probability, i.e., the number of long-range connections, in the network. For a value of the delay of $\tau/T_0 = 0.82$ and a small coupling $g_{max} = 0.2$ $mS$ $cm^{-2}$ the activity of the network is locally synchronized but not globally. While increasing the rewiring probability the activity of the network becomes globally more synchronized while locally the state remains unchanged.
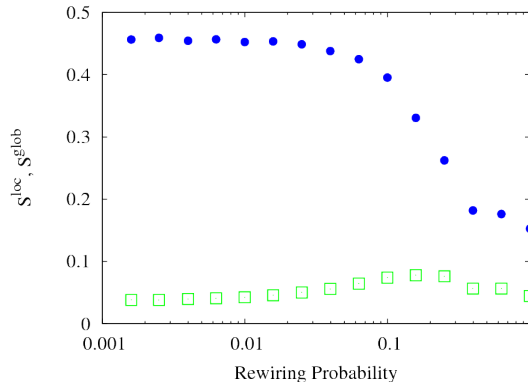


**Figure 5.5:** Rewiring dependence of $S^{loc}$ (green open squares) and $S^{glob}$ (blue circles) for a coupling value of $g_{max} = 0.2$ mS cm$^{-2}$ and delay time of $\tau = 12$ ms.

We also investigate the effect of increasing the number of connected neurons in the regular lattice. We observe a gradual transition from a global desynchronized state to a synchronized one for a fraction of neighbors around the 10% (see Figure 5.6). Afterwards, for these particular values of the coupling and delay, the synchronization quality slightly degrades as the number of connected neighbors increases. However, local and global measures remain identical above the mentioned percentage indicating that any local dynamic is reflected in the global behavior.
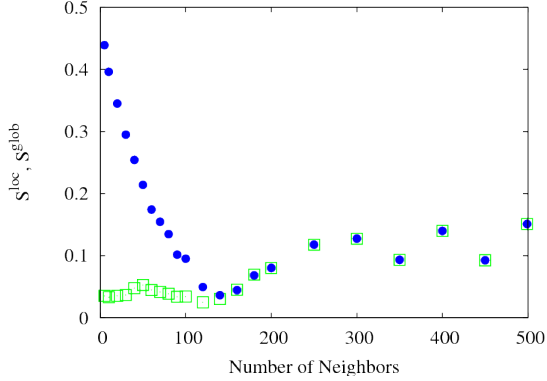
**Figure 5.6:** Dependence on the number of neighbors of $S^{loc}$ (green open squares) and $S^{glob}$ (blue circles) for a fixed coupling value of $g_{max} = 0.2$ mS cm$^{-2}$ and delay time of $\tau = 12$ ms.

### 5.2.3  **Order parameter clustering**

Despite the fact that all networks display the same local synchronization behavior, the way in which they reach it is different. To illustrate this we plot in Figure 5.7 the individual order parameter $s_i$ of each neuron versus the average value of its connected neighbors $\langle s_i \rangle_{nn}$.

In Figure 5.7 we show the results for a regular network. A transition of the local order parameter from a clustering in the complete desynchronized stated to a highly packed cloud of points around small values of $s_i$ in the locally synchronized state is observed. This transition is reached through an intermediate state of partial synchronization shown in the middle column. Other topologies show different transitions from desynchronized to synchronized states. The random network, for instance, does not exhibit the clustering of $s_i$ for the desynchronized state and the dispersion in the completely synchronized one is much larger than for the regular lattice. The mean-field topology, i.e., when all the neurons are connected with all other neurons in the network, exhibits a similar scenario than the random network.
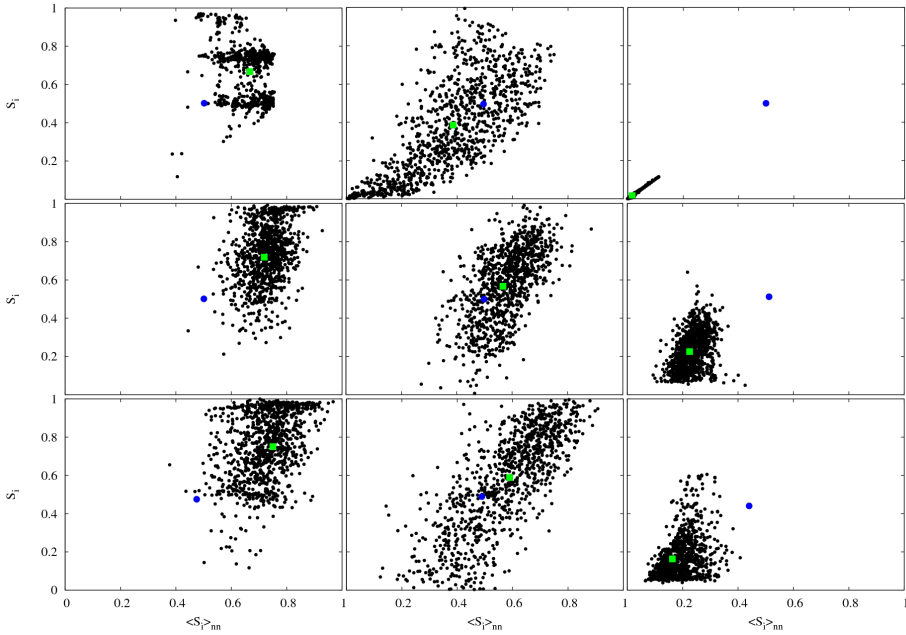
**Figure 5.7:** Plot of the individual local order parameter $s_i$ versus
the averaged value of its neighbors for three different situations.
Left column: $g_{max}$ = 0.2 mS cm$^{-2}$, $\tau$ = 4 ms. Middle column:
$g_{max}$ = 0.2 mS cm$^{-2}$, $\tau$ = 10 ms. Right column: $g_{max}$ = 0.2 mS cm$^{-2}$,
$\tau$ = 14 ms. Rows from top to bottom represent, simulations with
different topologies: regular, random and scale-free respectively.
Green square and blue dot represent the values of $S^{loc}$ and $S^{glob}$,
respectively.

### 5.2.4 **Effective fire frequency**

An important issue to be consider in the model is the frequency at which
the neurons, after a transient, fire due to the interaction with the other
elements of the network. To study this, we compute the density plot of
the histogram of the effective firing frequencies. Figure 5.8 shows the
evolution of the distribution of firing frequencies for different coupling
and delays.

In the left columns of Figure 5.8 it can be seen how, for a small coupling
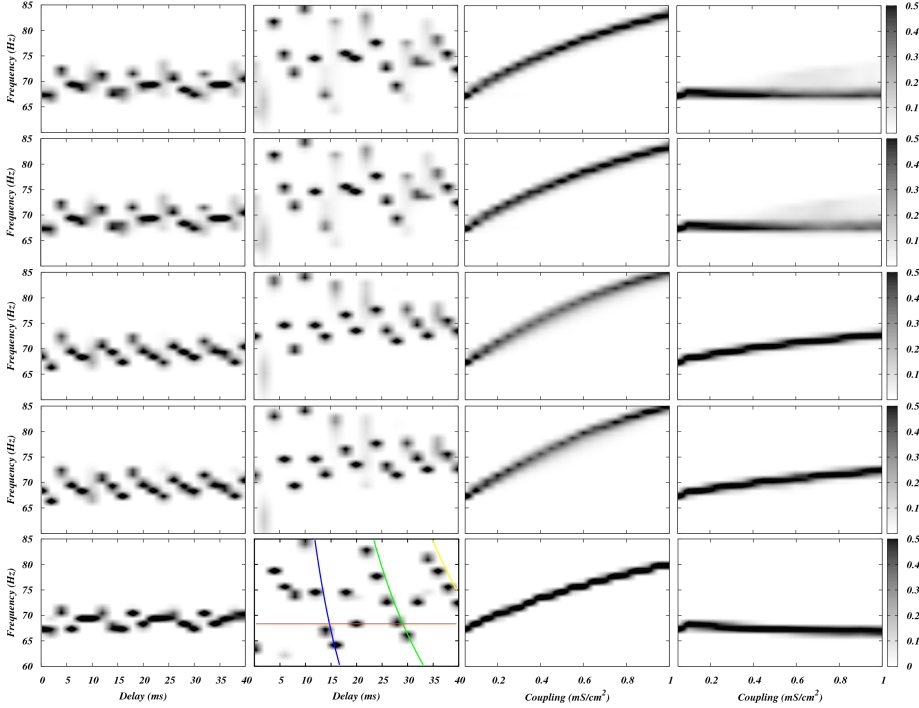
**Figure 5.8:** Density plot of the histogram of the effective firing frequencies. Columns, from left to right: $g_{max} = 0.2$ mS cm$^{-2}$, $g_{max} = 0.8$ mS cm$^{-2}$, $\tau = 4.0$ ms and $\tau = 14.0$ ms. Rows, from top to bottom, simulations with different topologies: regular, small-world, random, scale-free and all-to-all respectively. Blue line correspond to the isoline $\frac{1}{\tau}$, green line to $\frac{2}{\tau}$, yellow line to $\frac{3}{\tau}$ and the orange line indicated the value of the natural frequency of the neurons.

intensity, the frequencies tend to remain close together meanwhile for higher values of the coupling strength, the firing frequencies have a more irregular behavior exhibiting jumps from one value to anothers. Despite the apparent irregular behavior, the discrete jumps of the firing frequency follow the isolines corresponding to the harmonics $\frac{1}{\tau}$, $\frac{2}{\tau}$, etc. (see the colored lines in Figure 5.8). The two columns at the right side, which correspond to different values of the delay, show that the frequency tends to increase as the coupling strength becomes larger. On the other hand, for

a delay close to the intrinsic period, ($\tau$ = 14 ms), the frequency remains
locked to a fix value. This is a clear signature that the system is in a
synchronous state.

## 5.3

# Distribution of natural frequencies

The situation in which the natural frequency of all neurons are identical
is a simplification and is far from a realistic situation. For this reason, we
consider in this section a Gaussian distribution of the natural frequencies
of the neurons around a central frequency $f_0 = 70$ Hz with a dispersion
of $\sigma_{f_0} = 9$ Hz.
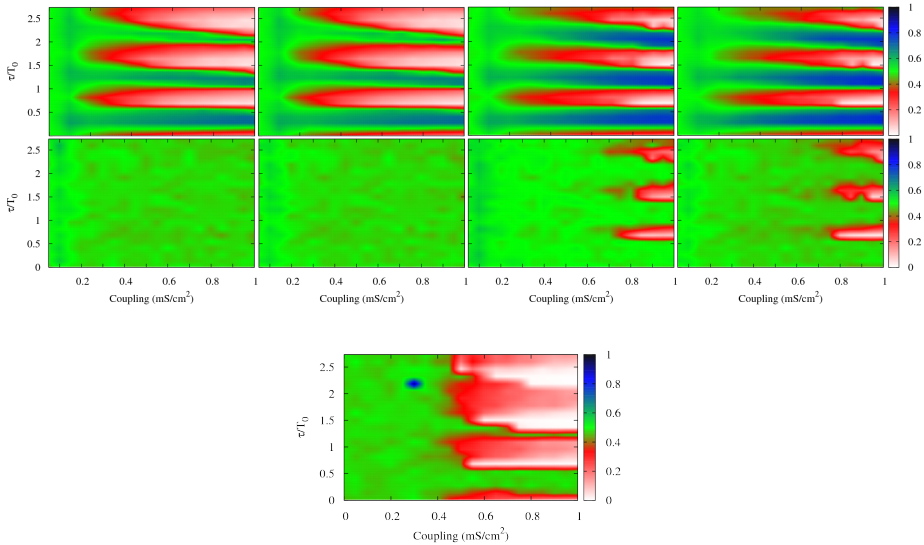


**Figure 5.9:** Upper panel: Contour plots of $S^{loc}$ (top row) and $S^{glob}$
(bottom row) in the coupling-delay phase space. Columns, from left
to right, correspond to simulations with different topologies: reg-
ular, small-world, random and scale-free. Bottom panel: Contour
plot of $S^{glob}$ for the globally connected network.

Basically, the effect of the distribution of the natural frequencies requires an increase of the coupling strength needed to achieve the synchronous state, as it can be seen in Figure 5.9. As expected, global synchronization is more difficult to achieve in this case. In the mean-field situation, the synchronization regions grow and they almost merges in a single region at high coupling values, losing the resonant character of the delay. As in the homogeneous situation, three different states appear. Regions where the neurons are spiking in-phase occur at delays different than the multiples of the intrinsic period, in contrast with the single frequency situation. These regions are indicated by white-red areas in Figure 5.9. There are other regions, corresponding to the blue areas in Figure 5.9, where the neurons spike in anti-phase. These regions are more pronounced in the random and scale-free networks. Separating the regions of in-phase and anti-phase dynamics, it exists an out-of-phase state where the neurons fire with random phases (green areas in Figure 5.9). In contrast with the homogeneous situation, this regime is predominant at low coupling intensities $g_{max} \lesssim 0.2 \ nS/cm^{-2}$ for all the considered delays. Concerning the global synchronization, in-phase synchronization is more difficult to achieve and only the random and scale-free networks exhibit this state at high coupling intensities but only for some particular values of the delay time. The predominant state is the one in which the neurons spike without a well defined phase relationship corresponding to the out-of-phase state indicated by green areas in Figure 5.9.

In order to illustrate the different dynamics that appear in our system, Figure 5.10 shows the raster plots of the firing activity of the neurons for the regular lattice, the random and the scale-free networks. Three different operation conditions corresponding to in-phase, out-of-phase and anti-phase synchronization states for a high coupling intensity are illustrated. For a delay smaller that the intrinsic period, it can be seen how, due to the distribution of frequencies, the in-phase state develops small deviations, more pronounced in the regular lattice. On the contrary, for a delay larger than the natural period, that in the homogeneous ensemble is an anti-phase state, the synchronized state is not well defined and the system operates close to the out-of-phase state. At delays close to the intrinsic

period the neurons fire out-of-phase. The regular lattice exhibits fronts of
propagating activity where the neurons spike consecutively.
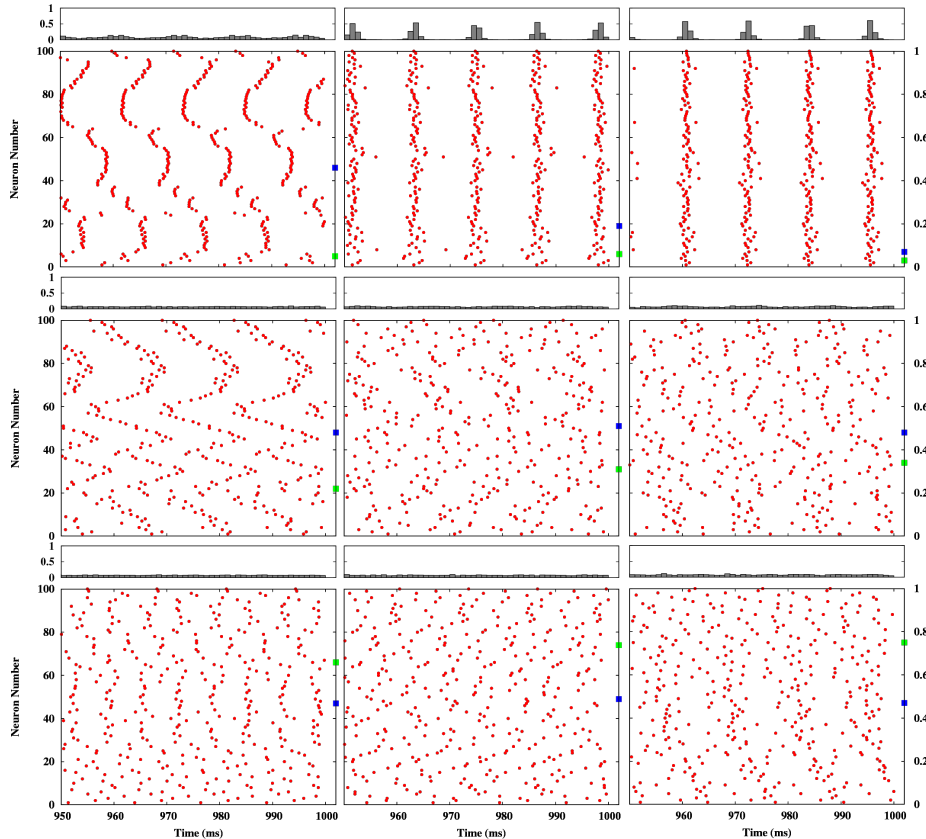


**Figure 5.10:** Raster plot for different values of the delay: $\tau/T_0 = 0.68$
(upper row), $\tau/T_0 = 0.96$ (middle row) and $\tau/T_0 = 1.23$ (bottom
row). The coupling strength is $g_{max} = 0.8$ mS cm$^{-2}$ Columns, from
left to right, correspond to simulations with different topologies:
regular, random and scale-free. Green square and blue dot plotted
at the right y-axis represent for each case the values of $S^{loc}$ and $S^{glob}$
respectively. Only the first one hundred neurons are shown. The
panel on top of each figure corresponds to the firing histogram of
the whole network in the corresponding situation.

### 5.3.1 **Role of the connectivity properties in the locking phenomena**

When the natural frequencies are distributed, at low coupling strength, the effective firing frequency behavior changes significantly with respect to the homogeneous case. Figure 5.11 shows the density plot of the histograms of the effective firing frequencies for different coupling and delay values for our heterogeneous ensamble.
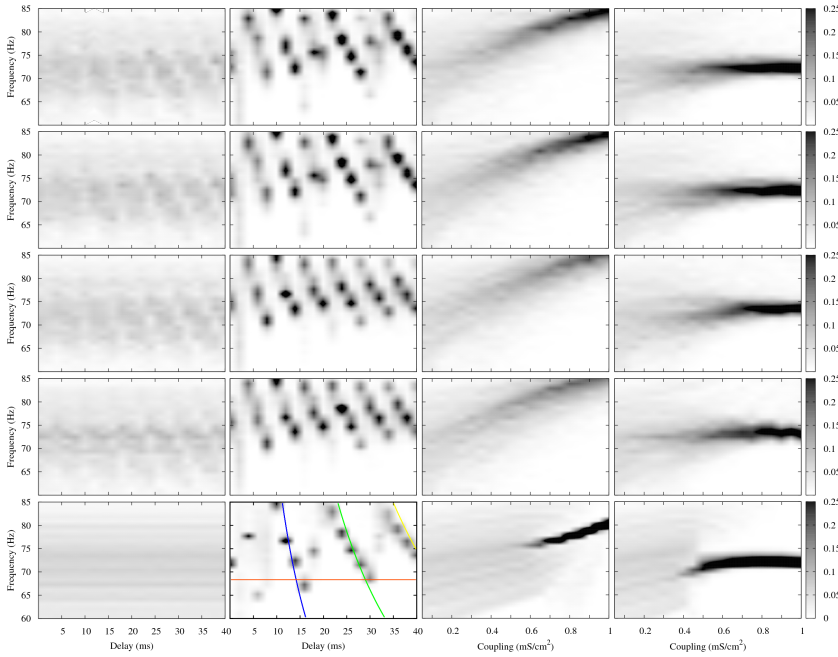


**Figure 5.11:** Density plot of the histogram of the effective firing frequencies. Columns, from left to right are: $g_{max} = 0.2$ mS cm$^{-2}$, $g_{max} = 0.8$ mS cm$^{-2}$, $\tau = 4.0$ ms and $\tau = 14.0$ ms. Rows, from top to bottom represent simulations with different topologies: regular, small-world, random, scale-free and all-to-all respectively. Blue line correspond to the isoline $\frac{1}{\tau}$, green line to $\frac{2}{\tau}$, yellow line to $\frac{3}{\tau}$ and the orange line corresponds to the value of the natural frequency of the neurons.

From left columns in Figure 5.11 it can be seen that for small values of
coupling intensity the firing frequency of the neurons remains disperse
while for higher values exhibits a saw-shape tendency going from higher
values of the firing frequency from desynchronized states to lower values
in the synchronized state. The right columns of Figure 5.11 show that,
for two different fixed values of the delay, a certain minimun coupling
intensity is needed for a well defined firing frequency to occur. For the
desynchronized state, delay of $\tau = 4$ ms, the firing frequency increases
as the coupling strength becomes larger. On the other hand, in the syn-
chronized state, for a delay of $\tau = 14$ ms and beyond a certain coupling
strength, the frequency remains locked to a fixed value close to the natural
mean frequency of the initial distribution.

We can still obtain more information about the distribution of the final
firing frequencies in the case of distributed natural frequencies. Figure
5.12 and 5.13 show the effective firing frequencies versus the natural
frequencies for different networks. In Figure 5.12, corresponding to the
regular lattice, for a fixed coupling strength $g_{max} = 0.2$ mS cm$^{-2}$ and the
two delay values that we have considered (top row), it can be seen a
linear response of the system, except for low frequencies, where a high
dispersion is obtained. When we increase the coupling to $g_{max} = 0.8$
mS cm$^{-2}$ (bottom row of Figure 5.12) we observe how the effective firing
frequency is locked around a certain value even in the desynchronized
case ($\tau = 4$ ms). In Figure 5.12 it can be clearly seen how different delays
induce different firing frequencies.
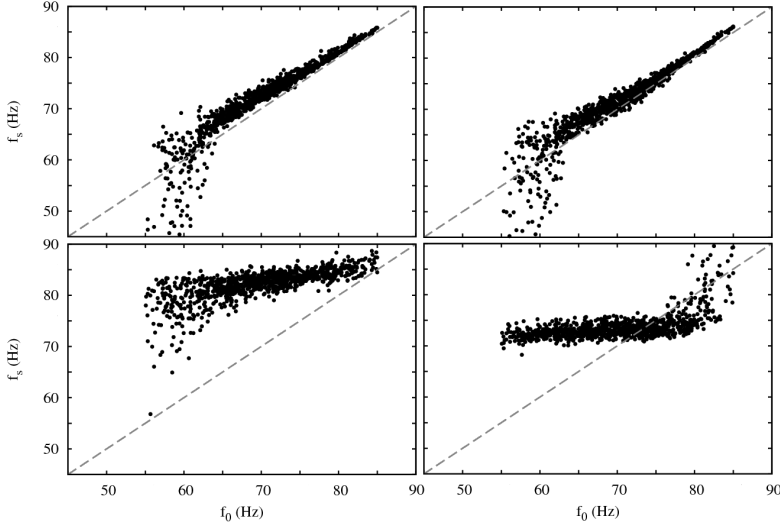
**Figure 5.12:** Effective firing frequencies versus the natural firing frequencies for the regular latice. Top row: fixed coupling of $g_{max}$ = 0.2 mS cm$^{-2}$ and delay of $\tau$ = 4 ms (left panel) and $\tau$ = 14 ms (right panel). Bottom row: fixed coupling of $g_{max}$ = 0.8 mS cm$^{-2}$ and delay of $\tau$ = 4 ms (left panel) and $\tau$ = 14 ms (right panel).

In the all-to-all network, the dispersion of the effective firing frequencies is drastically reduced, as it can be seen in Figure 5.13. For small coupling strength, a clear linear response is obtained. At high couplings, for a delay of 4 ms (desynchronized state), we can observe a cluster of neurons firing with the same frequency, but, due to the dispersion at low frequencies and the different response at high frequencies, this state is globally desynchronized. The synchronous state at high coupling and delay of 14 ms is characterized by a horizontal plateau, indicating that practically all neurons fire, after a transient, with the same frequency independently of its initial natural frequency value.
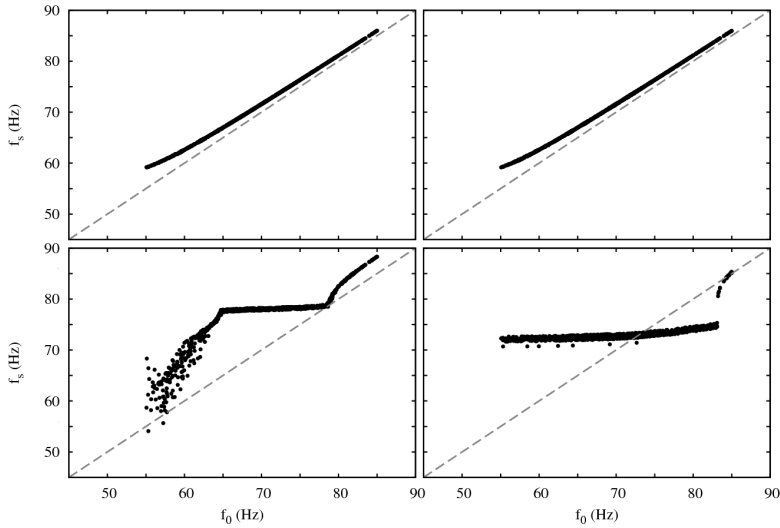
**Figure 5.13:** Effective firing frequencies versus the natural firing
frequencies for the globally coupled network. Top row, fixed cou-
pling of $g_{max} = 0.2$ mS cm$^{-2}$ and delay of $\tau = 4$ ms (left panel) and
$\tau = 14$ ms (right panel). Bottom row, fixed coupling of $g_{max} = 0.8$
mS cm$^{-2}$ and delay of $\tau = 4$ ms (left panel) and $\tau = 14$ ms (right
panel).

## 5.4

# Anatomical network case

As an example of a real anatomical network we investigate the synchro-
nization state in the macaque cortico-cortical network [90]. The network
is composed by 71 nodes representing different cortical areas with 746
links between them. Figure 5.14 shows an organic layout of the cortical
connectivity data set. We consider each node of the network following
the same dynamic as described in section 5.1. We estimate the local and
global degree of synchronization in the network using Eqs. (5.15) and
(5.17) respectively. Figure 5.15 shows $S^{loc}$ and $S^{glob}$ when the coupling
between the neurons and the delay time of the connections are varied.
We compared the results with a randomized version of the network pre-

**Figure 5.14:** Macaque cortical connectivity in a organic layout view.

serving the degree distribution. It can be first noticed that $S^{loc}$ and $S^{glob}$ are practically identical. A reason for this is that the macaque cortical network is densely connected, about 15% of the possible links. This result is in agreement with that obtained in section 5.2.2, where the global synchronization converges to the local one for a percentage of connected neurons above the 10%. The second remarkable feature is the coincidence between the macaque network and the randomized version of the network. A reason for that is that the macaque cortical network has a mean shortest path very similar to the randomized network (see Table 5.4). Another interesting feature is the absence of anti-phase states. Based only on the macaque network we cannot conclude if this fact is a general feature of live brains, but it raises the interesting question if this could happend in other anatomical networks. As it can be seen in Figure 5.15, there are practically no difference between both networks. The reason for this result might be that the original macaque cortico-cortical network has similar properties than a random network with the same degree distribution, as we said before.

Figure 5.16 illustrates the two different states observed in the system.
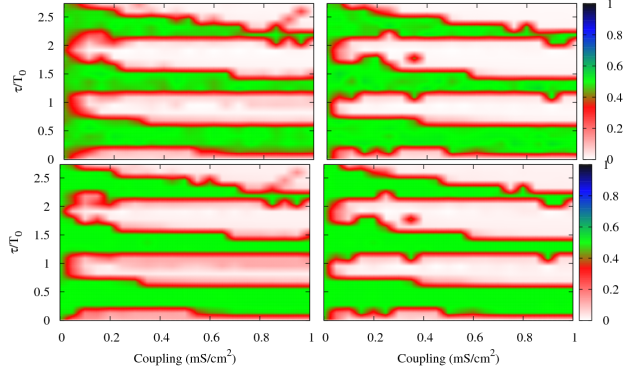
**Figure 5.15:** Top line: Contour plots of $S^{loc}$ (top panel) and $S^{glob}$ (bottom line) in the coupling-delay phase space for the macaque anatomical network. Left column: original macaque 71 cortico-cortical network. Right column: randomized version of macaque 71 cortico-cortical network preserving in and out node degree.

The raster plot of the network corresponding to a coupling intensity of $g_{max} = 0.8$ mS cm$^{-2}$ and delay of $\tau/T_0 = 0.96$ reveals an in-phase synchronous firing of the entire network. On the other hand, increasing the value of the delay to $\tau/T_0 = 1.36$, the firing activity becomes more out-of-phase. This is corroborated by a value of $S^{loc}$ (green square) and $S^{glob}$ (blue square) close to 0.5, represented in the right y-axis.

**Table 5.1:** Macaque Cortical Network properties

| Metric | Clustering | Average degree | Mean shortest path |
|---|---|---|---|
| Macaque Network | 0.46 | 10.5 | 2.33 |
| Randomized version | 0.24 | 10.5 | 2.06 |
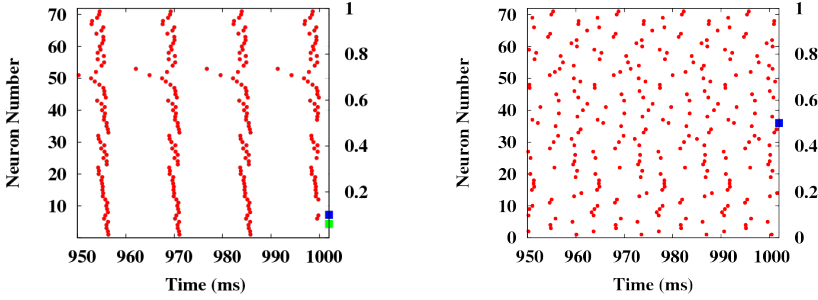
**Figure 5.16:** Rasterplots for different values of the delay: $\tau/T_0 = 0.96$ (left panel) and $\tau/T_0 = 1.36$ (right panel). The coupling strength is $g_{max} = 0.8$ mS cm$^{-2}$. Green and blue square at the right y-axis represent for each case the values of $S^{loc}$ and $S^{glob}$ respectively.

## 5.5

# Heterogeneous delay

In this section we consider the situation in which the interconnection delays are heterogeneous. This effect is modeled by a gamma distribution for the delays with a probability density given by

$$f(\tau_{ij}) = \tau_{ij}^{k-1} \frac{e^{-\tau_{ij}/\theta}}{\theta^k \Gamma(k)} \, , \tag{5.18}$$

where $k$ and $\theta$ are shape and scale parameters of the gamma distribution respectively. The mean time delay is given by $\langle \tau_{ij} \rangle = k\theta$ and the variance of the distribution is $\sigma^2 = k\theta^2$. We limit our study to distributions with a constant variance $\sigma^2 = 1 \, ms$ and we vary the mean value of the distribution in order to scan different conductance delays. As in the previous sections, we compute the local $S^{loc}$ and global $S^{glob}$ order parameters following Eqs. (5.15) and (5.17), respectively. The results are shown in Figure 5.17. As it can be seen, a distribution of the delays with such variance does not have a significant effect in the synchronization regions determined by $S^{loc}$ and $S^{glob}$. At a local scale, the effect that a distribution of delays has in the dynamics of the neurons is illustrated in Figure 5.18. This figure

135
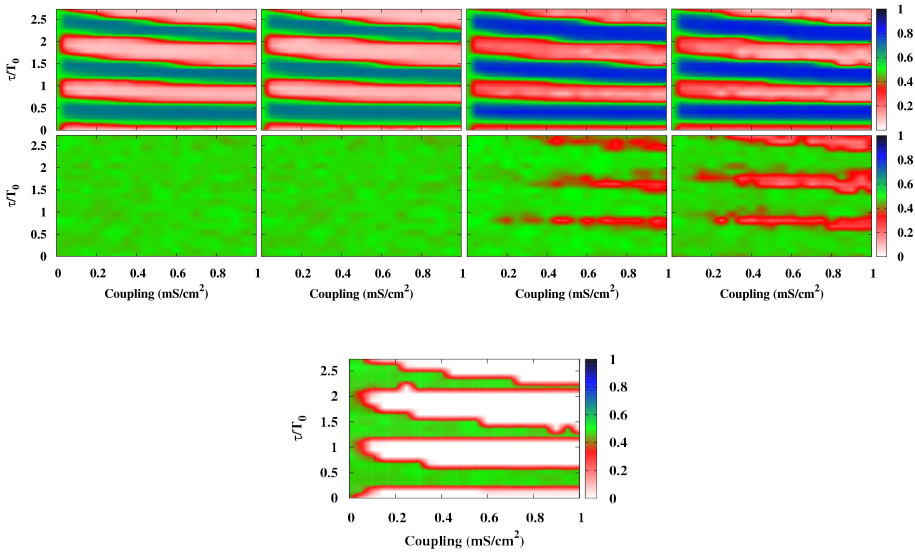
**Figure 5.17:** Upper panel: Contour plots of $S^{loc}$ (top row) and $S^{glob}$ (bottom row) in the coupling-delay phase space for heterogeneous delay. Columns, from left to right, correspond to simulations with different topologies: regular, small-world, random and scale-free. Bottom panel: Contour plot of $S^{glob}$ for the fully connected network.

shows the raster plots for three different topologies: regular, random and scale-free in different operating regimes. Comparing with the single delay situation (Figure 5.3), the distribution of delays induces a small dispersion in the phases of the neurons, but still the same three states (in-phase, out-of-phase and anti-phase) are present. Interestingly, the regular network maintain the sequential propagation of activity conforming the characteristic v-shape patterns. This robust mechanism, that persists even in the presence of heterogeneous delay, could play an important role in signal transmittion in anatomical networks.
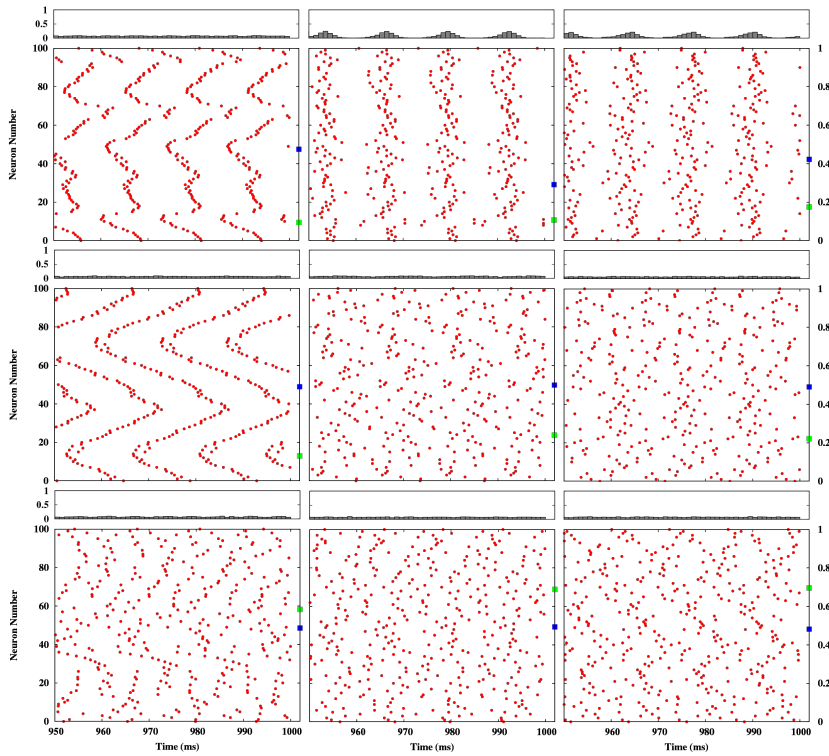
**Figure 5.18:** Raster plots for different values of the delay: $\tau/T_0 = 0.82$ (upper row), $\tau/T_0 = 0.96$ (middle row) and $\tau/T_0 = 1.1$ (bottom row). The coupling strength is $g_{max} = 0.8$ mS cm$^{-2}$ Columns, from left to right, correspond to simulations with different topologies: regular, random and scale-free. Green and blue squares plotted at the right y-axis represent the values of $S^{loc}$ and $S^{glob}$ respectively. Only the fist one hundred neurons are shown. Panel on top of each figure correspond to firing histogram of the entire network in each situation.

5.6 ──────────────────────────────────────

# Conclusions

Our results, based on extensive simulations of Hodgkin-Huxley type
of neurons in an oscillatory regime, indicate that only certain network
topologies allow for a coordinated firing at a local and long-range scale
simultaneously. At a local level, we have found that all the topologies
considered present three different operating regimes defining different
relationships between the phases of the neurons. Besides network ar-
chitecture, axonal conduction delays are also observed to be another
important factor in the generation of coherent spiking. We report that
such communication latencies not only set the phase difference between
the oscillatory activity of remote neural populations but also determine
whether the interconnected cells can set in any coherent firing at all. In this
context, we have also investigated how the balance between the network
synchronizing effects and the dispersive drift caused by inhomogeneities
in natural firing frequencies across cells is resolved. The presence of in-
homogeneities in the natural firing frequency difficults the occurrence of
coordinated firing states and a strong interaction between the neurons is
needed to appear. We have also shown that the observed role of con-
duction delays is not particular to canonical networks but experimentally
measured anatomical networks, such as the macaque cortical network,
can display the same type of behavior. Interestingly, the macaque cortical
network does not exhibit an anti-phase operating regime, leading open
the interesting question if this behavior is particular of the macaque cor-
tex topology or is a general feature of any anatomical network. Finally,
we have observed that heterogeneous delays do not have a significant
impact in the synchronization regions of the system, resulting in the same
features than in the single delay situation, for a low variance of their
distribution.

# Consistency in a neuronal network

Consistency is defined as the ability of a nonlinear system to generate the same response every time a complex input is used as driving signal, while the system starts from different initial conditions [91]. Any complex waveform such as deterministic chaos or stochastic noise can be used as driving signal. This signal, that is sent repeatedly to the nonlinear dynamical system which starts from arbitrary initial conditions, generates an output. If the correlation between two of these outputs is high, it is said that the system responds consistently. If this does not happen it is said to be inconsistent. Figure 6.1 illustrates the concept of consistency of a nonlinear dynamical system.
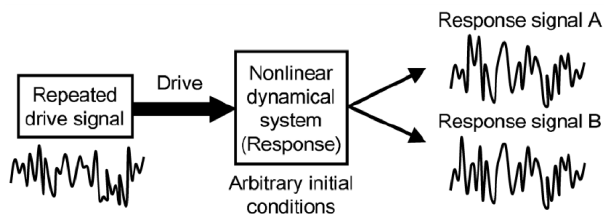


**Figure 6.1:** Concept of consistency.

Study the consistency of dynamical systems is essential for information transmission in biological, and neuronal systems in particular, and for reproduction of spatiotemporal patterns in nature. Previously, consistency has been studied in lasers systems and electronic circuits [91, 92]. In biological system, the reliability of the firing sequence of a neuron has also been studied demonstrating that a neuron that is repeatedly driven by a random drive signal can fire a consistent spike train with a high temporal precision [93].

In this chapter we study the consistency of a neuronal network composed of neurons described by the integrate-and-fire model, presented in chapter 1. The role of the synaptic plasticity in the consistency and synchronization of the network is also considered.

## 6.1

# Model

The system is composed of one thousand integrate-and-fire (IF) neurons coupled through a chemical synapses modeled by an alpha function. To take into account a more realistic situation, we consider our network composed of 80% excitatory neurons and 20% inhibitory neurons. We interconnect them conforming a sparse network, with 10% randomly chosen connections between the neurons. To keep balanced the network, we consider the ratio 1/4 in the strength of the excitatory to inhibitory connections, i.e. the inhibitory synapses are four times stronger than the excitatory ones. We assume an independent poissonian spike train acting over each neuron as an external signal with amplitude $D_n$.

The membrane potential $v_i(t)$ of neuron $i$ ($i = 1, ..., N$) at its soma obeys the following equation

$$\dot{v}_i(t) \quad = \quad -\frac{1}{\tau_m} v_i(t) + \frac{1}{C_m} I_i(t), \qquad (6.1)$$

where $\tau_m = 10 \ ms$ is the membrane time constant, $C_m = 250 \ pF$ is the capacitance of the membrane and $I_i(t)$ is the synaptic current arriving at the soma. This synaptic current is the sum of the contributions of spikes arriving at different synapses coming from recurrent connections or from

the external drive input. These spikes contributions are modeled as delta functions in our basic IF model:

$$I_i(t) = \frac{1}{N_c} \sum_j w_{ij} \sum_k f(t - t_j^k - D),$$ (6.2)

where the first summation is over different synapses with postsynaptic potential (PSP) amplitude $w_{ij}$, while the second one represents the different spikes arriving at synapse $j$, at time $t = t_j^k + D$, where $t_j^k$ is the emission time of $k$th-spike at neuron $j$, and $D = 10$ $ms$ is the transmission delay. The function $f(t)$ stands for the contribution of the incoming spikes and is represented as an $\alpha$-function:

$$f(t) = \frac{e}{\tau_\alpha} t e^{-t/\tau_\alpha},$$ (6.3)

where $\tau_\alpha$ is the rise time. We consider in this study the situation of homogeneous interaction between the neurons, i.e., $w_{ij} = w, \forall\, i, j$.

Simulation were done using the neuronal simulator package NEST [94]. This program is optimized for large networks of spiking neurons and can represent spikes in continuous time because it uses a precise time-driven algorithm to avoid integration errors occurring if spikes are constrained to times that are integral multiples of the simulation step.

6.2

# STDP synaptic rule

As it was introduced in chapter 1, Spike Timing Dependent Plasticity (STDP) is a phenomenon related to the change in the synaptic weights $w$ between a pair of neurons. For a single pair of presynaptic and postsynaptic action potentials with time difference $\Delta t = t_{post} - t_{pre}$ it induces a change in the synaptic efficacy $\Delta w$ given by [95]

$$\Delta w = \begin{cases} -\lambda f_-(w) \times K(\Delta t) & if\ \ \Delta t \leq 0 \\ \lambda f_+(w) \times K(\Delta t) & if\ \ \Delta t > 0 \end{cases}$$

The temporal filter $K(\Delta t) = exp(-|\Delta t|/\tau)$ implements the spike-timing dependence of the learning. The time constant $\tau$ determines the temporal extent of the learning window. The learning rate $\lambda$ scales the magnitude of individuals weight changes. The temporal asymmetry of the learning is represented by the opposite signs of the weight changes for positive and negative time differences. The updating functions $f_+(w) = (1-w)^\mu$ and $f_-(w) = \alpha w^\mu$, scale the synaptic changes and implement synaptic potentiation for $\Delta t > 0$, and depression otherwise. NEST has already implemented this synaptic plasticity rule and in our simulations we used the typical parameter values: $\tau = 20\ ms$, $\mu = 0.4$, $\alpha = 1.05$ and $\lambda = 0.005$.

## 6.3
## Measurement

To characterize both consistency and synchronization in the activity of our network, we consider the phase of each neuron defined as [96]:

$$\phi_i(t) = 2\pi \frac{t - \tau_k}{\tau_{k+1} - \tau_k} \tag{6.4}$$

where $\tau_k$ is the time of the $k$th firing of the neuron $i$. To measure the consistency of the responce of the network in different realizations, we define the quantity:

$$c_i(t) = \frac{1}{n} \sum_{k=1}^{n} \sin^2 \left( \frac{\phi_i(t) - \phi_i^k(t)}{2} \right) \tag{6.5}$$

where $\phi_i^k(t)$ is the phase of the neuron $i$ obtained in the $k$th realization starting from different initial conditions. The summation runs over $n$ different realizations. A spatiotemporal average of $c_i$,

$$C = \lim_{T \to \infty} \frac{1}{T} \int_0^T \left( \frac{1}{N} \sum_{i=1}^{N} c_i \right) dt \tag{6.6}$$

measures the degree of consistency of the response of the system. The idea of this measure is to quantify the phase difference between the response

patterns of the system when it start form different initial conditions when it is subject to the same driving signal. For a consistent response of the system, the phase difference between the patterns is zero, giving a value of $C = 0$. On the other hand, any inconsistent response of the system gives a phase difference larger than zero, resulting in values of $C > 0$.

To measure synchronization between the neurons, we use a similar index,

$$s_i(t) \;=\; \frac{1}{n_c(i)} \sum_{j \in neigh(i)} \sin^2\left(\frac{\phi_i(t) - \phi_j(t)}{2}\right) \tag{6.7}$$

where $\phi_j(t)$ is the phase of the neuron $j$ and the summation runs now over the $n_c(i)$ connected neighbors of neuron $i$. Averaging over the neurons and in time, we obtain a measure of the synchronization of the network in a particular realization

$$S \;=\; \lim_{T \to \infty} \frac{1}{T} \int_0^T \left(\frac{1}{N} \sum_{i=1}^{N} s_i\right) dt \tag{6.8}$$

When the network has a pattern response where the neurons fire in synchrony, this measure gives $S = 0$. On the contrary, for a desynchronous patterns we get $S > 0$.

## 6.4

# Consistency region

Our first goal is to determine if our neuronal network responds consistently when an external drive is applied. As a external drive signal we consider an independent Poisson spike train for each neuron. To illustrate the scenario, Figure 6.2 shows the raster plot of the activity of the network for different coupling strengths and a fixed value of the external drive amplitude. As it can be seen, the consistent responce of the network diminishes when the interaction between the neurons increases.
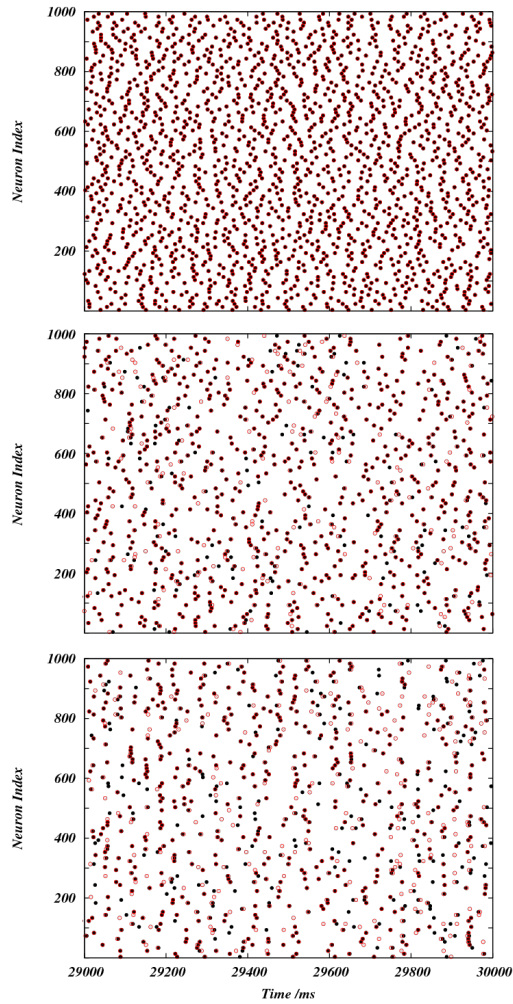
**Figure 6.2:** Raster plot for two simulation starting from different initial conditions (red circles and black dots). The parameters are: top: $w = 0.0 \ pA$, middle: $w = 1.0 \ pA$ and bottom: $w = 1.9 \ pA$. $D_n = 2.15 \ pA$.

We compute the index $C$ for different coupling intensities and drive signal strengths. The region where the system responds consistently is indicated by the black area in Figure 6.3. The upper panel stands for the usual homogeneous static connections, i.e., $w_{ij} = w$. The middle panel shows the consistency regions determined by $C$ when STDP synaptic plasticity rule is applied to the excitatory-excitatory connections. As it can be seen in the bottom panel, representing the difference between the two previous results, the inclusion of the STDP synaptic plasticity rule increases the region of consistency (red area) at moderate coupling strengths and at high drive amplitudes.

In order to illustrate what is the effect of the plasticity, Figure 6.4 shows the raster plot of the network for the same coupling intensity and drive amplitude in both cases: without learning rule (upper panel) and when STDP rule is applied to excitatory synapses (lower panel). It can be seen that the inclusion of plasticity has two main effects. On one hand, there is an increase of the activity of the network due to the reinforcement of the excitatory weights. On the other hand, this increase of the activity leads to an enhancement of the consistency of the system. The neurons are now capable of reproducing the same pattern of activity even when the system starts from different initial conditions.
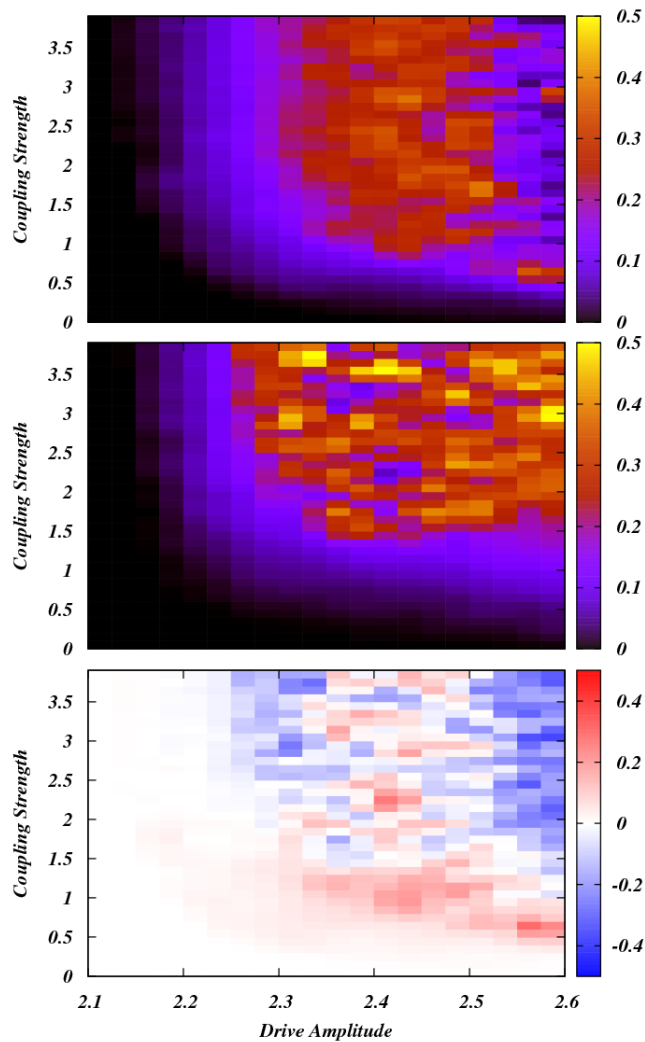
**Figure 6.3:** Consistency region determined by C. Perfect consistency is indicated by $C = 0$ (black areas) while an inconsistent response of the network correspond to $C > 0$. Upper panel: no STDP is applied to the network. Middle panel: nonlinear STDP is applied between excitatory connections. Bottom panel: difference between the two previous regions. An increase (decrease) of consistency is codified by red (blue) color.
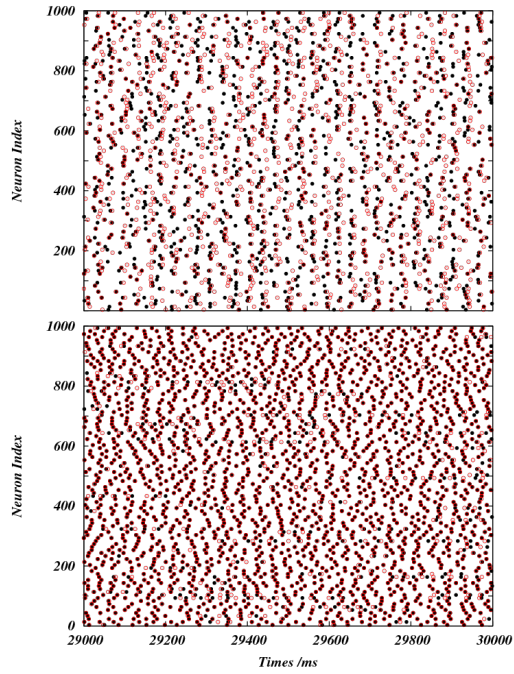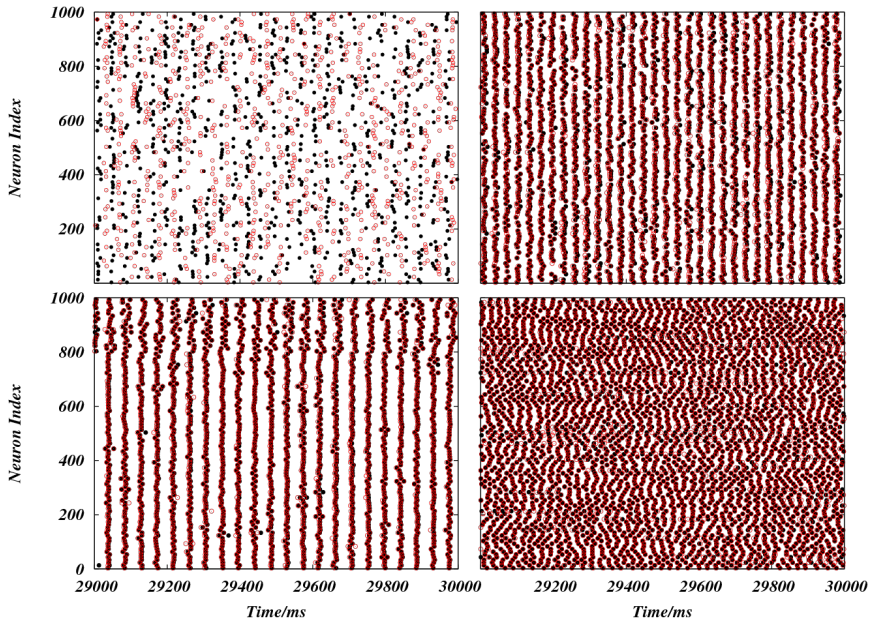
**Figure 6.4:** Raster plot for two simulation starting from different initial conditions. Top panel corresponds to a simulation without learning synaptic rule. Bottom panel: the same simulation with STDP synaptic rule. The parameters are: $w = 1.1\ pA$ and $D_n = 2.375\ pA$.

## 6.5

# Synchronization region

We also compute the synchronization region determined by the quantity $S$. Figure 6.5 shows, codified in colors, the values of the parameter $S$. The upper panel corresponds to the case of static conventional synapses while the middle row stands for simulations where the STDP synaptic rule is applied to the excitatory synapses.  Perfect synchronization is codified by a value of $S = 0$ (black color) while any other state differing from perfect synchrony has a value $S > 0$.  The bottom panel corresponds to the difference between the two regions.  An increase (decrease) of the synchronization in the system is codified by a red (blue) color.  As it can be seen, we do not observe perfect synchronization in our simulations, and for static synapses, desynchronization is predominant (yellow area). Only at high drive amplitudes a region where the parameter $S$ is close to zero appears.  On the contrary, the inclusion of STDP synaptic rule dramatically changes the scenario.  At intermediates drive amplitudes and high coupling intensities, a large area of values of $S$ close to zero appears indicating a region where the neurons fire more synchronously. To illustrate these results, Figure 6.6 displays the raster plot of the network for different coupling strengths and drive amplitudes.  The upper row corresponds to simulations with static conventional synapses and the bottom row stands for simulations where the STDP synaptic rule is applied to the excitatory synapses. This figure corroborates the effect of the STDP synaptic rule.  The reinforcement of the excitatory synapses leads to an increase of the activity of the network, and make the neurons to fire more synchronously as it can be seen in the left panel of Figure 6.6.  But plasticity can have the opposite effect as well.  At high drive amplitudes and moderates coupling strengths STDP diminishes drastically the synchrony of the network. Theses results suggest that synaptic plasticity can have a crucial role in the control of the pattern response of the network, modulating also the synchronous response of the neurons to an external stimulus.
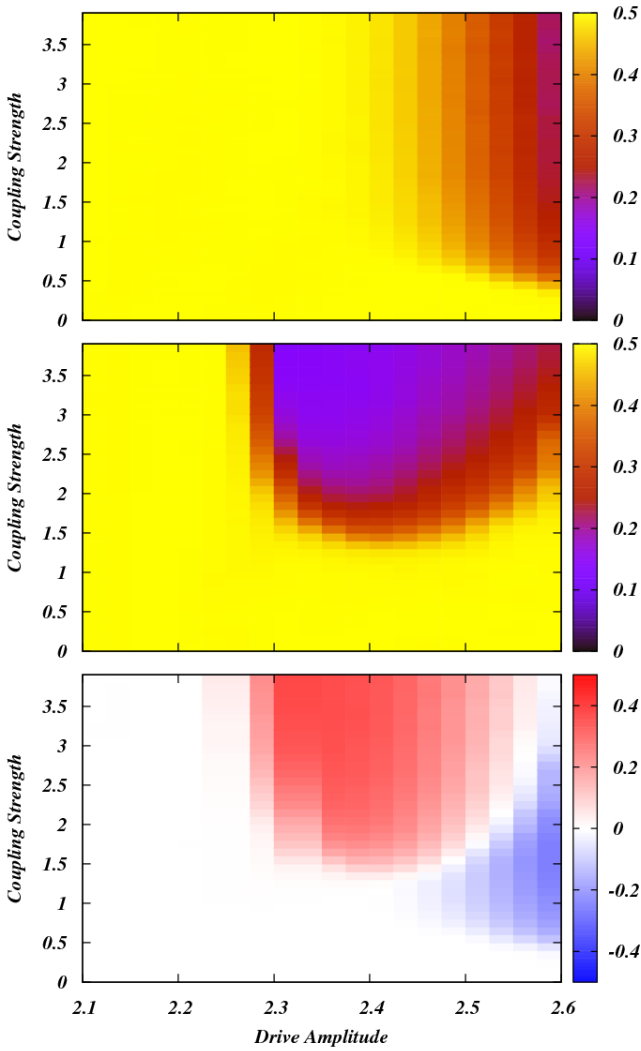
**Figure 6.5:** Synchronization region determined by S. Perfect synchronization is indicated by $S = 0$ while an asynchronous response of the network correspond to $S > 0$. Upper panel: no STDP is applied to the network. Middle panel: nonlinear STDP is applied between excitatory connections. Bottom panel: difference between the two previous regions. An increase (decrease) of synchronization is codified by red (blue) color.

**Figure 6.6:** Raster plots for two simulation starting from two different initial conditions. Top row correspond to a simulation without learning synaptic rule. Bottom row: the same simulation with STDP synaptic rule. Parameters used: left column, $w = 3.0 \, pA$ and $D_n = 2.35 \, pA$; right column, $w = 1.0 \, pA$ and $D_n = 2.6 \, pA$.

## 6.6

# Conclusions

In summary, we have studied the consistency and synchronization of a network of interacting neurons described by the integrate-and-fire model. We have found that the system can respond consistently to an external driving stimulus and we have quantified the regions where consistency occurs by means of an order parameter based on the phase differences of the different pattern responses. Interestingly, we have found that synchronization appears in different region of the phase space than consistency, indicating that consistency and synchronization can be considered, in this

case, as different features of the system.

We have also studied the effect induced by STDP rule between excitatory connections. We have found that STDP has a modulatory effect in both the consistency and synchronization of the system, increasing or decreasing the regions where consistency or synchronization appear. This result suggests that synaptic plasticity has a crucial role in shaping the response of the network to an external stimulus.

Chapter 7

# Concluding Remarks

In this thesis we have explored the dynamics and synchronization of different neuronal systems. The results we have presented were mainly based on numerical simulations of nonlinear differential equations describing the dynamics of interacting neurons. The most important results and conclusions extracted from the work presented in this thesis are summarized as follow.

In Part I we have studied the effect of different sources of disorder such as external noise acting on neurons or the presence of heterogeneity in the constituents of a neuronal network. In particular, in Chapter 2, we studied the effect of the synaptic noise, modeled as colored noise, when it acts over a population of motoneurons subject to an external weak modulation. We have demonstrated that noise can have a constructive role when acting over a group of motorneurons belonging to the spinal cord. The enhancement of the response of an ensemble of motoneurons to a weak modulation was reported as a stochastic resonance phenomenon. Our numerical results were supported with the first experimental measurements confirming that stochastic resonance occurs at the spinal cord level.

In chapter 3 we proposed a neuronal architecture involved in the generation of a motor activity such as the scratching. We reported both numerically and experimentally a rostro-caudal signal propagation oc-

curring during this motor activity. Our model allowed us to reproduce the observed spontaneous failures or absences of electrical activity in the motoneurons of the spinal cord by means of changes in the excitability of part of the network. We have also predicted a new kind of deletion, not observed experimentally yet, that recovers during the propagation. Study and understanding the mechanisms of deletions become essential to unveil the neuronal circuits involved in the generation of specific motor activities. Further experimental measurements are needed to elucidate the validity of the assumptions of our model and to corroborate our predictions. In our study, we have neither taken into account the spontaneous or background activity of the surrounding neurons nor the afferent feedback coming from the muscles and sensory neurons. It is well known that these features play an important role affecting the motor activities and it is consequently essential to include them in future versions of the model.

The role of the diversity present in an ensemble of interacting neurons was explored in chapter 4. We have studied different neuronal models under different coupling configurations observing an enhancement of the response of the system to an external weak modulation produced by the diversity of the units. In our study we have considered the variation of the ratio between excitatory and inhibitory connections obtaining an increase in the response of the system when this ratio is balanced. It would be of interest to explore the situation in which the synaptic weights of excitatory and inhibitory synapses are also balanced and the effect that plasticity plays into this novel behaviour.

In Part II we have studied the effect of the topology and delay in the connections in the synchronization properties of neuronal networks. In Chapter 5 we explored how the topological properties and conduction delays of several classes of neural networks affect the capacity of their constituent cells to establish well-defined temporal relations among the firing of their action potentials. We have found that only certain networks topologies allow for a coordinated firing at a local and long-range scale simultaneously. We have reported that the existence of latency delays

in the communication not only establish the phase difference between the oscillatory activity of remote neural populations but also determine whether the interconnected cells can respond in a coherent firing. We have shown that the role played by the delay is not particular to canonical networks. Experimentally measured anatomical networks, such as the macaque cortical network, can display the same type of behavior. Further studies exploring different delays distribution are needed in order to determine the robustness of the synchronized state.

Finally, in Chapter 6, we have studied the consistency and synchronization of a neuronal network of integrate-and-fire neurons subject to an external drive. We have quantified the regions where consistency and synchronization occur. We have found that synchronization occurs at different values of the coupling strength and drive amplitude than consistency, suggesting that consistency and synchronization can be considered as different features of the system. We have reported the modulatory effects induced by the synaptic plasticity in the excitatory connections observing both an increasing and decreasing of the regions where consistency and synchronization appear. This result confirms the crucial role played by synaptic plasticity in the response of the network to an external stimulus. The design of experiments devoted to determine consistency in different systems becomes essential for a deeper understanding of the phenomena.

We expect that the work presented in this thesis opens new perspectives into the experimental research in the central nervous system.

# List of Figures

LIST OF FIGURES

LIST OF FIGURES

# List of Tables

# References

[1] L. Lapicque, "Recherches quantitatives sur l'excitation électrique des nerfs traitée comme une polarization.," *J. Physiol. Pathol. Gen.* **9**, p. 620, 1907.

[2] R. Stein, "Structure of nerve fibers and synapses in some invertebrates.," *Quant. Biol.* **4**, p. 1, 1936.

[3] K. Cole, *Membranes, ions and impulses*, Berkeley: University of California Press., Berkeley, first ed., 1968.

[4] A. L. Hodgkin and A. Huxley, "A quantitative description of membrane current and it applications to conduction and excitation in nerve.," *J. Physiol.* **117**, p. 500, 1952.

[5] R. FitzHugh, "Impulses and physiological states in theoretical models of nerve membrane.," *Biophysical J.* **1**, p. 445, 1961.

[6] C. Morris and H. Lecar, "Voltage oscillations in the barnacle giant muscle fiber.," *Biophysical J.* **35**, p. 193, 1981.

[7] A. L. Hodgkin, A. Huxley, and B. Katz, "Measurements of current-voltage relations in the membrane of the giant axon of loligo.," *J. Physiol.* **116**, p. 424, 1952.

[8] A. L. Hodgkin and A. Huxley, "Currents carried by sodium and potassium ions through the membrane of the giant axon of loligo.," *J. Physiol.* **116**, p. 449, 1952.

[9] A. L. Hodgkin and A. Huxley, "The components of membrane conductance in the giant axon of loligo.," *J. Physiol.* **116**, p. 473, 1952.

[10] A. L. Hodgkin and A. Huxley, "The dual effect of membrane potential on sodium conductance in the giant axon of loligo.," *J. Physiol.* **116**, p. 497, 1952.

[11] A. L. Hodgkin and B. Katz, "The effect of sodium ions on the electrical activity of the giant axon of the squid.," *J. Physiol.* **108**, p. 37, 1949.

[12] B. Hille, *Ionic channels of excitable membranes*, Sinauer Associates, Sunderland, Mass., second ed., 1992.

[13] S. H. Strogatz, *Nonlinear dynamics and chaos*, Addison-Wesley, Reading, Mass., second ed., 1994.

[14] R. Stein, "A theoretical analysis of neuronal variability.," *Biophys. J.* **5**, p. 173, 1965.

[15] B. Lindner, J. Garcia-Ojalvo, A. Neiman, and L. Schimansky-Geier, "Effects of noise in excitable systems.," *Phys. Rep.* **392**, p. 321, 2004.

[16] E. M. Izhikevich, "Neural excitability, spiking and bursting.," *Int. J. Bifurcation Chaos* **10**, p. 1171, 2000.

[17] A. L. Hodgkin, "The local electric changes associated with repetitive action in a non-medullated axon.," *J. Physiol.* **107**, p. 165, 1948.

[18] E. M. Izhikevich, *Dynamical systems in neuroscience*, The MIT Press, Cambridge, Mass., first ed., 2007.

[19] J. Rinzel, "A formal classification of bursting mechanisms in excitable systems.," in *Mathematical topics in population biology, Morphogenesis and Neuroscience.*, E. Teramoto and M. Yamaguti, eds., pp. 267–281, Springer, Berlin, 1987.

[20] R. Bertram, M. J. Butte, T. Kiemel, and A. Sherman., "Hybrid integrate-and-fire model of a bursting neuron," *Bulletin of mathematical Biology* **57**, p. 413, 1995.

[21] D. Hebb, *The organization of behavior: a neuropsychological theory.*, Weley, New York, first ed., 1949.

[22] A. Morrison, M. Diesmann, and W. Gerstner, "Phenomenological models of synaptic plasticity based on spike timing.," *Biological Cybernetics* **98**, p. 459, 2008.

[23] H. Markram, J. Lubke, M. Frotscher, and B. Sakmann, "Regulation of synaptic efficacy by coincidence of postsynaptic aps and epsps.," *Science* **275**, p. 213, 1997.

## REFERENCES

[24] G. Bi and M. Poo, "Synaptic modifications in cultured hippocampal neurons: dependence on spike timing, synaptic strength, and postsynaptic cell type.," *Journal of Neuroscience* **18**, p. 10464, 1998.

[25] G. Bi and M. Poo, "Synaptic modification by correlated activity: Hebb's postulated revisited.," *Annu. Rev. Neurosci.* **24**, p. 139, 2001.

[26] A. Pikovsky, M. Rosenblum, and J. Kurths, *Synchronization: A universal concept in nonlinear sciences.*, Cambridge University Press, New York, first ed., 2001.

[27] W. Singer, "Neuronal synchrony: A versatile code for the definition of relations?," *Neuron* **24**, p. 49, 1999.

[28] P. Tass, *Phase Resetting in Medicine and Biology. Stochastic Modelling and Data Analysis.*, Springer-Verlag, Berlin, first ed., 1999.

[29] F. Varela, J. Lachaux, E. Rodriguez, and J. Martinerie, "The brainweb: Phase synchronization and large-scale integration.," *Nature Reviews Neuroscience* **2**, p. 229, 2001.

[30] M. Gray, "The temporal correlation hypotesis of visual feature integration: Still alive and well.," *Neuron* **24**, p. 31, 1999.

[31] R. Traub, M. Whittington, and J. Jeffreys, *Fast Oscillations in Cortical Networks*, MIT Press, Cambridge, first ed., 1999.

[32] A. Engel, A. Kreiter, P. Konig, and W. Singer, "Synchronization of oscillatory neural responses between striate and extrastriate visual cortical areas of the cat.," *Proc. Nati. Acad. Sci. USA* **88**, p. 6048, 1991.

[33] A. Frien, R. Eckhorn, R. Bauer, T. Woelbern, and H. Kehr, "Stimulus-specific fast oscillations at zero phase between visual areas v1 and v2 of awake monkey.," *Neuroreport* **5**, p. 2273, 1994.

[34] S. Bressler, "Large-scale cortical networks and cognition.," *Brain Res.* **20**, p. 288, 1995.

[35] P. Girard, J. Hupe, and J. Bullier, "Feedforward and feedback connections between v1 and v2 of the monkey have similar rapid conductions velocities.," *J. Neurophysiol.* **85**, p. 1328, 2001.

[36] L. Pecora and T. Carroll, "Synchronization in chaotic systems.," *Phys. Rev. Lett.* **64**, p. 821, 1990.

[37] M. Rosenblum, A. Pikovsky, and J. Kurths, "From phase to lag synchronization in coupled caotic oscillators.," *Phys. Rev. Lett.* **78**, p. 4193, 1997.

[38] N. Rulkov, M. Sushchik, L. Tsimring, and H. Abarbanel, "Generalized synchronization of chaos in directionally coupled chaotic systems.," *Phys. Rev. E.* **51**, p. 980, 1995.

[39] H. Abarbanel, N. Rulkov, and M. Sushchik, "Generalized synchronization of chaos: The auxiliary system approach.," *Phys. Rev. E.* **53**, p. 4528, 1996.

[40] M. Rosenblum, A. Pikovsky, and J. Kurths, "Phase synchronization of caotic oscillators.," *Phys. Rev. Lett.* **76**, p. 1804, 1996.

[41] S. Bocaletti, J. Kurths, G. Osipov, D. Valladares, and C. Zhou, "The synchronization of chaotic systems.," *Phys. Rep.* **366**, p. 1, 2002.

[42] R. Brown, "A brief account of microscopical observations made in the months of june, july and august, 1827, on the particles contained in the pollen of plants; and on the general existence of active molecules in organic and inorganic bodies.," *Phil. Mag.* **4**, p. 161, 1828.

[43] A. Einstein, "Uber die von der molekularkinetischen theorie der warme geforderte bewegung von in ruhenden flussigkeiten suspendierten teilchen.," *Annalen der Physik* **322**, p. 549, 1905.

[44] M. von Smoluchowskii, "Zur kinetichen theorie der brownschen molekularbewegung und der suspensionen.," *Annalen der Physik* **21**, p. 756, 1906.

[45] P. Langevin, "Sul la théorie du movement brownien.," *Comptes. Rendues* **146**, p. 530, 1908.

[46] K. Falconer, *Fractal Geometry.*, John Weley and Sons, London, first ed., 1990.

## REFERENCES

[47] T. Gard, "Introduction to stochastic differential equations.," in *Monograph and Textbooks in Pure and Applied Mathematics.*, M. Dekker, ed., -, 1987.

[48] M. S. Miguel and R. Toral, "Stochastic effects in physical systems.," in *Instabilities and Nonequilibrium Structures VI.*, , ed., Kluiver Ac. Press, 1999.

[49] J. Douglas, L. Wikens, E. Pantazelou, and F. Moss, "Stochastic resonance and the benefits of noise: from ice ages to crayfish and squids.," *Nature* **365**, p. 337, 1993.

[50] J. Levin and J. Miller, "Broadband neural encoding in the cricket cereal sensory system enhanced by stochastic resonance." *Nature* **380**, p. 165, 1996.

[51] A. Longtin, A. Bulsara, and F. Moss, "Time-interval sequences in bistable systems and the noise-induced transmission of information by sensory neurons." *Phys. Rev. Lett.* **67**, p. 656, 1991.

[52] P. Cordo, J. Inglis, S. Verschueren, J. Collins, D. Merfeld, S. Rosenblum, S. Buckley, and F. Moss, "Noise in human muscle spindles," *Nature* **383**, p. 769, 1996.

[53] A. Destexhe, Z. Mainen, and T. Sejnowski, "An efficient method for computing synaptic conductances based on a kinetic model of receptor binding." *Neural Comput.* **6**, p. 14, 1994.

[54] C. Tessone, C. Mirasso, R. Toral, and J. Gunton, "Diversity-induced resonance," *Phys. Rev. Lett.* **97**, p. 194101, 2006.

[55] L. Mendell and E. Henneman, "Terminal of single ia fibers: distribution within a pool of 300 homonymous motro neurons." *Science* **160**, p. 96, 1968.

[56] P. Gogan, J. Gueritaud, G. Horcholle-Bossavit, and S. Tyc-Dumont, "Direct excitatory interactions between spinal motoneurones of the cat." *J. Physiol.* **272**, p. 755, 1977.

[57] A. Destexhe, M. Rudolph, J. Fellows, and T. Sejnowski, "Fluctuating synaptic conductances recreate in vivo-like activity in neocortical neurons.," *Neuroscience* **107**, p. 13, 2001.

[58] K. Bayev and P. G. Kostyuk, "Primary afferent depolarization evoked by the activity of spinal scratching generator.," *Neuroscience* **6**, p. 205, 1981.

[59] C. Cuellar, J. Tapia, V. Juárez, J. Quevedo, P. Linares, L. Martínez, and E. Manjarrez, "Propagation of sinusoidal electrical waves along the spinal cord during a fictive motor task.," *J. Neurosci.* **29**, p. 798, 2009.

[60] C. Sherrington, "Observation of the scratch-reflex in the spinal dog.," *J. Physiol.* **34**, p. 1, 1906.

[61] M. Berkinblit, T. Deliagina, A. Feldman, I. Gelfand, and G. Orlovsky, "Generation of scratching. i. activity of spinal interneurons during scratching.," *J. Neurophysiol.* **41**, p. 1040, 1978.

[62] D. McCrea and I. Rybak, "Organization of mammalian locomotor rhythm and pattern generation.," *Brain. Res. Rev.* **57**, p. 134, 2008.

[63] G. Brown, "The intrinsic factors in the acts of progression in the mammal.," *Proc. Roy. Soc. Lond. B. Biol. Sci.* **84**, p. 308, 1911.

[64] S. Grillner, "Control of locomotion in bipeds, tetrapods, and fish," in *Handbook of Physiology. The nervous system. Motor control*, J. Brookhart and V. Mountcastle, eds., American Physiological Society, Bethesda, first ed., 1981.

[65] R. Burke, A. Degtyarenko, and E. Simon, "Patterns of locomotor drive to motoneurones and last-order interneurones: clues to the structure of the cpg," *J. Neurophysiol.* **86**, p. 447, 2001.

[66] S. Grillner and P. Zangger, "On the central generation of locomotionin the low spinal cat," *Exp. Brain Res.* **34**, p. 241, 1979.

[67] O. Kiehn, "Locomotor circuits in the mammalian spinal cord," *Annu. Rev. Neurosci.* **29**, p. 279, 2006.

## REFERENCES

[68] M. Lafreniere-Roula and D. McCrea, "Deletions of rhythmic motoneuron activity during fictive locomotion and scratch provide clues to the organization of the mammalian central pattern generator.," *J. Neurophysiol.* **94**, p. 1120, 2005.

[69] I. Rybak, N. A. Shevtsova, M. Lafreniere-Roula, and D. McCrea, "Modelling spinal circuitry involved in locomotor pattern generation: insights from deletions during fictive locomotion.," *J. Physiol.* **577**, p. 617, 2006.

[70] V. Turkin and T. Hamm, "Changes in locomotor drive potential and cycle characteritics associated with deletions during fictive locomotion.," *Soc. Neurosci. Abstr.* **34**, p. 883, 2004.

[71] P. Stein, "Neural control of turtle hindlimb motor rhythms.," *J. Comput. Physiol. A Sens. Neural Behav. Physiol. Neuroethol.* **191**, p. 213, 2005.

[72] S. Grillner, "Biological pattern generation: the cellular and computational logic of networks in motion.," *Neuron* **52**, p. 751, 2006.

[73] K. Pearson, "Central programming and reflex control of walking in the cockroach.," *J. Exp. Biol.* **56**, p. 173, 1972.

[74] R. Brownstone and J. Wilson, "Strategies for delineating spinal locomotor rhythm-generating networks and the possible role of hb9 interneutones in rhythmogenesis.," *Brain. Res. Rev.* **57**, p. 64, 2008.

[75] J. Rinzel and B. Ermentrout, *Analysis of neural excitability and oscillations. In: Methods in neuronal modelling: from ions to networks.*, The MIT Press, Cambridge, MA, first ed., 1998.

[76] A. Winfree, "Biological rhythms and the behavior of populations of coupled oscillators," *J. Theoret. Biol.* **16**, p. 15, 1967.

[77] Y. Kuramoto in *International Symposium on Mathematical Problems in Theoretical Physics.*, , ed., Lecture Notes in Physics. Springer, 1975.

[78] E. Glatt, M. Gassel, and F. Kaiser, "Noise-induced synchronisation in heterogeneous nets of neural elements," *Eur. Phys. Lett.* **81**, p. 40004, 2008.

170

[79] S.D.Monte and F.D'Ovidio, "Dynamics of order parameters for globally coupled oscillators," *Europhys. Lett.* **58**, p. 21, 2002.

[80] S.D.Monte, F.D'Ovidio, H. Chaté, and E. Mosekilde, "Effects of microscopic disorder on the collective dynamics of globally coupled maps," *Physica D* **205**, p. 25, 2005.

[81] H. Abarbanel, M. Rabinovich, A. Selverston, M. Bazhenov, R. Huerta, M. Suschchik, and L. Rubchinskii, "Synchronisation sn neural networks," *Phys. Usp.* **39**, p. 337, 1996.

[82] M. Ravinovich, P. Varona, A. Selverston, and H. Abarbanel, "Dynamical principles in neuroscience," *Rev. Mod. Phys.* **78**, p. 1213, 2006.

[83] P. Fries, D. Nikolic, and W. Singer, "The gamma cycle," *Trends Neurisci.* **30**, p. 309, 2007.

[84] G. Stepan, "Delay effects in brain dynamics," *Phil. Trans. R. Soc. A* **367**, p. 1059, 2009.

[85] A. Roxin, N. Brunel, and D. Hansel, "Role of delays in shaping spatiotemporal dynamics of neuronal activity in large networks," *Phys. Rev. Lett.* **94**, p. 238103, 2005.

[86] F. Atay, J. Jost, and A. Wende, "Delays, connection topology, and synchronization of coupled chaotic maps," *Phys. Rev. Lett.* **92**, p. 144101, 2004.

[87] D. J. Watts and S. Strogatz, "Collective dynamics of 'small-world' networks," *Nature* **393**, p. 40910, 1998.

[88] A. L. Barabási and R. Albert, "Emergence of scaling in random networks," *Science* **286**, p. 509, 1999.

[89] A. Pikovsky, M. Rosenblum, G. Osipov, and J. Kurths, "Phase synchronization of chaotic oscillators by external driving," *Physica D* **104**, p. 219, 1997.

[90] M. Young, "The organization of neural systems in the primate cerebral cortex," *Proc. R. Soc. London, Ser. B* **252**, p. 13, 1993.

[91] A. Uchida, R. McAllister, and R. Roy, "Consistency of nonlinear system response to complex drive signals.," *Phys. Rev. Lett.* **93**, p. 244102, 2004.

[92] A. Uchida, M. Kawano, and S. Yoshimori, "Dual synchronization of chaos in colpitts electronic oscillators and its applications for communications.," *Phys. Rev. E* **68**, p. 056207, 2004.

[93] Z. Mainen and T. Sejnowski, "Reliability of spike timing in neocortical neurons.," *Science* **268**, p. 1503, 1995.

[94] M.-O. Gewaltig and M. Diesmann, "Nest (neural simulation tool)," *Scholarpedia* **2**(4), p. 1430, 2007.

[95] R. Gutig, R. Aharonov, S. Rotter, and H. Sompolinsky, "Learning input correlations through nonlinear temporally asymetric hebbian plasticity.," *J. Neurosci.* **23**, p. 9, 2003.

[96] L. Gammaitoni, F. Marchesoni, and S. Santucci, "Stochastic resonance as a bona fide resonance," *Phys. Rev. Lett.* **74**, p. 1052, 1995.

**Part III**


# Appendices

# CURRICULUM VITAE

*Toni Pérez López*

## Personal Data

| | |
|---|---|
| First name | : Toni |
| Surnames | : Pérez López |
| Date of birth | : 03/10/1978 |
| Place of birth | : Jerez de la Frontera, (Spain) |
| Nationality | : Spanish |
| Civil Status | : Single |
| DNI | : 31705457A |
| Address | : 18 1E Pasaje Son Real, Palma de Mallorca |
| Post Code | : 07008 |
| Office Phone | : +34 971 173369 |
| e-mail | : toni@ifisc.uib-csic.es |
| URL | : http://www.ifisc.uib.es/~toni |

## Academic Degrees

Degree:   M.Sc. in Physics
Center:   University of Barcelona
Date:    03/08/2004

## Current Affiliation

1. PhD student since 01/01/2005 at the Instituto de Física Interdisciplinar y Sistemas Complejos, IFISC (CSIC-UIB)

## Awarded Fellowships

1. Fellowship of Ayuda al Estudio del Ministerio de Educación y Cultura in the years 1997/98, 1998/99 and 2000/01.

2. Collaboration Fellowship under the European Community project OCCULT from 01/01/2005 to 08/31/2005 under the supervision of Dr. Claudio Mirasso.

3. "Beca predoctoral para la formación de personal investigador", a PhD fellowship funded by the Conselleria d'Economia, Hisenda i Innovació of the Govern de les Illes Balears since 09/01/2005 under the supervision of Dr. Claudio Mirasso.

## Other Merits

1. Assistant Student for the Optoelectronic Group of the Physics Department of the University of the Balearic Islands, 2002/03.

2. Teaching Assistant under the project: "Convocatòria d'ajudes d'alumne col·laborador per a les experiències d'aplicació del sistema de crèdits europeus" of OCIHE at University of Balearic Island, from 10/2006 to 06/2007; from 10/2007 to 06/2008 and 10/2008 to 06/2009

# Specialization Courses

Ph.D. courses in the University of the Balearic Islands

- *Métodos estocásticos de computación*. Dr. Raúl Toral and Pere Colet. UIB, 2005 [3 credits]

- *Computación distribuida, Grid y E-ciencia*. Dr. Joan Massó. UIB, 2005 [3 credits]

- *Fenómenos no lineales en biología*. Dr. Raúl Toral, Dr. Claudio Mirasso, Dr. Tomás M. Sintes and Dr. Oreste Piro. UIB 2005 [4 credits]

- *Dinámica de dispositivos y sistemas fotónicos*. Dr. Claudio Mirasso and Dr. Josep Mulet. UIB 2005 [3 credits]

- *Sistemas dinámicos no lineales y complejidad espacio-temporal*. Dr. M. San Miguel, Dr. Emilio Hernández and Dr. Oreste Piro. UIB 2005 [4 credits]

Other specialization courses

- 2$^{nd}$ *International School Topics in Nonlinear Dynamics*, 07/09/2003 to 07/11/2003 , Siena, Italy. Organized by the Italian Society for Chaos and Complexity and Center for Complex Systems Studies.

- *IV Days of Introduction to Dynamical Systems (JISD 2005)*, 06/27/2005 to 07/01/2005 , Barcelona, Spain. Organized by the Doctorate Program of Applied Mathematics of the Universitat Politècnica de Catalunya.

- *Non-equilibrium in Physics and in Biology (PHYSBIO 06)*, 08/13/2006 to 10/08/2006, Sant Etienne de Tineè (France). Organized by the European Union Marie Curie Series of Conferences.

- *Theoretical Neuroscience & Complex Systems*, 08/06/2006 to 08/25/2007, Frankfurt (Germany). Organized by the Frankfurt Institute of Advanced Studies (FIAS).

## Stays at foreign research centers

- *06/20/2005 to 06/24/2005 at the Institute für Physik, Humboldt Universität*, Berlin, Germany, under the supervision of Professor H. J. Wünsche.

- *02/19/2006 to 03/06/2006 at the Institute für Physik, Humboldt Universität*, Berlin, Germany, under the supervision of Professor H. J. Wünsche.

- *05/20/2006 to 07/23/2006 at the Institute of Neurophysiology, Benemerita Universidad de Puebla*, Puebla, Mexico, under the supervision of Professor Elías Manjarrez.

- *12/02/2006 to 12/10/2006 at the Institute für Physik, Humboldt Universität*, Berlin, Germany, under the supervision of Professor H. J. Wünsche.

- *18/05/2008 to 24/05/2008 at the Max-Planck-Institute for Brain Research*, Frankfurt, Germany, in collaboration with Dr R. Vicente.

- *21/08/2008 to 14/11/2008 at the Department of Information and Computer Sciences Interdisciplinary, Saitama University*, Saitama, Japan, under the supervision of Professor Atsushi Uchida.

## Seminars

- *"Chaos Synchronization: Applications to Data Encryption"*, 06/23/2005, Weierstrass Institute for Applied Analysis and Stochastic (WIAS), Berlin, Germany.

- *"Synchronization in Biophysical Systems"*, 07/13/2006, Institute of Neurophysiology, Benemerita Universidad de Puebla, Puebla, Mexico.

- *"Resonance in Biophysical Systems"*, 12/18/2007, IFISC, University of Balearic Islands, Palma de Mallorca, Spain.

- *"Introduction to neuronal systems: basics concepts about modeling neurones"*, 10/17/2008, Saitama University, Saitama, Japan.

- *"Resonance in Biophysical Systems"*, 10/18/2008, Saitama University, Saitama, Japan.

- *"Effects of topology and delayed connections in a neuronal network"*, 05/06/2008, IFISC, University of Balearic Islands, Palma de Mallorca, Spain.

## Congress presentations

- *Synchronization of Chaotic Semiconductor Lasers and its Applications to Optical Communications*, 09/27/2004, XX Trobades científiques de la Mediterranea, Mahon (Spain). Poster.

- *Optical-Mode Commutation in Semiconductor Ring Lasers*, 06/27/2005, XIII Congreso de Física Estadística (FISES 2005), Madrid (Spain). Poster.

- *All-Optical Two-modes Switching in Semiconductor Ring Lasers.*, 04/03/2006, Photonics Europe 2006, Strasbourg (France). Oral.

- *Chaos Synchronization of Unidirectionally Coupled Multisection Lasers*, 11/26/2006, Cleo Focus Meeting 2006, Cannes (France). Oral.

- *All-Optical Two-modes Switching in Semiconductor Ring Lasers.*, 09/25/2006, Cleo Focus Meeting 2006, Cannes (France). Poster.

- *Synchronization of chaotic unidirectionally coupled multisection lasers*, 03/30/2007, PHASE & IPSSO 2007, Metz (France). Oral.

- *Bistability and Optical Switching in Semiconductor Ring Lasers*, 06/20/2007, CLEO Europe/IQEC 2007, Munich (Germany). Poster.

- *Synchronization of chaotic unidirectionally coupled multisection lasers*, 06/21/2007, CLEO Europe/IQEC 2007, Munich (Germany). Oral.

- *Study of the Role of diversity of Synaptically-Coupled Neurons*, 11/08/2007, Noise in Life 07, Dresden (Germany). Poster.

- *Diversity-induced resonance in a FitzHugh-Nagumo neuronal network*, 10/09/2008, Dynamics Days Asia Pacific 5 Nara (Japan). Poster.

## Congress assistance

- *XX Trobades científiques de la Mediterranea*, 09/26/2004 to 09/29/2004, Mahon (Spain)

- *XIII Congreso de Física Estadística (FISES 2005)*, 06/27/2005 to 06/27/2005, Madrid (Spain).

- *4a. Reunió de la Xarxa Temàtica: Dinàmiques No Lineals d'Auto-organització Espai-temporal*, 02/01/2006 to 02/03/2006, Barcelona (Spain).

- *Photonics Europe 2006*, 04/03/2006 to 04/07/2006 , Strasbourg (France).

- *Conference on Mathematical Neuroscience (Neuromath 06)*, 09/01/2006 to 09/04/2006, Sant Julià de Lòria (Andorra).

- *9th Granada Seminar on Computational Physics*, 09/11/2006 to 09/16/2006, Granada (Spain).

- *Cleo Focus Meeting 2006*, 09/24/2007 to 09/27/2006, Cannes (France).

- *PHASE & IPSSO 2007*, 03/28/2007 to 03/30/2007, Metz (France).

- *CLEO Europe/IQEC 2007*, 06/17/2007 to 06/22/2007, Munich (Germany)

- *Cobenn*, 10/17/2007 to 10/20/2007, Palma de Mallorca (Spain)

- *Noise in Life 07*, 11/07/2007 to 11/09/2007, Dresden (Germany)

- *Dynamics Days Asia Pacific 5*, 09/09/2008 to 12/09/2008, Nara (Japan).

## Publications

### Articles

- R. Vicente, T. Pérez, and C.R. Mirasso, "*Open- versus Closed- Loop Performance of Synchronized Chaotic External Cavity Semiconductor Lasers*", IEEE Journal of Quantum Electronics **38**, pp. 1197-1204 (2002).

- J.M. Buldú, R. Vicente, T. Pérez, C.R. Mirasso, M.C. Torrent, and J. García-Ojalvo, "*Periodic Entrainment of Power Dropouts in Mutually Coupled Semiconductor Lasers*", Applied Physics Letters, **81**, pp. 5105-5107, (2002).

- J.M. Buldú, M.C. Torrent, J. García-Ojalvo, R. Vicente, T. Pérez, and C.R. Mirasso, "*Low Frequency Fluctuations Entrainment is Enhanced by Coupling*", Fluctuation and Noise Letters, **3**, pp.127-134, (2003).

- C.R. Mirasso, R. Vicente, P. Colet, J. Mulet, and T. Pérez, "*Synchronization Properties of Chaotic Semiconductor Lasers and Applications to Encryption*", Comptes Rendus de l'Académie de Sciences, Physique, **5**, pp. 613-622, (2004).

- Pérez,Toni; Radziunas, Mindaugas; Wunsche, Hans-Jurgen; Mirasso, Claudio R.; Henneberger, Fritz, "*Synchronization Properties of Two Coupled Multisection Semiconductor Lasers Emitting Chaotic Light*", IEEE Photonics Technology Letters, **18**, 2135-2137. (2006)

- Valerio Annovazzi-Lodi, Mauro Benedetti, Sabina Merlo, Toni Pérez, Pere Colet and Claudio R. Mirasso, "*Message Encryption by Phase Modulation of a Chaotic Optical Carrier* ", IEEE Photonics Technology Letters, **19**, 76-78. (2007)

- Martínez, Lourdes; Pérez, Toni; Mirasso, Claudio; Manjarrez, Elías, "*Stochastic Resonance in the Motor System: Effects of Noise on the Monosynaptic Reflex Pathway of the Cat Spinal Cord*", Journal of Neurophysiology, **97**, 4007-4016. (2007)

- Pérez, Toni; Scirè, Alessandro; Van der Sande, Guy; Colet, Pere and Mirasso, Claudio, "*Bistability and all-optical switching in semiconductor ring lasers*", Optics Express, **20**, 12941-12948. (2007)

- Pérez, Toni; Claudio; Tapia, Jesus; Mirasso, Claudio; García-Ojalvo, Jordi; Quevedo, Jorge; Cuellar, Carlos; Manjarrez, Elias, "*An intersegmental neuronal architecture for deletion-proof spinal wave propagation*", Journal of Neuroscience, **29**, 10254-10263. (2009)

182

- Pérez, Toni; Vicente, Raúl; Eguíluz, Victor; Mirasso, Claudio; Pipa, Gordon, *"Effect of the topology and delayed connections in a neuronal network"*, submitted to PLoS Computational Biology.

- Pérez, Toni; Mirasso, Claudio; Toral, Raúl; Gunton, James, *"The role of diversity in coupled neurons: a comparison between chemical and electrical coupling"*, in preparation.

## Proceedings

- T. Pérez, R. Vicente, and C.R. Mirasso, *"Dynamical Entrainment of Unidirectionally Coupled Single-Mode Diode Lasers"*, SPIE Proceedings, **4646**, pp. 479-486, (2002).

- Scirè, A; Sorel, M; Giuliani, G; Colet, P; Pérez, Toni; Mirasso, C.R., *"All-optical two-mode switching in semiconductor ring lasers"*, Proc. SPIE Proceedings, **6184**, pp. 70-75, (2006).

- Scirè, A. ; Pérez-Serrano, A. ; Pérez, T. ; Van der Sande, G. ; Colet, P. ; Mirasso, C.R. ; Balle, S.,*"Bistability and all optical switching in semiconductor ring lasers"*, Proceeding of 9th International Conference on Transparent Optical Networks, ICTON, (2007).

# Computer experience and languages

- Programming: Fortran, C, IDL, Mathematica and Matlab.

- Operative systems: UNIX and Windows.

- Languages: Spanish (native), Catalan (good), English (good).

*"I do not fear computers. I fear the lack of them."* — Isaac Asimov